SEA
GRANT
PROJECT
OFFICE

WAVE FORCES ON A SUBMERGED OBJECT

By

John E. Halkyard

Massachusetts Institute of Technology

Cambridge, Massachusetts 02139

Report No. MITSG 72-4
November 1, 1971

Wave Forces On A Submerged Object

By

John E. Halkyard

Report No. MITSG 72-4
November 1, 1971

WAVE FORCES ON A SUBMERGED OBJECT

by

John E. Halkyard

Abstract

An experimental and theoretical investigation is conducted into the nature of the wave motion past (and under) a semi-circular cylinder suspended a short distance above the sea bottom. Particular attention is drawn to the flow through the gaps at the cylinder's edges.

The flow is represented by replacing the gaps by a fluid source and a fluid sink respectively. The strength of the source and sink is found by a semi-intuitive matched asymptotic expansion scheme. The pressures both inside and outside the cylinder are computed and the resulting forces plotted.

A significant reduction in the horizontal force is noted for very small gap widths. This result is supported by force measurements in the wave tank, as is the discovery that the vertical force is largely affected by a first order constant pressure acting inside the cylinder.

Reflection coefficients measured in the tank showed less correlation to the theory, mostly due to sensitivity to beach reflected waves.

The extension of this theory to three-dimensional objects is discussed, and a comparison is made with other investigators' data.

ACKNOWLEDGMENTS

The author would like to express his appreciation to the Chicago Bridge and Iron Company for their support of this work, and especially to Mr. James Stevens who introduced the author to the problems of wave forces.

Throughout the work, Professor Jerome Milgram has offered enthusiastic and enlightening supervision.

Mr. Robert Peterson assisted in the collection of data, and a program donated by Mr. Richard Sidell allowed the digitized data to be used on the System 360 computer.

The author would like to thank Mr. Dean Lewis and his staff of the Marine Hydrodynamics Laboratory for their help, as well as that of Mr. Edward Kern.

Mrs. Viola Liddell is responsible for the typing, and is to be thanked for a superb job under rather hurried circumstances. Computations for this thesis were conducted on the IBM 360 M65 computer of the MIT Information processing Center.

MASSACHUSETTS INSTITUTE OF TECHNOLOGY
CAMBRIDGE, MASS. 02139

SEA GRANT PROJECT OFFICE

ADMINISTRATIVE STATEMENT

The study resulting in this report, "Wave Forces on a Submerged Object" was carried out as a research project for Chicago Bridge and Iron Company and concurrently fulfilled the author's Doctoral Thesis requirements.

The information in this report is of particularly timely interest in view of the many and varied proposals for offshore petroleum storage systems inspired by the original and successful Chicago Bridge and Iron Company installation in the Middle East. This research on the nature of wave motions is an important contribution to understanding the resultant effects on such underwater structures. This understanding is important in providing some of the engineering considerations that can be applied, thereby enhancing the system design and reducing pollution potential.

The printing and distribution of this special edition of the report was organized by the M.I.T. Sea Grant Project Office under the project established to expedite dissemination of important studies and/or research findings developed at M.I.T. under other than Sea Grant support.

This valuable information dissemination is made possible with funds from a grant by the Henry L. and Grace Doherty Charitable Foundation, Inc. to the M.I.T. Sea Grant Program and in part by the research support from Chicago Bridge and Iron Company.

Alfred A. H. Keil
Director

November 1, 1971

TABLE OF CONTENTS

Appendices

* Appendices F, G and H have been omitted from this report due to their size. Anyone wishing to refer to them may refer to the original thesis or contact the author c/o Department of Ocean Engineering, M.I.T., Cambridge, Massachusetts 02139.

NOMENCLATURE

(x,y), $\vec{r}$, (ξ,η), $\vec{\rho}$	Cartesian coordinates from center of cylinder
(X_L,Y_L), (X_R,Y_R)	Inner coordinates
(r,θ)	Cylindrical coordinates
(X_L,Y_L), (X_R,Y_R)	Intermediate variables
Z_L, Z_R	Complex Inner Coordinates
A	Source strength of gap flow
B	Bernoulli constant for inside flow
B_{11}	Damping coefficient
C_D	Drag coefficient in Morison equation
C_M	Mass coefficient in rison equation
C_{W1}, C_{W2}, ...	Calibration coeffic ts for wave probes
C_1, C_2, ...	Capacitance
C_L, C_R	Bernoulli's constan for inner flow
D	Water depth
$F(x,y)$	Function used in th erivation of the second order outsid low
F_H	Horizontal force
F_V	Vertical force
$G(x,y\|\xi,\eta)$	Green's function
$H(x,y)$, H_L, H_R	Function in second ler outside flow
I	Impedance

$J(x,y)$	Function in second order inside flow
K	Wave number
M	Moment
$P(x,y,t)$	Pressure
$Q(\varepsilon)$	Source strength of gap flow in radiation problem
R	Cylinder radius
R_i	Resistance of i^{th} resistor
S_i	Signal of i^{th} channel
T	Wave period
T_V	Natural period of cylinder in vertical direction
T_H	Natural period of cylinder in horizontal direction
U_m	Maximum horizontal particle velocity
U	Horizontal velocity
V	Volume enclosed by cylinder
V_n	n^{th} harmonic of vertical force
V_H	Voltage of horizontal force channel
V_V	Voltage of vertical force channel
(X_s,Y_s)	Inner coordinates defining cylinder surface
a	Wave amplitude
d	Gap width
g	Gravitational acceleration
k_i	Calibration coefficient for i^{th} load cell
$\vec{u}$	Velocity
r	$\sqrt{(x-\xi)^2 + (y-\eta)^2}$
r_L	$\sqrt{(x+1)^2 + y^2}$
r_R	$\sqrt{(x-1)^2 + y^2}$

(x_s, y_s)	Coordinates defining cylinder surface
$\alpha(\varepsilon)$	Gage functions
δ	Ka
ε	Ratio of gap width to cylinder radius
η, η_1, η_2	Wave elevations
Γ	Circulation
λ	Wave length
ω	Circular frequency
ν	ω^2/g
ρ	Density
τ	Transmission coefficients
$\Phi(x,y,t)$	Velocity potential
$\bar{\phi}$	Velocity potential outside cylinder
$\tilde{\phi}$	Velocity potential inside cylinder
$\hat{\phi}$	Velocity potential near gaps
ϕ_s	Scattered velocity potential
ϕ_{xo}	First order scattered potential

LIST OF FIGURES

[Figures marked with (G) are graphs]

List of Figures (continued)

PLATES

LIST OF TABLES

BIBLIOGRAPHY

Ashley, Holt (1966) "Machine Computation of Aerodynamic Loads in Linear and Non-Linear Situations", MIT Fluid Dynamics Res. Lab. Rpt. No. 66-5.

Black, J. L. and Mei, C. C. (1970) "Scattering and Radiation of Water Waves", MIT Water Resources and Hydro. Lab. Report No. 121. Also Journal of Fluid Mechanics, 46, 151-164.

Blackman, R. B. and Tuckey, J. W. (1958) "The Measurement of Power Spectra", Dover Publications, New York.

Borgman, L. E. (1967) "Ocean Wave Simulation for Engineering Design", Hydraulic Engrg. Lab. Report HEL 9-13, University of Calif., Berkeley.

Chamberlin, R. S. (1969) "Design Considerations - Offshore Storage", Oceanography Conference, Brighton, England.

Cole , J. D. (1968) "Perturbation Methods in Applied Mathematics" , Ginn Blaisdell, Waltham, Massachusetts

[illegible] Field Theory of Guided Waves, New York, McGraw Hill

Davenport, W. B. Jr. and Root, W. L. (1958), An Introduction to the Theory of Random Signals and Noise, New York, McGraw Hill.

Den Hartog, J. P. (1956), Mechanical Vibrations, New York, McGraw Hill.

Garrison, C. J., Rao, R. S. and Snider, R. H. (1970, "Wave Interaction with Large Submerged Objects", ASCE Nat'l. Structural Engineering Mtg., Portland, Oregon.

Garrison, C. J. (1971), personal communication.

Grace, R. A. and Casciano, F. M. (1969), "Ocean Wave Forces on a Submerged Sphere", Jour. Waterways and Harbors Div. A.S.C.E., WW3, August

Guiney, D. C. (1971), "Transmission of Water Waves through a Gap in a Thin Barrier", unpublished paper, Dept. of Applied Math., Univ. of Adelaide, Australia.

Haskind, M. D. (1957), "The Exciting Forces and Wetting of Ships in Waves (in Russian), Izvestia Akademii Nauk, U.S.S.R., Otdelenie Tekhnicheskikh Nauk, #7, pp. 65-79 (English translation available as David Taylor Model Basin Translation No. 307, March, 1967).

Havelock, Sir Thomas (1955), "Wave Forces due to a Floating Sphere Making Periodic Heaving Oscillations", Proc. Royal Soc., London, v.231

Herbich, J. B. and Shank, G. E. (1970), "Forces Due to Waves on Submerged Structures", Texas A. & M. Sea Grant Report TAMU-SG-70-212

Itokawa, H. (1969), "Undersea Oil Storage System", Technical Research Society for Undersea Oil Storage, Tokyo, Japan.

John, F. (1950), "On the Motion of Floating Bodies", I, II Comm. Pure Appl. Math., 2, pp. 13-57.

Kaplun, S. (1954), "The Role of Coordinate Systems in Boundary Layer Theory", Z. Angew. Math. Phys. 5, 111-135.

Kern, Edward C., Jr. (1971), "Exciting Forces on Oil Pollution Control Barriers in Waves and Currents", MIT M.S. Thesis, Dept. of Ocean Engineering.

Kreisel, G. (1949), "Surface Waves", Quart. Appl. Math., Vol. VII, p. 21.

Lagerstrom, P. A. and Cole, J. D. (1955), "Examples Illustrating Expansion Procedures for the Navin Stokes Equations", J. Rat. Mech. Anal. 4, 817-882.

Lewin, Myra (1963), "The Effect of Vertical Barriers on Progressing Waves", J. Math. Phys., 42, p. 287.

McCamy, R. C. and Fuchs, R. A. (1954), "Wave Forces on Piles: a Diffraction Theory", U.S. Army Corps of Engrs., Beach Erosion Board, Tech. Memo. No. 69.

Mei, C. C. (1969), "Weak Reflection of Water Waves by Bottom Obstacles", Proc. A.S.C.E., Engrg. Mech. Div., 95, EM1.

Milgram, J. N. and Halkyard, J. E. (1971), "Wave Forces on Submerged Objects in the Sea", Jour. Ship Research, 15, No. 2.

Morison, J. R., O'Brien, M. P., Johnson, J. W., and Schaaf, S. A. (1950), "The Force Exerted by Surface Waves on Piles", Petroleum Trans., Amer. Inst. Mining Engrs., Vol. 189, pp. 149-154.

Morse, P. M., and Feshbach, H. (1953), "Methods of Theoretical Physics", New York, McGraw-Hill.

Motora, S. and Koyama, T. (1966), "Wave Excitationless Ship Forms", Proc. Sixth Symp. on Naval Hydrodynamics, 383-413.

Newman, J. N. (1962), "The Exciting Forces on Fixed Bodies in Waves", J. Ship Research, Dec.

Newman, J. N. (1965) "Propagation of Water Waves Past Long Low Two-dimensional Objects" J. Fluid Mechs., 23

Newman, J. N. (1969) "Lateral Motion of a Slender Body Between two Parallel Walls" J. Fluid Mechs., 39

Newman, J. N. (1970) "Marine Hydrodynamics", lecture notes for a course at M. I. T., Dept. of Ocean Engineering.

Newman, J. N. (1971) "Diffraction of Water Waves" to be published in Applied Mechanics Reviews

O'Brien, M. P. and Morison, J. R. (1952), "The Force Exerted by Waves on Objects", Trans. Amer. Geophys. Union, V. 33, No. 1

Prandtl, L. (1905), Über Flüssigkeiten bei sihr kleiner Reibung. Verh. III, Internat. Math. Kongr., Heidelberg, (English trans.: "Motion of Fluids with Very Little Viscosity", Tech. Memo. N.A.C.A., No. 452, 1928).

Prandtl, L. and Tiejtens, O. J. (1934), Applied Hydro. and Aero. Mech., New York, McGraw-Hill.

Rayleigh, Lord (1877), "On Progressive Waves", Proc., London Math. Soc., V. 9.

Thorne, R. C. (1953), "Multipole Expansions in the Theory of Surface Waves", Proc. Camb. Phil. Soc., 49.

Tuck, E. O. (1970), "Transmission of Water Waves Through Small Apertures", J. Fluid Mech., 49.

Ursell, F. (1950), "Surface Waves on Deep Water in the Presence of a Submerged Circular Cylinder", I and II, Proc. Camb. Phil. Soc., 46.

Van Dyke, M. (1964), Perturbation Methods in Fluid Mechanics, Acad. Press, N. Y.

Widnall, S. and Barrows, T. (1970), "Wings in Ground Effect", J. Fluid Mech., 41, 4.

Wiegel, R. L. (1964), Oceanographical Engineering, New York, Prentice-Hall.

Wiegel, R. L., Beebe, K. E., and Moon, J. (1957), "Ocean Wave Forces on Circular Cylindrical Piles", J. Hyd. Div., A.S.C.E., 83, HY2, paper 1199.

I. INTRODUCTION

Recent discovery and subsequent production of oil fields
far offshore has spurred considerable interest in the concept
site storage and loading of crude oil as an alternative
lizing long pipelines. The economic savings in both
l expenditures and operating costs introduced by
ing structures for the submerged storage of oil have
iscussed by Chamberlin (1969)*. The Chicago Bridge and
installed the first submerged oil storage tank
n Gulf in August, 1969. This tank consists of
steel structure approximately 250 feet in
75 feet high. A 30-foot diameter riser pene-
ee surface. The tank has a capacity of 500,000
ude oil (about 75,000 tons), and sits in 156
. The tank operates on a water displacement
t is free flooding through ducts and openings
e ringwall so that as oil is pumped down the
ie tank water passes out the bottom.

.1 shows schematically the operation of the

submerged oil storage design has been tested at
e stage (see Itokawa, 1969). This model was con-
a hemispherical cap of flexible material and

ire listed in alphabetical order by the first
l, and by the year of publication for different
e same author, in the Bibliography.

of c
to u
cap
uti
bee
Iron Compa
in the Per
a dome-sha
diameter a
trates the
barrels of
feet of wa
principle.
about its
riser into

Figur
tank.

Anoth
the protot
structed w

*Reference
author ci
works by

a steel ellipsoidal base and was capable of holding up to 10,000 gallons.

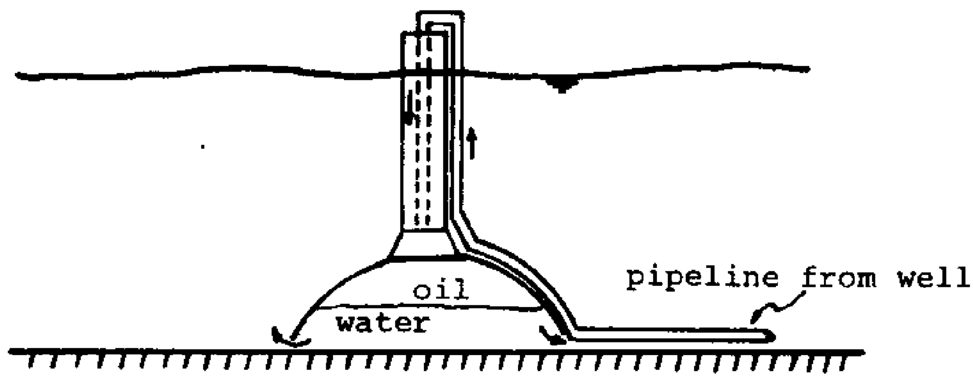

Figure I.1

SCHEMATIC DRAWING OF SUBMERGED OIL STORAGE TANK (CB&I)

In addition to their obvious use in oil st
underwater structures have been studied as poss
of the future.*

Naturally, one of the greatest engineering
the design of these structures is the predictio
design loadings under the influence of surface
problems related to the prediction of these for

*See, e.g., Commission on Marine Science, Engin
Resources, "Our Nation and the Sea," Jan. 1969
and Environment," Vols. 1-3, Feb. 1969, both a
the Superintendent of Documents. Also of inte
report "The Ocean Engineering Program of the U
Sept. 1967, Office of the Oceanographer of the

age, large
le cities

allenges in
of maximum
ves. The
s are

ring and
and "Science
ilable from
st is the
. Navy,"
avy.

complicated by the fact that the structures are large compared with the wave lengths encountered so that significant scattering of the waves takes place. Traditional civil engineering methods for calculating forces on piles and other small objects in the coastal zone are no longer sufficient.

This realization has slowly crept into the engineering community as witnessed by the proliferation of studies into the forces on submerged objects in recent years.

I.1 The Problem of Exciting Forces

In many ways, the problems associated with wave interaction with large submerged objects are the same as those which have been under study for years by naval architects in connection with the exciting forces on ships and other floating objects.

Haskind (1957) derived in exact (within linear theory) relationship between the exciting (wave) forces on an object and its damping coefficient in harmonic motion thus leading to a simplification in most cases of the work involved in calculating the forces. Earlier work by Havelock (1955), Ursell (1950) and others provided theories for the damping coefficients and added mass of simple geometries, both floating and submerged, which could subsequently be utilized to compute wave forces via Haskind's relations.

Newman (1960) utilized Haskind's relations to find the exciting forces on a submerged ellipsoid (in three dimensions) and an ellipse (in two dimensions).

I.2 Survey of the Methods

The methods used in the calculation of wave forces (or the added mass and damping in the case of radiation) vary in their numerical complexity and in the information which they yield. Usually the complexity increases as more information is desired.

I.2.1 Matching Polynomial Coefficients

Ursell's method (Ursell, 1950) has been the most popular approach until recently. This method involves the following procedure: describe the flow by a polynomial expansion, including a source term, about the origin plus a radiated wave of unknown amplitude. Divide the object into a finite number of grids, N, and write the boundary condition on each of the grids in terms of the polynomial expansion. The equations may then be solved algebraically for the unknown polynomial coefficients if the solution is approximated by a polynomial of degree N-1. This method leads to a near field solution for the flow to any degree of approximation desired, depending only on the number of grid points taken.

I.2.2 Integral Equation Method

the solution of [illegible] John (1950) has discussed in deta[illegible]

al equation. The [illegible] water wave problems via a Fredholm int[illegible] numerical solution of the integral equation has been widely used in the prediction of loads on airfoils (see, e.g., Ashely, 1966), but the complexity of the Green's function with the inclusion of free surface effects has discouraged its use in water wave problems. Recent advances in computer design and performance have largely reduced the difficulties, however, and this approach offers many practical advantages for engineering purposes. The solution to the integral equation provides an exact (within the limits of linear theory and numerical computations) value for the pressures acting on the surface of the object. A computer program may be written to account for a wide variety of general shapes, and may even be incorporated in a general design program to calculate tradeoffs for various shapes, depths, etc.

Kim (1962) used the integral equation method to find the damping and added mass coefficients of rolling or heaving disk in the free surface. The forces on submerged three-dimensional objects have been calculated by Milgram and Halkyard (1971) and Garrison, et al (1970). Garrison in addition performed some experiments on a submerged dome. Mei (1969) calculated t weak reflection of waves by a bottom obstacle using an a oximate solution to the Fredholm integral equation.

I.2.3 The Variation Method

A scheme with nsiderably more finesse than either of the previously stat methods is the variational method.

This method has been utilized extensively in electromagnetic theory (see, e.g., Collin, 1960, Chapter 8), and has been applied to scattering and radiation of surface waves by Miles (1967), Black et al (1971), and Miles and Gilbert (1969) among others. The variational approach allows the computation of radiated waves (and thus the exciting forces via Haskind's relations) with greatly reduced numerical effort. This method does not, however, yield the near field flow conditions. For engineering purposes, the net forces computed by such a scheme may be helpful in foundation design, but the distribution of pressures is essential information for structural considerations. Either of the previous methods would be preferable from this point of view.

A complete discussion of scattering, or diffraction, of ocean waves is beyond the scope of this thesis. A general and thorough discussion of wave interactions may be found in Wehausan and Laitone (1960), and an up-to-date review of the literature is given by Newman (1971).

I.2.4 Other Approaches

Running a parallel, though seemingly unassociated, course with the investigations mentioned above, which were mainly associated with naval architectural problems, was the "coastal engineering" approach. This approach was initially developed for the determinations of wave loads on vertical piles such as those used as dock supports and as structural members in the "Texas Tower" type oil rigs. An extensive dependence on empirical observation, plus the combined conclusions of hydrodynamicists back to the studies of pendulums in a viscous fluid by G. G. Stokes in 1851, led Morison and his co-investigators (Morison, et al, 1950) to the conclusion that the total force on an ocean structure could be divided into two components: a drag force and an inertial force. This conclusion gives rise to the well known "Morison equation" which has been almost universally adopted by the coastal engineering community:

$$F = F_D + F_M = \frac{1}{2} C_D \rho A_p u|u| + C_M \rho F \frac{\partial u}{\partial t} \qquad \text{I.1}$$

where

F = total force on an object in the direction of u

F_D = drag force

F_M = inertial force

C_D = drag coefficient

ρ = mass density of fluid (sea water = 2.0)

A_p = area of object projected on plane perpendicular to the direction of flow

u = velocity of fluid

C_M = inertial coefficient

V = submerged volume of the object

A great deal of study has been done on the forces on submerged objects under the assumption that the Morison equation correctly accounted for the forces. O'Brien and Morison (1952), and more recently Grace and Casciano (1969) have correlated C_M and C_D to experimental observations of forces on small submerged spheres. Extensive measurements and further correlation of C_M and C_D for vertical piling was carried out by Wiegal, Beebe and Moon (1957). Their tests, conducted in an open ocean environment, showed considerable scatter of data (see Figures I.2 and I.3) which was subsequently explained and corrected by Borgman (1967) through a spectral analysis of the wave records.

Considerably better correlation of C_M and C_D with experiment was obtained by Keulegan and Carpenter (1958) under laboratory conditions, and with the allowance that C_M and C_D may vary over a wave cycle. A detailed discussion of their approach is included in Chapter VI of this thesis.

Other tests have been undertaken. Wiegel (1964) offers an extensive survey of these tests and some of the theoretical advances.

Since the Morison formula was originally introduced as a device to predict wave forces on small diameter piles, its acceptability for objects which exhibited scattering was not well understood until subsequent developments, some of which were mentioned above. In particular, MacCamy and Fuchs (1954) calculated the effect of diffraction of piles and concluded that diffraction not only affected the <u>magnitude</u> of

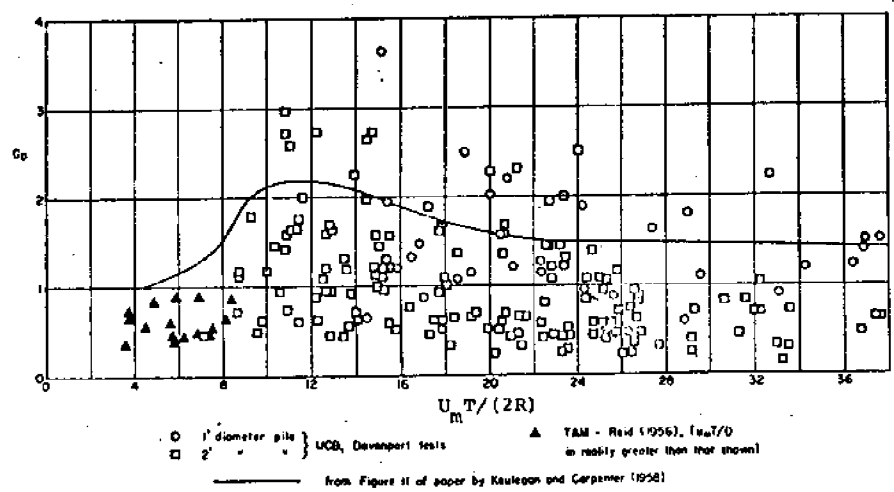

Figure I.2

C_D PLOTTED AGAINST $U_mT/(2R)$ FROM TEST DATA (from Wiegel, 1964). VERTICAL CYLINDER RADIUS = R.

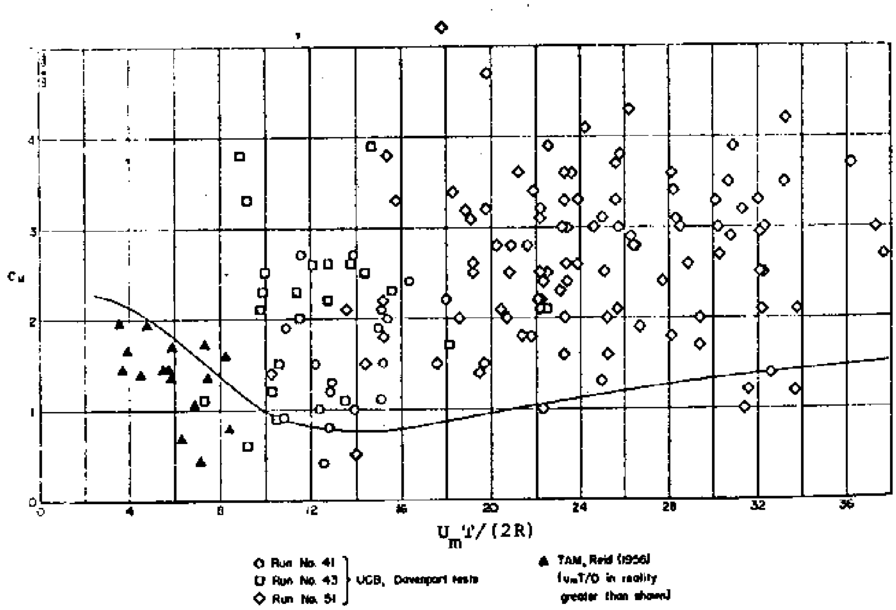

Figure I. 3

C_M PLOTTED AGAINST $U_mT/(2R)$ FROM TEST DATA (from Wiegel, 1964). VERTICAL CYLINDER RADIUS = R.

C_M, but that the phase of the inertial force must also be altered if diffraction is to be taken into account. This result led to later generalizations of the Morison equation, such as that used by Motora and Koyama (1966):

$$F = k_1 \frac{\partial u}{\partial t} + k_2 u|u| + k_3 u \qquad \text{I.2}$$

where k_1, k_2 and k_3 are coefficients to be determined either experimentally or theoretically.

This equation certainly has more appeal for large ocean structures. A simplification of the equation is made for the case of large structures by observing that, for all but the largest waves, the drag forces are of a second order to the inertial forces.

In this thesis Morison's equation is introduced in a modified form allowing C_M to take on complex values to account for the phase shift. The magnitude of C_M then provides a non-dimensional horizontal force measurement as well as a coefficient for engineering comparison.

I.3 Recent Work on Large Submerged Objects

The advent of large submerged objects in the sea has brought the theoretical approaches of the naval architects into the field of coastal or "ocean" engineering. Recent diffraction studies, primarily those of Milgram and Halkyard (1971) and Rao and Garrison (1970) have been motivated by the Chicago Bridge and Iron Company's oil storage tank, as have been the experimental studies of Herbich and Shank (1970). This author's work has been largely sponsored by that company, while, needless to say, many proprietary studies have been conducted by various concerns.

There is yet to appear a comprehensive theory to take into account all the factors influencing the force on these types of structures. Even if we restrict ourselves to linear theory (where everything is proportional to the wave height) the following questions have not been satisfactorily answered:

1. What effect does structural deflection have on the total loads?
2. How much energy is transmi[illegible] to the oil/water interface inside the tank?
3. What effect does the flow o[illegible]ater under the tank have on the net loads?
4. How can these effects be ut[illegible]zed in the improvement of the design?

The most conspicuous failure o[illegible]heories to date has been the failure to account for flo[illegible]nderneath the structure, an effect which surely takes [illegible]ce in the full scale tank and, except under the most car[illegible]lly devised experiment, in the model tests as well. In thi[illegible]egard, it is interesting to note that Rao and Garrison ([illegible]0), in conducting force measurements on submerged hemispher[illegible]l shapes, actually had to correct for the bottom effects b[illegible]easuring the pressures inside the model and subtracting the uplift resulting from this pressure from the total measured loads. This corrected force compared reasonably well with their diffraction theory, which accounted for only the pressures on the outside of the hemisphere.

The present work is aimed at gaining an understanding of the effect of flow about the bottom of a submerged object. A cylinder is selected, rather than the more realistic hemisphere, since the theory in this case is simpler and a more meaningful experiment could be carried out in the facilities available. In principle, the methods used here could be used to compute the effects on a three-dimensional object, provided more computation time could be afforded and a large wave tank were available to compare results.

I.4 Scope of the Thesis and the Approach

The present problem was selected because it offers the opportunity to develop a "complete" diffraction theory for a physically realizable situation which can be tested in the laboratory. The geometry selected is that of a semi-circular cylinder mounted close to the horizontal bottom.

The flow through the slits at the bottom of each side of the cylinder is accounted for by assuming a source of unknown strength at one gap and a sink of equal strength at the other. Locally, the flow through the gaps is treated as the flow through an orifice in an infinite wall, and the source strength is adjusted so that these two approximations agree within a certain "intermediate" region.

This approach is a simple and straightforward application of the method of matched asymptotic expansions as used by Tuck (1971). Strictly speaking, it is only valid for small gap widths, as determined by the ratio of gap width to cylinder radius ($=\varepsilon$), although recent exact solutions by Guiney (1971) have shown Tuck's solution to be valid for rather large values of his small parameter (equivalent to $\varepsilon \approx .4$).

The theoretical problem is solved in Chapters II, III and IV. Chapter V discusses the forces resulting from the computed flow, and compares the results with measured forces by other investigators. Chapter VI discusses the experimental setup and the analytical procedures used to reduce the data, as well as the results of the experiments. Chapter VII presents a summary of the results and conclusions drawn therefrom, including comments concerning the three-dimensional problem and the oil/water interface problem. The Appendices contain an extended discussion of the matching process of Tuck, as well as the solution for the case of an oscillating structure which is used as a check on the computer program. Finally, a listing of the computer programs and a complete compilation of the test results are included.

II. STATEMENT OF THE PROBLEM

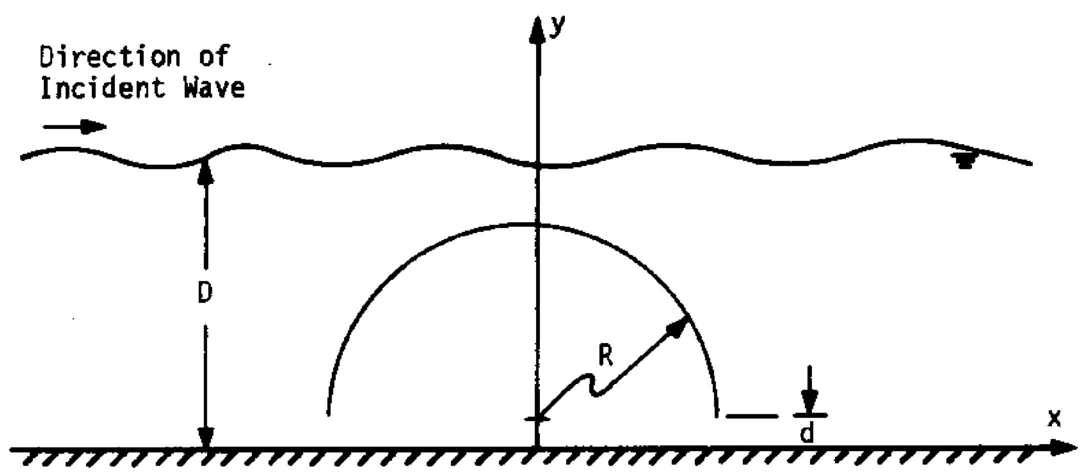

Figure II.1

Consider an infinitely long semi-circular cylinder situated as shown in Figure II.1. The cylinder is fixed and rigidly held so that its edges are a distance d off the sea bottom. "Small" gravity waves pass the cylinder with crests parallel to its axis, and the cylinder in turn reflects some of the wave energy and experiences a force.

Define the velocity potential function, $\Phi(x,y,t)$, such that

$$\vec{u}(x,y,t) = \nabla\vec{\Phi}(x,y,t) \qquad \text{II.1}$$

where $\vec{u}(x,y,t)$ is the velocity vector of the fluid at the point (x,y).

Throughout this discussion we will assume the motion to be simple harmonic so that the time dependence may be separated:

$$\Phi(x,y,t) = \mathrm{Re}[\phi(x,y)e^{-i\omega t}] \qquad \text{II.2}$$

All dependent variables will henceforth be written as spacial functions only, with the time dependence implied by II.2 assumed.

Non-dimensionalize independent variables as follows:

$$(x,y) = R(\hat{x},\hat{y}) \qquad \text{II.3.1}$$

$$t = \hat{t}/\omega, \qquad \text{II.3.2}$$

where the variables on the right are dimensionless.

The dependent variables are non-dimensionalized as follows:

wave elevation	$\eta(x)$	$= a\hat{\eta}(x)$	II.4.1
velocity	$u(x,y)$	$= \frac{gaK}{\omega}\hat{u}(x,y)$	II.4.2
velocity potential	$\phi(x,y)$	$= \frac{ga}{\omega}\hat{\phi}(x,y)$	II.4.3
pressure	$p(x,y)$	$= \rho g a\hat{p}(x,y)$	II.4.4
force	$F(x,y)$	$= \frac{\pi\rho g a R}{2}\hat{F}(x,y)$	II.4.5

where $K \tanh KD = \omega^2/g$

a = wave amplitude

Henceforth all variables will be assumed dimensionless unless stated otherwise, and the caps over the variables will be omitted. It will be convenient to define

$$\varepsilon = d/R \qquad \text{II.5.1}$$

$$\delta = Ka \qquad \text{II.5.2}$$

It will be necessary to examine the flow in the regions exterior and interior to the cylinder separately. For this purpose, define as the "outside region" that for which

$$x^2 + (y-\varepsilon)^2 > 1$$
$$0 < y < D,$$

and the "inside region" that for which

$$x^2 + (y-\varepsilon)^2 < 1$$
$$y > 0$$
$$|x| < 1$$

The flow in the outside region will be identified by the velocity potential $\bar{\phi}(x,y)$. If this is taken to be a two

ser expansion in ε and δ, we may write ... perturbation para

. (45) (cf. Newman, 197

$\delta\phi_1(x,y,\varepsilon) + \delta^2\phi_2(x,y,\varepsilon) + \ldots$ $\bar{\phi}(x,y) =$

$y,\varepsilon) = \phi_{10}(x,y) + \alpha_1(\varepsilon)\phi_{11}(x,y)$ where $\phi_1($

$+ \alpha_2(\varepsilon)\phi_{12}(x,y) + \ldots$ II.6

e gage functions as yet undetermined. The $\alpha_1(\varepsilon)$'s

II.6 to obtain We may expan

$\delta\phi_{10}(x,y) + \delta\alpha_1\phi_{11}(x,y) + \ldots$ $\bar{\phi}(x,y)$

$+ \delta^2\phi_{20}(x,y) + \ldots$

ng we will neglect terms of $O(\delta^2)$ and In the follo

$O(\delta\alpha_1)$. This theory is thus valid only calculate terms o if those terms included are much greater than those neglected, i.e., if

$$\delta\alpha_1 >> \delta^2$$

In the following discussion we have incorporated the δ implicitly in our non-dimensionalization. Also, it will be convenient to write $\overline{\phi}$ as the "incident" plus the "scattered" wave

$$\overline{\phi}(x,y) = \phi_o(x,y) + \phi_s(x,y, \;)$$

where

$$\phi_o(x,y) = ie^{iKx}\,\frac{\cosh Ky}{\cosh KD} \qquad \text{II.7}$$

We will find that this representation is non-uniformly valid. Near the gaps it will be necessary to find another solution. We will solve for the flow in each of these regions and match them in an overlap domain in order to find the complete solution inside and outside of the cylinder.

II.1 Outside Region

Denote the velocity potential for flow in the outside region by $\overline{\phi}(x,y)$. This function satisfies the following boundary value problem:

$$\nabla^2\overline{\phi} = 0 \qquad \text{II.8}$$

$$\overline{\phi}_y(x,D) - \frac{\omega^2 R}{g}\,\overline{\phi}(x,D) = 0 \qquad \text{II.9}$$

$$\overline{\phi}_y(x,0) = 0 \qquad \text{II.10}$$

$$\overline{\phi}(x_s,y_s)\cdot\hat{n}(x_s,y_s) = 0 \qquad y_s > \varepsilon \qquad \text{II.11}$$

where $x_s^2 + (y_s-\varepsilon)^2 = 1$

$$\hat{n} = x_s\hat{i} + y_s-\varepsilon)\hat{i}$$

Define (x_s^0, y_s^0) such that

$$(x_s^0)^2 + (y_s^0)^2 = 1$$

defines cylinder when $\varepsilon = 0$. Then note that

$$x_s^0 = x_s$$
$$y_s^0 = y_s-\varepsilon, \qquad \text{and that}$$

$$\nabla\overline{\phi}(x_s,y_s)\cdot\hat{n}(x_s,y_s) =$$

$$\nabla\overline{\phi}(x_s^0,y_s^0)\cdot\hat{n}(x_s^0,y_s^0) + \varepsilon\,\frac{\partial}{\partial y}\,[\nabla\overline{\phi}(x_s^0,y_s^0)\cdot\hat{n}(x_s^0,y_s^0)]$$
$$+ \ldots$$

Using only the first term, write the linear boundary condition on the surface of the cylinder as

$$\nabla\overline{\phi}(x_s,y_s)\cdot\hat{n}(x_s,y_s) = 0 \qquad \text{II.11.1}$$
$$y > 0$$
$$\text{where } x_s^2 + y_s^2 = 1$$

Introducing the mathematical order notation (cf. Van Dyke), notice that equation II.12 is valid to $o(\varepsilon)$. To complete the boundary value problem add the condition that the surface waves far from the object must consist of the incident wave plus outgoing waves (radiation condition). If we separate the function $\overline{\phi}(x,y)$ into the incident wave (undisturbed flow) plus a scattered wave as

$$\overline{\Phi} = \phi_o + \phi_s \qquad \text{II.12}$$

condition II.11.1 becomes

$$\vec{\nabla}\phi_s(x_s,y_s)\cdot\hat{n}(x_s,y_s) = -\vec{\nabla}\phi_o(x_s,y_s)\cdot\hat{n}(x_s,y_s) \qquad \text{II.13}$$

$$y_s > 0$$

Since the boundary condition (II.13) does not specify the normal velocity at the position $(\pm 1,0)$, the problem has not been completely posed.

The use of a matched asymptotic expansion allows us to replace this boundary condition with a flow singularity, and to solve the outer solution to $O(\alpha_1)$.

The indeterminency of the boundary conditions at $(\pm 1,0)$ suggests the division of $\overline{\Phi}(x,y)$ into two parts, one satisfying homogeneous boundary conditions and one behaving singularly at $(\pm 1,0)$. In particular, assume

$$\phi_s(x,y) = \phi_{so}(x,y) + A[\ln(r_L/r_R) + H(x,y)] \qquad \text{II.14}$$

where $r_L = \sqrt{(x+1)^2 + y^2}$, $r_R = \sqrt{(x-1)^2 + y^2}$,

which represents a regular scattered wave potential plus a source at one gap and a sink of equal strength at the other gap. The function $H(x,y)$ is necessary to satisfy II.11.1, and is regular throughout the outside region. The source strength, A, is naturally a function of the incident wave parameters and ε, and must approach zero as ε decreases;

$$\lim_{\varepsilon \to 0} A = 0 \quad . \qquad \text{II.15}$$

The selection of a source/sink combination (II.14) to describe the perturbation caused by the gaps satisfies the physical condition that fluid must leave the outside region at one gap and enter it from the other. The selection of higher singularities may be ruled out, at least to $O(\varepsilon)$, on the basis of the "Principle of Minimum Singularity" (Van Dyke, 1964) or, more formally, through the matching of the expansion for $\phi_s(x,y)$ with another expansion describing the flow through the gaps.

This matching procedure is necessitated by the fact that II.14 cannot accurately represent the flow "close" to the gaps since the source term becomes arbitrarily large as r_L or r_R become small.

II.2 The Inside Region

The flow inside the cylinder must satisfy the following conditions:

$$\nabla^2 \tilde{\phi} = 0 \qquad \text{II.16.1}$$

$$\frac{\partial \tilde{\phi}}{\partial y} (x,0) = 0 \qquad \text{II.16.2}$$

$$\overline{\nabla} \tilde{\phi} (x_s, y_s) \cdot \hat{n} (x_s, y_s) = 0 \qquad \text{II.16.3}$$

$$x_s^2 + y_s^2 = 1$$

$$y_s > 0$$

where II.16.3 is the linearized boundary condition analagous to II.11.

II.16 leads to a trivial result for the case of no gap. We expect from the nature of the outside solution (II.14) that $\tilde{\phi}(x,y)$ takes the form

$$\tilde{\phi}(x,y) = B + A[\ln r_R/r_L + J(x,y)] \qquad \text{II.17}$$

where B = a constant dependent on ε and the outside flow.

$J(x,y)$ is a regular function necessary to satisfy II.16. Equation II.17 also satisfies the condition of continuity of flow through the gaps if A is taken to be the same as that in II.14. In order to find A and B the flow through the gaps must be examined in detail.

II.3 Flow Adjacent to Gaps

In order to examine the flow through the gaps it becomes necessary to alter the coordinate system heretofore used in such a manner as to magnify the area under consideration, namely, the regions adjacent to the gaps. This may be accomplished by defining new independent variables.

$$Y_R = Y_L = y/\varepsilon \qquad \text{II.18.1}$$

$$X_R = (x-1)/\varepsilon \qquad \text{II.18.2}$$

$$X_L = (x+1)/\varepsilon \qquad \text{II.18.3}$$

It should be noted that the selection of this particular stretching of coordinates cannot be known *a priori* to be correct. In particular, the condition required for proper stretching is that a point corresponding to fixed values of (X_L,Y_L) or (X_R,Y_R) will remain in the "inner" flow region in the limit as $\varepsilon \to 0$ (Lagerstrom and Cole, 1955).

Figure II.2

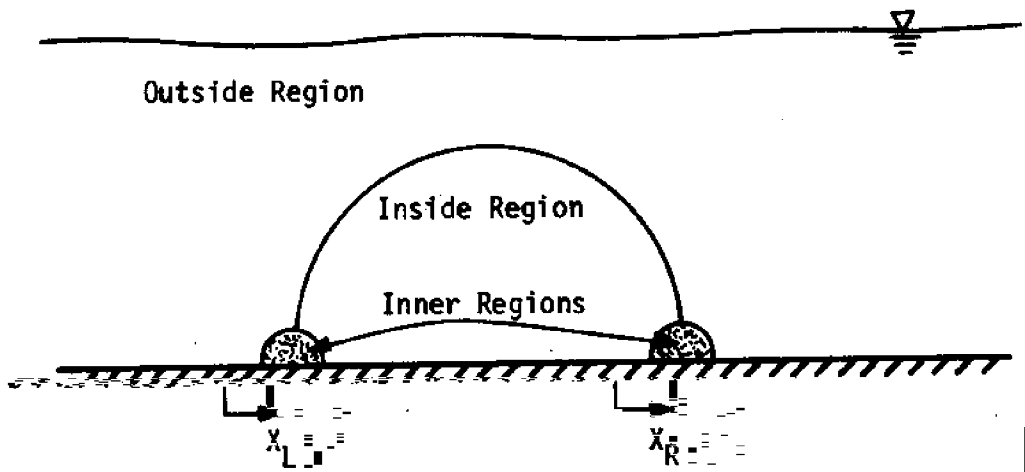

For example, referring to Figure II.2 we can define the "inner" region as that region where the solutions indicated by II.14 and II.17 become invalid. This is the case (using the left gap as the example) when A $\ell n\ r_L = 0(1)$, or when

$$r_L = 0(e^{1/A}) \qquad \text{II.19}$$

Thus, if we consider a point described by

$$R_L = r_L e^{-1/A},$$

and hold R_L fixed while taking $\varepsilon \to 0$, r_L will always be within a semi-circle wherein the outside solutions are not valid. It will be shown later that $A = 0(1/\ell n\varepsilon)$, so that

$$R_L = r_L/\varepsilon$$

is indeed the proper stretching. It can be argued on purely physical grounds, however, that the point $(-1,\varepsilon)$ must always be included in the inner region so that any stretching other than II.18 would be inadmissible. For example, if we had said

$$Y_L = y_L \varepsilon^{-1/2}$$

$$\text{or } Y_L = y_L e^{1/\varepsilon}$$

the point $y_L = \varepsilon$ does not correspond to a fixed Y_L for $\varepsilon \to 0$.

Given the change in coordinates II.18, we can formulate the problem for the inner flow velocity potential:

$$\nabla^2 \hat{\phi}(X,Y) = 0 \qquad \text{II.20.1}$$

$$\frac{\partial \hat{\phi}}{\partial Y}(X,0) = 0 \qquad \text{II.20.2}$$

$$\overline{\nabla}\hat{\phi}(X_s,Y_s)\cdot\hat{n}(X_s,Y_s) = 0 \qquad \text{II.20.3}$$

Again we may linearize the boundary condition on the cylinder wall. Equation II.20.3 may be written

$$\nabla\hat{\phi}(X_s,Y_s)\cdot\overline{\nabla}f(X_s,Y_s) = 0 \qquad \text{II.21}$$

where $$f(X_s,Y_s) = (\varepsilon X_s - 1)^2 + (\varepsilon Y_s - \varepsilon)^2 - 1. \qquad \text{II.22}$$

This function applies to the left gap, an analagous function applies to the right gap. Expanding II.21,

$$\frac{\partial \hat{\phi}}{\partial \overline{X}}(X_s,Y_s)(\varepsilon X_s - 1) + \frac{\partial \hat{\phi}}{\partial Y}(\varepsilon Y_s - \varepsilon) = 0$$

and expanding the whole expression in a Taylor series about $\bar{x}_s = 0$,

$$- \frac{\partial \hat{\phi}}{\partial X} \, 0, Y_s) + \varepsilon (Y_s - 1) \frac{\partial \hat{\phi}_s}{\partial Y} (0, Y_s)$$

$$+ X_s \left[\varepsilon \frac{\partial}{\partial X} (0, Y_s - \frac{\partial^2 \hat{\phi}}{\partial X^2} (0, Y_s) + \varepsilon (Y_s - 1) \frac{\partial^2 \hat{\phi}_s}{\partial X \partial Y} \right] + \ldots = 0$$

Noting the $f(x_s, y_s) = 0$, from II.22 we see that

$$X_s \approx \varepsilon \frac{(Y_s - 1)^2}{2} + 0(\varepsilon^2)$$

and may thus conclude that II.20.3 may be written

$$\frac{\partial \hat{\phi}}{\partial X} (0, Y_s) = 0, \qquad \text{II.20.3.1}$$

which is valid to $0(\varepsilon)$. Thus to the same order linearization as the outer problem, the inner flow may be characterized as the flow through a slit in a vertical wall (e.g., Tuck, 1969). We may now proceed to solve the "inner" problem and the "outer" problems in each region.

III. SOLUTION

Although the statement of the problem to $0(\varepsilon)$ as discussed in Chapter II is straightforward, the exact solution is difficult, if not impossible to obtain. Various approximate methods exist, however (viz., Milgram and Halkyard, 1971), of which a direct approach will be used in conjunction with a modeling scheme to account for the gaps. The accuracy of the results will thus depend on the accuracy of the numerical scheme employed.

III.1 Solution for the Outside Region

We may first consider the function $\overline{\phi}(x,y)$ which satisfies II.8-II.11, the function $\phi_s(x,y)$ defined by II.12 satisfying II.8-II.10 and II.13, and the function $\phi_{so}(x,y)$ defined by II.14. If we take the limit of II.14 as $\varepsilon \to 0$, recognizing II.15, we obtain

$$\phi_{so}(x,y) = \lim_{\varepsilon \to 0} \phi_s(x,y) \qquad \text{III.1}$$

(not uniformly valid)

Thus $\phi_{so}(x,y)$ satisfies II.8-II.10, and II.13. In particular, write II.13 in the limiting case $\varepsilon \to 0$ to obtain

$$\overline{\nabla}\phi_{so}(x_s,y_s)\cdot\hat{n}(x_s,y_s) = -\overline{\nabla}\phi_o(x_s,y_s)\cdot\hat{n}(x_s,y_s) \qquad \text{III.2}$$

$$y_s \geq 0$$

$\phi_{so}(x,y)$ is simply the scattered potential outside the cylinder for the case of no gap, and may be solved by the direct application of Green's theorem to the region external to the cylinder (cf. Morse and Feshbach, Chapter 7). This method is equivalent to the distribution of sources and dipoles over the surface of the cylinder, and can be shown to be equivalent to a solution consisting of sources only or dipoles only distributed over the surface (cf. Lamb, 1945, p. 59).

Define the Green's function $G(x,y|\xi,\eta)$ to be the potential at (x,y) of a pulsating source at (ξ,η) in the fluid bounded by the free surface and the flat bottom extending in both directions to infinity. This potential may be characterized by the following boundary value problem:

$$\nabla^2_{xy} G = -2\pi\delta(x-\xi,y-\eta) \qquad \text{III.3}$$

$$\frac{\partial G}{\partial y}(x,0|\xi,\eta) = 0 \qquad \text{III.4}$$

$$\frac{\partial G}{\partial y} - \frac{\omega^2 R}{g} G(x,D|\xi,\eta) = 0 \qquad \text{III.5}$$

In addition, $G(x,y|\xi,\eta)$ must represent an outgoing wave at distances far upstream and far downstream from the source point (ξ,η). $G(x,y|\xi,\eta)$ may be presented by its real and imaginary parts:

$$G(x,y|\xi,\eta) = g_1(x,y|\xi,\eta) + i\, g_2(x,y|\xi,\eta) \qquad \text{III.6}$$

where g_1 and g_2 are real functions (see Appendix B).

Applying Green's theorem to the region external to the cylinder (but in the fluid) yields the following integral representation for $\phi_{so}(x,y)$:

$$\phi_{so}(\overline{\rho}) = -\frac{1}{2\pi}\int_C \left[\phi_{so}(\overline{r})\frac{\partial G}{\partial n}(\overline{\rho}|\overline{r}) - G(\overline{\rho}|\overline{r})\frac{\partial \phi_{so}(\overline{r})}{\partial n}\right] d\ell_{\overline{r}} \qquad \text{III.7}$$

$$\text{where} \quad \overline{r} = (x,y)$$
$$\overline{\rho} = (\xi,\eta)$$

The integration is performed over the cylinder surface assuming a unit axial dimension. Introducing III.2, and letting $\overline{\rho}$ approach the surface of the cylinder, we obtain:

$$\phi_{so}(\overline{\rho}) = -\frac{1}{\pi}\int_C \phi_{so}(\overline{r})\frac{\partial G}{\partial n}(\overline{\rho}|\overline{r})\, d\ell_{\overline{r}} - \frac{1}{\pi}\int_C G(\overline{\rho}|\overline{r})\frac{\partial \phi_o(r)}{\partial n}\, d\ell_{\overline{r}} \qquad \text{III.8}$$

The second term of III.8 is known since both $G(\overline{\rho}|\overline{r})$ and $\partial\phi_o(r)/\partial n$ are known. The equation may be solved numerically by dividing the cylinder into a finite number (N) of elements, such that the point $\overline{r}_i$ represents the midpoint of each element.

$$\overline{r}_i = (\cos\theta_i,\ \sin\theta_i)$$
$$\theta_i = (i-1/2)\pi/N \qquad \text{III.9}$$
$$i = 1,\ 2,\ \ldots,\ N-1,\ N$$

III.8 may then be written in finite element form

$$\phi_{so_j} = \sum_{i=1}^{N} K_{ij}\ \phi_{so_i} + F_{so_j} \qquad \text{III.10}$$

where $K_{ij} = \frac{\pi}{N} \overline{\nabla} G(r_j r_i) \cdot \hat{n}_i \qquad (i \neq j)$

$$F_{so_j} = - \frac{1}{N} \sum_{i=1}^{N} G(r_j | r_i) \overline{\nabla} \phi_o(r_i) \cdot \hat{n}_i$$

The value of K_{ii} is found by separating $\overline{\nabla} G(r_j/r_i)$ into a regular part plus a singular part, integrating the singular part analytically over the i^{th} element, and adding the value of the regular part at the point r_i.

Rewriting III.10 yields

$$\sum_{i=1}^{N} \phi_{so_i}(\delta_{ij} - K_{ij}) = F_{so_j} \qquad \text{III.11}$$

which may readily be solved by matrix inversion or least squares techniques. A value of N=35 provides a numerical accuracy of better than 1% for all frequencies of interest. Computation time for these cases averages less than one minute.

It will be convenient to define the following quantities:

$$\lim_{\overline{r} \to (-1,0)} \phi_{so}(\overline{r}) \simeq \phi_{so_N} \qquad \text{III.12.1}$$

$$\lim_{\overline{r} \to (1,0)} \phi_{so}(\overline{r}) \simeq \phi_{so_1} \qquad \text{III.12.2}$$

It remains to determine the function H(x,y) which, as was pointed out earlier, represents a regular function necessary to insure that the second term of II.14 satisfies the boundary conditions. The function $\ell n(r_L/r_R) + H(x,y)$ may actually be considered the sum of two Green's functions, that for a source at (-1,0) and for a sink at (1,0) satisfying the following boundary value problem

$$\nabla^2[\ell n(r_L/r_R) + H(x,y)] = -2\pi[\delta(x+1,y) - \delta(x-1,y)] \quad \text{III.11.1}$$

$$\frac{\partial}{\partial y}[\ell n(r_L/r_R) + H(x,D)] - \frac{\omega^2 R}{g}[\ell n(r_L/r_R) + H(x,D)] = 0 \quad \text{III.11.2}$$

$$\frac{\partial}{\partial y}[\ell n\left|\frac{x+1}{x-1}\right| + H(x,0)] = 0 \qquad |x| \geq 1 \quad \text{III.11.3}$$

$$\frac{\partial}{\partial n}[\ell n(r_L/r_R) + H(x_s,y_s)] = 0 \qquad |x| < 0 \quad \text{III.11.4}$$

Recalling the definition of the Green's function, $G(x,y|\xi,\eta)$, we may write

$$\ell n(r_L/r_R) + H(x,y) = G(x,y|-1,0) - G(x,y|1,0) + F(x,y) \quad \text{III.12}$$

Noting the conditions satisfied by $G(x,y|\xi,\eta)$ in III.3.5, we may then find the conditions satisfied by $F(x,y)$ by substituting III.12 into III.11:

$$\nabla^2 F(x,y) = 0 \quad \text{III.13.1}$$

$$\frac{\partial F(x,D)}{\partial y} - \frac{\omega^2 R}{g} F(x,D) = 0 \quad \text{III.13.2}$$

$$\frac{\partial F(x,0)}{\partial y} = 0 \qquad |x| \geq 1 \quad \text{III.13.3}$$

$$\frac{\partial}{\partial n}F(x_s,y_s) = \frac{\partial}{\partial n}[G(x_s,y_s|1,0) - G(x_s,y_s|-1,0)] \quad \text{III.13.4}$$

F(x,y) must also satisfy the radiation conditions. Applying Green's theorem to the region external to the cylinder, and allowing the source point to approach the cylinder's boundary in the same manner as III.8, yields the integral equation for F(x,y):

$$F(\vec{\rho}) = -\frac{1}{\pi}\int F(\vec{r})\,\frac{\partial G}{\partial n}(\vec{\rho}\,|\,\vec{r})\,d\ell_r + \frac{1}{\pi}\int G(\vec{\rho}\,|\,\vec{r})\,\frac{\partial}{\partial n}\left[G(\vec{r}\,|\,\vec{r}_r) - G(\vec{r}\,|\,\vec{r}_\ell)\right]d\ell_r \qquad \text{III.14}$$

where $\vec{r}_r = (1,0)$

$\vec{r}_\ell = (-1,0)$

Since $G(\vec{\rho}\,|\,\vec{r})$ is a known function, equation III.14 may be solved in the same manner as III.8.

For the purposes of matching, it is convenient to calculate H(-1,0) and H(1,0). From III.12, we see that

$$H(x,y) = G(x,y)\,|-1,0) - G(x,y\,|\,1,0) + F(x,y) - \ln(r_L/r_R) \qquad \text{III.15}$$

Writing

$$G(x,y\,|\,\xi,\eta) = \ln r + g(x,y\,|\,\xi,\eta),$$

we obtain

$$H(x,y) = g(x,y\,|-1,0) - g(x,y)\,|\,1,0) + F(x,y) \qquad \text{III.16}$$

which may be calculated directly once F(x,y) has been computed. For convenience, we will denote

$$H_R = H(1,0) \qquad \text{III.17.1}$$

$$H_L = H(-1,0) \qquad \text{III.17.2}$$

III.2 Solution for the Inside Region

The flow inside the cylinder takes the form indicated by equation II.17:

$$\tilde{\phi}(x,y) = B(\varepsilon) + A(\varepsilon)[\ell n(r_R/r_L) + J(x,y)] \qquad \text{II.17}$$

The function $J(x,y)$, like $H(x,y)$ in the outside region, is required in order to satisfy the boundary condition on the surface of the cylinder:

$$\vec{\nabla}J(x_s,y_s)\cdot\hat{n}(x_s,y_s) = \vec{\nabla}\ell n(r_L/r_R)\cdot\hat{n}(x_s,y_s) \qquad \text{III.18}$$

$$x_s^2 + y_s^2 = 1$$

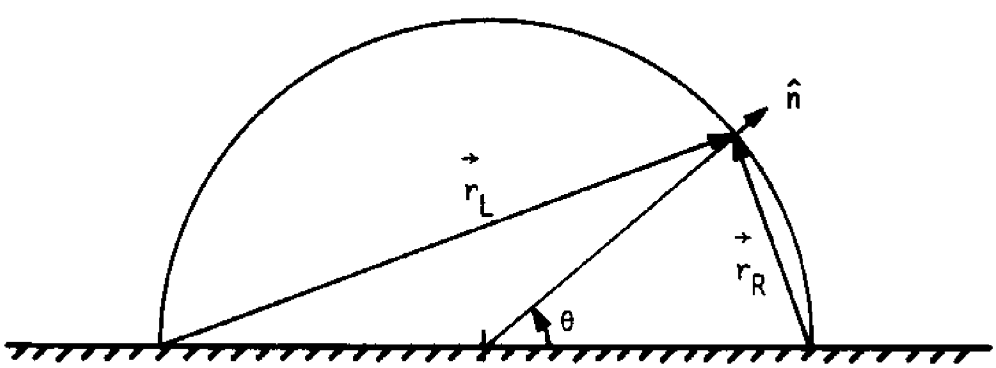

Figure III.1
RELATIONSHIP OF r_L AND r_R ON INSIDE BOUNDARY

This can be evaluated by observing that

$$\hat{n}(x_s,y_s) = \cos\theta\ \hat{i} + \sin\theta\ \hat{j} \qquad y_s > 0$$

$$= -\hat{j} \qquad y_s = 0$$

where the normal direction is taken outward from the region.

Also, writing again

$$r_L = \sqrt{(x+1)^2 + y^2}$$

$$r_R = \sqrt{(x-1)^2 + y^2}$$

we get

$$\vec{\nabla}\ell n(r_L/r_R) = [\hat{i}\ \frac{\partial}{\partial x} + \hat{j}\ \frac{\partial}{\partial y}]\ \ell n(r_L/r_R)$$

$$= [\frac{1}{r_L}\ \frac{\partial r_L}{\partial x} - \frac{1}{r_R}\ \frac{r_R}{\partial x}]\ \hat{i}$$

$$+ [\frac{1}{r_L}\ \frac{\partial r_L}{\partial y} - \frac{1}{r_R}\ \frac{\partial r_R}{\partial y}]\ \hat{j}$$

$$= [\frac{x_s+1}{r_L{}^2} - \frac{x_s-1}{r_R{}^2}]\ \hat{i} + y[\frac{1}{r_L^2} - \frac{1}{r_R^2}]\ \hat{j}$$

Now rewrite the boundary condition, III.18,

$$\vec{\nabla}J(x_s,y_s)\cdot\hat{n}(x_s,y_s) = \cos\theta\ [\frac{x_s+1}{r_L{}^2} - \frac{x_s-1}{r_R{}^2}] + y_s\sin\theta[\frac{1}{r_L^2} - \frac{1}{r_R^2}].$$

$$y_s > 0$$

Letting $x_s = \cos\theta$ and $y_s = \sin\theta$, and applying the law of cosines:

$$r_R{}^2 = 2(1 - \cos\theta)$$

$$r_L{}^2 = 2(1 + \cos\theta),$$

we can write

$$\vec{\nabla}J(x_s,y_s)\cdot\hat{n}(x_s,y_s) = \cos\theta \ [\ \frac{\cos\theta+1}{2(\cos\theta+1)} + \frac{\cos\theta-1}{2(\cos\theta-1)}\ ]$$

$$+ \frac{\sin^2\theta}{2}\ [\ \frac{\cos\theta+1 + \cos\theta-1}{\cos^2\theta-1}\ ]$$

$$= \cos\theta - \cos\theta \equiv 0 \qquad \text{III.19}$$

$$y_s > 0$$

Hence we arrive at the conclusion that $J(x,y)$ satisfies the homogeneous Neumann boundary condition on the surface $x_s^2 + y_s^2 = 1$. This could have been deduced immediately by simply noting that the circular shape of the cylinder corresponds to a streamline for the source/sink combination represented by $\ell n(r_L/r_R)$ (Lamb, 1945, p. 70). Since the x-axis (y_s=0) also represents one of the streamlines for this motion, we arrive at the fortuitous conclusion that $J(x,y)$ satisfies the homogeneous boundary condition over the entire inside region. $J(x,y)$ is at most, therefore, a constant, which can be set equal to zero with no loss of generality.

For the present it will be instructional to include $J(x,y)$ in the analysis, even though its value is zero for the circular cylinder. For other shapes its value will obviously be non-zero (except for other shapes which correspond to source/sink flow lines), and some numerical scheme (such as the integral equation method) would have to be employed to find its value. Assuming that this can be done, we will denote:

$$J_L = J(-1,0) \qquad \text{III.20.1}$$

$$J_R = J(1,0). \qquad \text{III.20.2}$$

These quantities will be necessary in the matching procedure.

III.3 Solution for the Inner Flow

The flow through the gaps was shown in Chapter II to be equivalent to $O(\varepsilon)$ to the flow through a slit in a vertical barrier. This result follows from the coordinate stretching II.18, and is represented in Figure III.2.

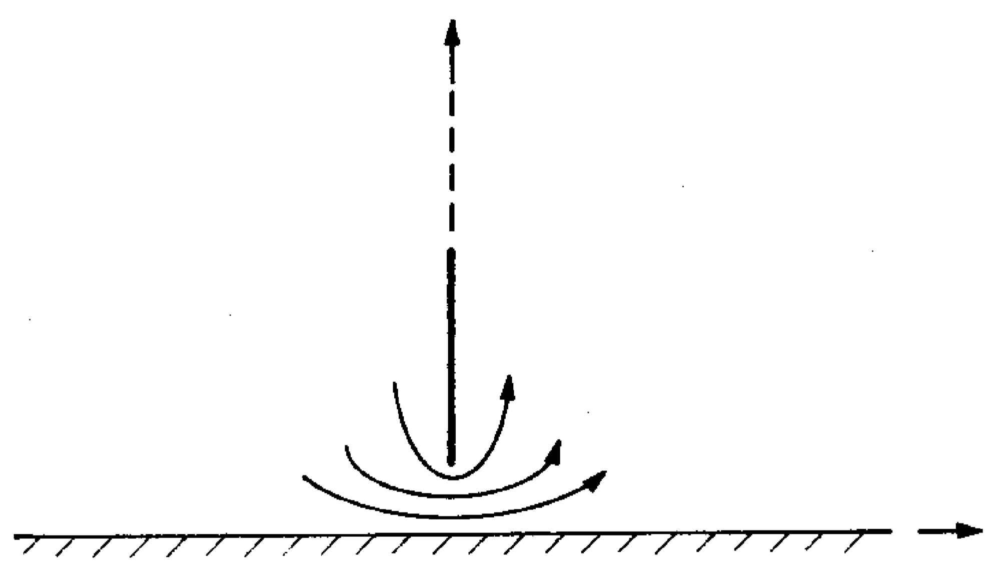

Figure III.2
FLOW THROUGH GAP

By the method of images, this flow can be found by replacing the rigid boundary Y=0 by the image of the vertical barrier x=0, $y \geq 1$, (Figure III.3).

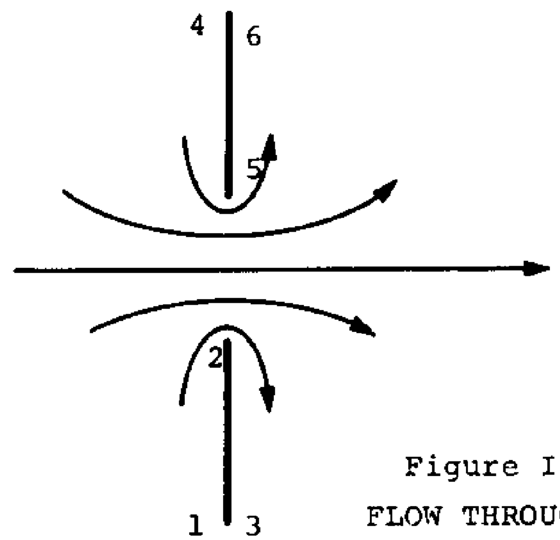

Figure III.3
FLOW THROUGH SLIT

Since the curvature of the cylinder does not enter this problem, the flow through either gap is identical.

To evaluate this flow, map the region shown in Figure III.3 into that shown in Figure III.4 by using the following mapping function:

$$Z = -i \cosh \zeta \qquad \text{III.21}$$

$$\text{where } Z = X + iY$$

$$\zeta = \xi + \eta$$

The numbered points in Figure III.3 map into the corresponding points of Figure III.4.

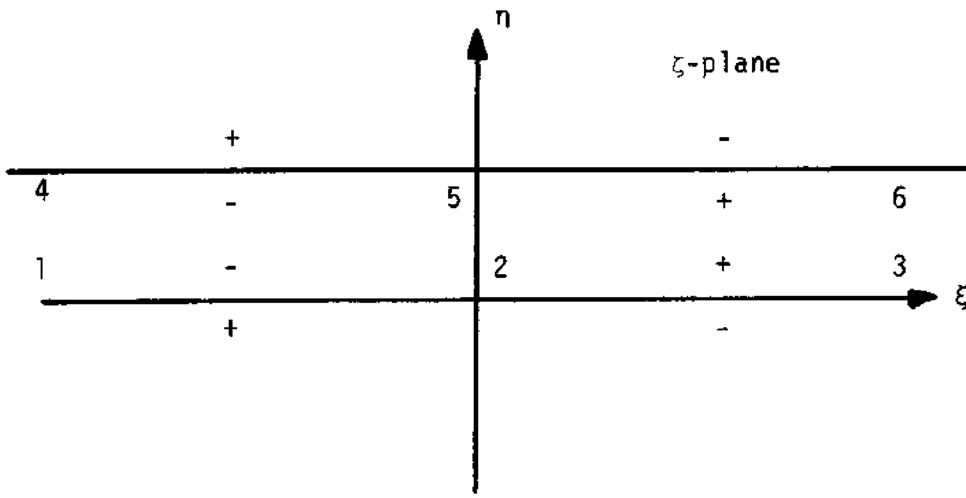

Figure III.4

Note that for ζ along the real axis in the ζ-plane, or the line $\eta = \pi$, $Z(\zeta)$ lies along the imaginary axis in the Z plane. The points $\zeta = 0$ and $\zeta = i\pi$ correspond to the edges, $Z = -i$ and $Z = i$, respectively. If we introduce the complex velocity potential, $W(Z)$, such that

$$\frac{dW(Z)}{dZ} = u + iv$$

$$= \frac{\partial\phi}{\partial X} + i\,\frac{\partial\phi}{\partial Y}$$

$$= \frac{dW[Z(\zeta)]}{d\zeta}\,\frac{d\zeta}{dZ}$$

We obtain the expected result that the velocities become infinite at the edges, since

$$\frac{d\zeta}{dZ} = \frac{i}{\sinh\zeta}$$

becomes infinite at these points (assuming $dW/d\zeta$ takes on non-zero values there).

The η axis in the ζ-plane between $\eta = 0$ and $\eta = \pi$ corresponds to the gap ($-1 < \text{Im}Z < +1$) in the Z plane. Passing through this line in either plane must correspond to passing from one side of the gap to the other. In order to show this, write

$$\zeta = \alpha + i\beta$$

so that, from III.21,

$$Z = \sinh\alpha \sin\beta - \cosh\alpha \cos\beta.$$

Now with $0 < \beta < \pi$, the region $\alpha < 0$ corresponds to the left side of the gap (Re $Z < 0$), the region $\alpha > 0$ corresponds to the right side (Re $Z > 0$). Figures III.3 and III.4 indicate these mapping regions.

The flow in the ζ-plane corresponding to flow through the gap in the Z plane thus becomes simple streaming flow:

$$W(\zeta) = U\zeta + C,$$

which, upon substitution of ζ from III.21 becomes

$$W(Z) = U \cosh^{-1} iZ + C. \qquad \text{III.22}$$

This form is also given by Lamb (op. cit., p. 73). U and C must be found from matching. In order to compare III.22 with the outer expansions, both inside and outside the cylinder, write the potential as

$$\hat{\phi}(X,Y) = U \text{ Re } [\cosh^{-1} iZ] + C \qquad \text{III.23}$$

where U and C may be complex (reflecting the phase of the flow) and functions of ε.

III.4 Accuracy of the Solutions

While equation III.23 re sents the flow through a gap in an infinite barrier, we ha shown that it represents as well the flow through either of the cylinder to $O(\varepsilon)$. Thus we have derived in this pter and the preceding chapter expressions for the velocity entials in each of the areas of interest (inside the cylin, outside the cylinder and adjacent to each gap) to with an approximate error of $O(\varepsilon)$. The accuracy of the re ts, therefore, will be limited by the size of the ga

In addition, the results rived herein do not take into account real fluid effects or e finite thickness of the cylinder wall - both of which come important for small ε. These effects will be discuss in detail in a later chapter.

IV. MATCHING THE SOLUTIONS

The method of matched asymptotic expansions is treated by Van Dyke (1964), Cole (1968), and in considerable detail by Lagerstrom and Cole (1955). The particular problem of concern here, that of flow through a small aperture, has been treated by Tuck (1971) in finding the reflection and transmission coefficients for a vertical barrier with a submerged slit. The method used by Tuck is virtually the same as that used here, and it is instructional to consider his problem in some detail. Appendix A includes, therefore, a discussion of Tuck's problem using the alternate matching schemes. Newman (1967) used an identical matching technique to compute the flow past a ship of large draft in shallow water. Widnall and Barrows (1969) used a more complicated, but straightforward, matched asymptotic expansion scheme to find the lift on two-and three-dimensional wings in ground effect.

Before turning to the explicit solution of the problem at hand, it may be helpful to review the rationale behind employing the method of matched asymptotic expansions and the basic techniques of its implementation.

First, we have assumed that the correct solution for the flow has been altered only slightly by the occurrence of a small gap at the cylinder edges. Solving this problem involved the postulation of a perturbation potential, $\phi_s(x,y)$ which would approximate the correct correction for the gap for finite values of ε, and would approach the exact correction asymptotically for small ε.

In particular, if $\phi_p(x,y)$ represents the <u>exact</u> solution for our problem (which we cannot calculate), we have shown that the solutions derived in Chapter III approximated ϕ_p with an error of $O(\varepsilon)$, or, in other words,

$$\lim_{\varepsilon \to 0} \left[\frac{\phi_p(x,y) - \phi_s(x,y)}{\varepsilon}\right] = K \qquad \text{IV.1}$$

where $\phi_s(x,y)$ is represented in II.14, and K is some constant which numerically is of order unity.

The above limit states that the error, for sufficiently small values of ε, is directly proportional to ε. This is, in fact, the precise definition of what is meant by the asymptotic representation

$$\phi_p(x,y) = \phi_s(x,y) + O(\varepsilon),$$

(cf. Lagerstrom, 1957).

We have further postulated that the correct form for the function $\phi_s(x,y)$ is that of a source/sink combination plus a regular function of (x,y), as indicated by II.14. This solution satisfies all the conditions of the problem (Chapter II) except that it does not provide the correct representation of the flow near the edges of the cylinder, thus leading to the fact that IV.1 becomes invalid in those regions. Because of this, the complete problem cannot be solved, even to $o(\varepsilon)$, without special consideration for what goes on in the vicinity of the gap.

This leads to the formulation of the "inner" problem to describe the flow through the gaps (Section II.3). The inner problem results from a coordinate transformation and stretching which magnifies the region of non-uniformity (the region where IV.1 is not valid) so that the perturbation potential becomes a first order function. That is, while the effect of ε on the "outer" solution (II.14) is presumed small, its effect on the inner solution is, by definition, of $O(1)$.

Both the "inner" and the "outer" problems are incomplete. The outer problem does not specify a boundary condition at the edges of the cylinder, and the inner problem does not specify the boundary conditions far from the edges. The complete solution cannot be found, therefore, without the added condition that both the solutions match within some intermediate region.

This condition implies the existence of an "overlap domain". That is, there must be a region in which both the outer and inner solutions are equally accurate representations of the exact solution. We may illustrate this with reference to the present problem. As we have seen, the "outer" solution (both inside and outside the cylinder) consists of log terms plus regular terms:

$$\phi_s(x,y) = A[\ell n(r_L/r_R) + H(x,y)] + \phi_{so}(x,y)$$

Approaching the left gap from the left along the x axis yields

$$\phi_s(x,0) = A[\ell n(\frac{|x+1|}{|x-1|}) + H(x,0)] + \phi_{so}(x,0) \qquad \text{IV.2}$$

Near the point x = -1 the log term becomes singular, but the other terms are well behaved. We can therefore expand all terms except the log in a Taylor series about x = -1:

$$\phi_s(x,0) \underset{\lim x\to -1}{\simeq} A[\ell n(x+1) - \ell n(2) + H(-1,0)] + \phi_{so}(-1,0) + \ldots \qquad \text{IV.3}$$

which may be written

$$\phi_s(x,0) \underset{\lim x\to -1}{=} A[\ell n(x+1) + Q_L] + P + \ldots \qquad \text{IV.4}$$

Q_L and P are the constants indicated by IV.3.

As we have mentioned, the above solution is non-uniform, since our assumption that ϕ_s approaches the exact scattered potential for $\varepsilon\to 0$ is not valid when $|x+1|$ becomes too small. This is the case when $x+1 = 0(e^{-1/A})$, since the term $A\ell n(x+1)$ then becomes 0(1). On the other hand, for sufficiently large values of $|x+1|$ the Taylor series (IV.3) must include more terms to provide the necessary accuracy. When $|x+1| = 0(A)$, for example, the error incurred in truncatin the Taylor series is equal to the term of interest, namely the leading term of IV.4.

Equation IV.4 holds, of course, no matter which path chosen to approach the gap point, provided (x+1) is replac by r_L. For the present we will stick to the x-axis, however, since the purpose here is to illustrate the method. For the general case, $\lim_{r_L \to 0} \phi_s(x,y)$ is referred to as the "inner limit of the outer solution". Speaking in terms of IV.4, we can say that this expression is valid to $0(A)$, provided

$$e^{-1/A} < |x+1| < A .$$

Turning our attention to the inner solution,

$$\hat{\phi}(X,Y) = C + A \text{ Re } \cosh^{-1} iZ$$

We may also examine its value along the x-axis:

$$\hat{\phi}(\overline{X},0) = C + A \text{ Re } \cosh^{-1} |X|$$

$$\hat{\phi}(x,0) = C + A \text{ Re } \cosh^{-1} i|x/\varepsilon| \qquad \text{IV.5}$$

For sufficiently large values of $|X|$, IV.5 becomes (see Appendix C):

$$\underset{\lim X\to\infty}{\hat{\phi}(X,0)} = C + A \, \ell n 2X + 0(\tfrac{1}{X^2}) \qquad \text{IV.6}$$

Rewriting IV.6 using outer variables yields:

$$\underset{\lim X\to\infty}{\hat{\phi}(x,0)} = B + A[\ell n(x+1) + \ell n 2 - \ell n\varepsilon] + 0(\frac{\varepsilon^2}{|x+1|}) \qquad \text{IV.7}$$

This expression will be valid to $0(A)$ provided $|x+1| > \varepsilon$.

In addition, in order for IV.7 to asymptotically approach the correct solution as $\varepsilon \to 0$, we observe that

$$A = 0(1/\ell n\varepsilon). \qquad \text{IV.8}$$

In addition to the requirement that $|x+1| > \varepsilon$ for the asymptotic form IV.7 to be valid to $0(1/\ell n\varepsilon)$, we must also recognize that the complete inner solution, IV.5, is only valid for values of r_L (or r_R) close to the gap, i.e.,

$$r_L < \gamma(\varepsilon).$$

In this regard we observe that, in particular, the curvature of the dome is not accounted for in IV.5. We must observe, therefore, at what radius the error in the wall boundary condition becomes $0(\varepsilon)$.

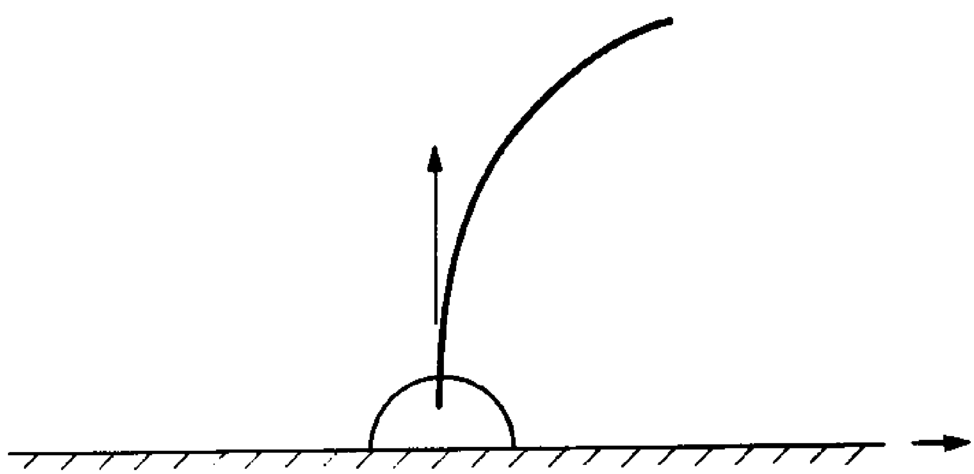

FIGURE IV.1 INNER FLOW REGION

Writing the potential

$$\hat{\phi}(x,y) = C + A[\mathrm{Re}\cosh^{-1} iZ] \qquad \text{IV.9}$$

and the condition on the surface of the cylinder that there be no velocity normal to the surface:

$$\vec{\nabla}\hat{\phi}(x_s,y_s)\cdot\hat{n}(x_s,y_s) = 0$$

$$\text{where} \quad x_s^2 + (y_s-\varepsilon)^2 = 1$$

$$\hat{n}(x_s,y_s) = x_s\hat{i} + (y_s-\varepsilon)\hat{j},$$

Now, let

$$\hat{f}(y_s,\varepsilon) = \text{error in boundary condition}$$
$$= \vec{\nabla}\hat{\phi}(x_s,y_s)\cdot\hat{n}(x_s,y_s) \qquad \text{IV.11}$$

It will be more convenient to evaluate this expression using complex variables. Thus, since we are only concerned here with velocities, represent the complex inner potential as

$$W(Z) = \cosh^{-1} iZ \qquad \text{IV.12.1}$$

where
$$\frac{1}{\varepsilon}\frac{dW(Z)}{dZ} = U + iV \qquad \text{IV.12.2}$$

$$U = \frac{\partial\hat{\phi}}{\partial x} \qquad \text{IV.12.3}$$

$$V = \frac{\partial\hat{\phi}}{\partial y} \qquad \text{IV.12.4}$$

$$Z = X + iY$$

Now we may evaluate $f(y_s,\varepsilon)$ as

$$f(y_s,\varepsilon) = A \operatorname{Re}\left[\frac{\bar{z}_s}{\varepsilon}\frac{dW(Z)}{dZ}\right] \qquad \text{IV.13}$$

where $\bar{z}_s = x_s - i(y_s-\varepsilon)$

Now

$$\frac{1}{\varepsilon}\frac{dW(Z)}{dZ} = \frac{1}{\varepsilon}\frac{d\cosh^{-1}(iZ)}{dZ} = \frac{1}{\sqrt{(Z+1)^2+\varepsilon^2}} \qquad \text{IV.14}$$

where use has been made of the coordinate stretching $z = \varepsilon Z + 1$.

So we may now write

$$f(y_s,\varepsilon) = A \text{ Re } \frac{\bar{z}_s}{\sqrt{(z_s+1)^2 + \varepsilon^2}}$$

Expanding for small ε yields

$$f(y_s,\varepsilon) \simeq A \text{ Re } \left\{ \frac{z_s}{(z_s+1)} \left[1 + \frac{\varepsilon^2}{z_s+1} + \ldots\right] \right\}$$

If we insert the values of $\bar{z}_s$ and z_s, and take only the real part, we obtain

$$f(y_s,\varepsilon) \simeq A \frac{1 + 2\varepsilon y_s - \varepsilon^2 - 2y_s^2 - \sqrt{1 - (y_s-\varepsilon)^2} + y_s\varepsilon}{2 + 2\varepsilon y_s - \varepsilon^2 - 2\sqrt{1 - (y_s-\varepsilon)^2}}$$

We find from this that $\lim\limits_{y_s \to \varepsilon} f(y_s,\varepsilon) = 0$, as it indeed should since the edge of the cylinder is exactly vertical. To find how this error function behaves for $y_s > \varepsilon$, expand in a Taylor series about $y_s = \varepsilon$. This yields

$$f(y_s,\varepsilon) \simeq A \frac{\varepsilon(y_s-\varepsilon)}{(1+\varepsilon^2)} \simeq A\varepsilon(y_s-\varepsilon) \qquad \text{IV.15}$$

when only the first term of the Taylor series has been retained.

If we match solutions to $0(\alpha_1)$, the inner solution remains valid to $f(y_s,\varepsilon) = \alpha_1$, or, from IV.15,

$$y_s = \varepsilon_s + \alpha_1/\varepsilon \text{ [illegible]}$$

We have noted that the outer solution becomes invalid to $0(1/\ln\varepsilon)$ for $r_L(r_R) = \varepsilon$, since the second term of II.14 becomes the same order as the first. The region between

$r_L = \varepsilon$ and $r_L = \varepsilon + \alpha_1/\varepsilon = \varepsilon + 1/\varepsilon\ell n\varepsilon$ is therefore an overlap domain wherein both solutions are equally valid.

Matching, therefore, is accomplished by simply setting these two limit processes equal. It is interesting to note that the discovery of the precise regions of validity of each solution confirms here the existence of an overlap region where both solutions are equally good, thus justifying the matching to be carried out here. In general the method would work even if there <u>weren't</u> an overlap region, due to the existence of an "intermediate" region lying between the inner and outer regions in which another solution (found by a suitable intermediate stretching of variables) may be found. By the Kaplun extension theorem (Kaplun, 1954), both the inner and outer regions would overlap into this intermediate region, thus permitting a double matching operation to be performed linking the inner and outer solutions.

It is also important to note the distinction between the
tching of two solutions valid in adjacent regions, and the
atching" of two solutions. This latter method, used, for
ample, in finite element calculations, is accomplished by
lecting a boundary common to two regions, and adjusting the
lutions in each region so that the numerical value of the
o solutions (or their derivatives) are equal on that
undary.

Matching, on the other hand, is based not on the exis-
nce of a common <u>boundary</u>, but of a common <u>region</u> of

validity. The two solutions must, of course, agree numerically throughout this common region (to within a specified accuracy) but must in addition (or as a consequence) be of the same functional form.

Figure IV.2 shows possible plots of the outer and inner solutions (IV.4 and IV.7 respectively) for the potentials along the x-axis.

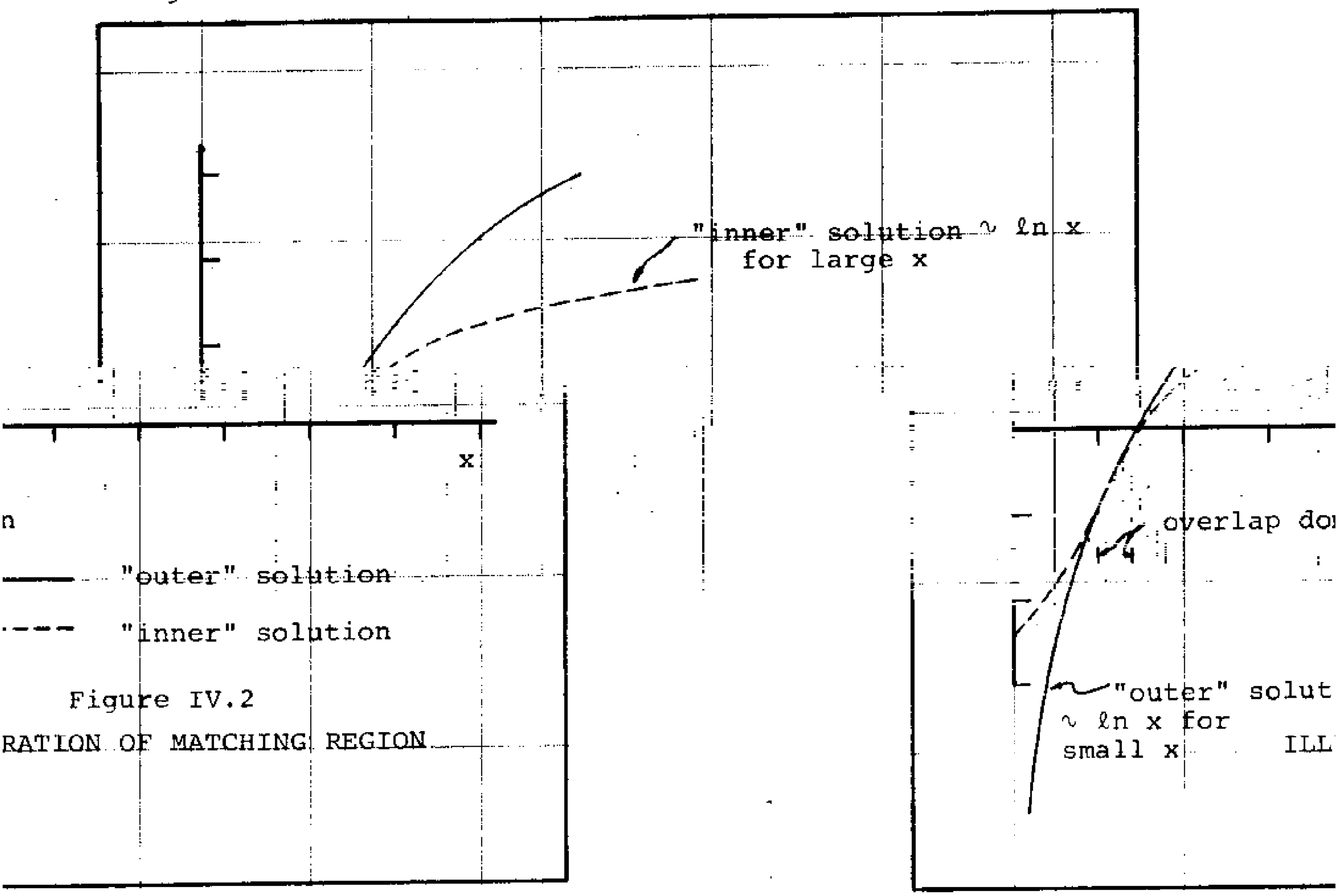

Figure IV.2

RATION OF MATCHING REGION

ILL

tching Schemes

IV.1 Heuristic vs. Formal

nt R_L^* or R_R^* in the inner region

) or (1,0) respectively as ε

points r_L^* or r_R^* remain a fixed

We have seen that a

moves toward the point (-

decreases. In addition,

distance from (-1,0) or (1,0) as ε decreases. We are thus led into the dilemma that the two regions of validity (the "inner" region associated with R_L or R_R, and the "outer" region associated with r_L or r_R) may not remain overlapping in the limit as $\varepsilon \to 0$, since R_L^* and R_R^* decrease as r_L^* and r_R^* remain fixed.

This problem has been associated with thin airfoil theory (Van Dyke, 1954, Chap. IV) and with low Reynold's number flow (Kaplun, 1957).

It should be noted, in this regard, that one may view these matching problems from either a heuristic or a rigorous point of view, depending on one's purpose. The method employed by Tuck (1971) and Newman (1967) may be classified as "heuristic", or, as Tuck has stated, "semi-intuitive".

The heuristic, or semi-intuitive, method may be conceptualized as follows (with credit to Professor Tuck): The inner flow may be described as that seen by a near-sighted "midget" seated in the middle of the gap. He is unaware of either the existence of the free surface or the shape of the cylinder (its curvature), and must conclude that he is simply experiencing a steady motion through an aperture in a straight barrier with no other factors affecting the flow other than the size of the gap and his own presence (which we ignore). If the midget views the flow far from the gap, through a telescope, say, he will see that the flow on one side is streaming toward him like a sink, and on the other side the flow is disappearing in a sourcelike fashion. Even with a telescope the midget would not be able to detect the subtleties of the outer flow such as the free surface.

The outer flow, on the other hand, may be considered as that seen by a farsighted giant who is, perhaps, lying face down in the water. The giant is capable of determining the shape of the object (the cylinder), and can feel the effect of the free surface, but he cannot see the gaps at the edge of the cylinder. He does, however, note that fluid is leaving his field of view at one edge of the cylinder and appearing at the other, but he is unable to see the flow through the gap. If the giant puts on a set of spectacles, he is able to perceive the details of the gap flow only to the extent that he can verify that there is indeed a source at one gap and a sink of equal strength at the other.

The heuristic matching process simply states that the flow as seen by the midget with the telescope must be exactly the same as that seen by the giant with his spectacles.

This approach to matching is usually referred to as the "limit matching principle", and is usually stated as follows:

> The inner limit (of the outer limit)
> = the outer limit (of the inner limit)

It was first used by Prandtl to solve the problems associated with the boundary layer effect on inviscid flow models. Its success hinges largely on the existence of an overlap domain wherein the two limit processes described above do actually apply, although it may succeed even in cases where no overlap domain exists.

A more rigorous and satisfactory solution was preferred by Kaplun (1957). According to Kaplun's extension theorem, even when no region existed in which both the limits described above were valid, there must exist another solution limit which is valid in the region between the two extremes of the inner and outer limits, and which may be matched to each of the two previous limits, therefore providing a link between the inner and outer solutions. This region spanning the "gap" (not the "gap" in our problem) between the inner and outer regions is known as the "intermediate region". It is obtained by introducing a coordinate stretching similar to the inner coordinate stretching, but not as strong, which would allow a variable in the intermediate region to remain between the inner region and the outer region as $\varepsilon \to 0$.

To see how this works, let us define an intermediate variable for our problem as:

$$\bar{R}_L = r_L/\varepsilon^{1/2} \qquad \text{IV.23.1}$$

$$\bar{R}_R = r_R/\varepsilon^{1/2} \qquad \text{IV.23.2}$$

Now, if we select a point r_L^* (dealing with only the left gap does not alter the generality of the discussion) which is some distance from the gap (-1,0), the same point written in intermediate and inner coordinates becomes:

$$\bar{R}_L^* = r_L^*/\varepsilon^{1/2}$$

and $$R_L^* = r_L^*/\varepsilon \; .$$

And if we solve the appropriate problem in each of the regions (with the appropriate coordinates inserted into the equations of motion and the boundary conditions), we obtain three different solutions:

$\bar{\phi}(r_L^*)$ outer solution

$\phi(\bar{R}_L^*)$ intermediate solution

$\hat{\phi}(R_L^*)$ inner solution.

If the asymptotic expression of each of these solutions is found by taking the limit as $\varepsilon \to 0$ with r_L^*, $\bar{R}_L^*$ and R_L^* fixed, respectively, we discover that the three points (in each region) do not remain a fixed distance from the gap (-1,0). In particular, r_L^* remains a fixed distance from the gap, $\bar{R}_L^*$ decreases like $\varepsilon^{1/2}$ and R_L^* decreases like ε. Thus the three points separate, the "inner" point approaching the gap faster than the intermediate point, and the outer point remaining fixed. It appears that, without Kaplun's theorem, the heuristic approach would be subject to considerable doubt. The success of the heuristic approach depends on the nature of the problem and on the dependent variables used in the matching. It works, for example, for the tangential velocity in a boundary layer but not for the normal velocity (Van Dyke, 1964).

IV.2 Matching by Means of an Intermediate Solution

We will herein write the matching equations for the

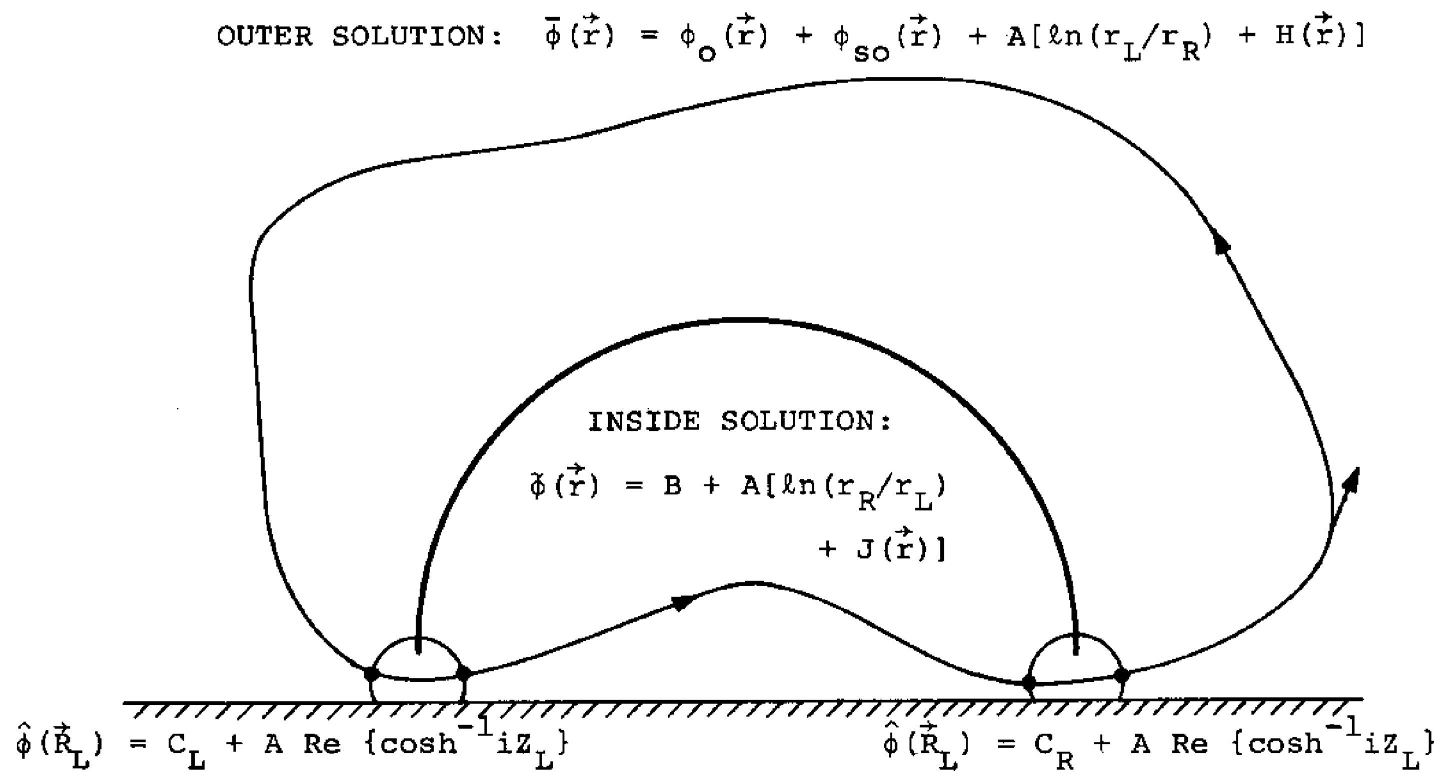

Figure IV.3

SOLUTIONS IN ALL REGIONS

or $\bar{R}_R$ remains within these regions as $\varepsilon \to 0$. Noting that

$$\lim_{\varepsilon \to 0} \alpha(\varepsilon) = 0,$$

we find that the solution for the flow in the inner region is also that for the flow through an aperture in a vertical barrier. This approximation is valid to $0(\alpha)$.

Thus there is no need to solve a separate problem for the intermediate regions. We simply have to write the outer solution and the inner solution (which is also the intermediate solution) in terms of the variables $\bar{R}_L$ and $\bar{R}_R$, take the limit $\varepsilon \to 0$, and set equal the corresponding limits. Thus we may proceed in a straightforward manner:

<u>Region 1</u>

Outer Solution

$$\phi_o(\vec{r}) + \phi_{so}(\vec{r}) + A[\ell n(r_L/r_R) + H(\vec{r})] \quad \text{IV.24.1}$$

Write in intermediate variables for region 1

$$\phi_o(\alpha\bar{X}_L-1,\alpha\bar{Y}_L) + \phi_{so}(\alpha\bar{X}_L-1,\alpha Y_L)$$

$$+ A[\ell n(\frac{\alpha\bar{R}_L}{\alpha\bar{R}_L+2}) + H(\alpha\bar{X}_L-1,\alpha\bar{Y}_L)] \quad \text{IV.24.2}$$

Take limit $\alpha \to 0$, $\bar{R}_L$ fixed

$$\phi_o(-1,0) + \phi_{so}(-1,0) + A[\ell n(\alpha\bar{R}_L/2) + H(-1,0)] \quad \text{IV.24.3}$$

Inner Solution

$$C_L + A\,\text{Re}\cosh^{-1}(iR_L) \quad \text{IV.25.1}$$

Write in intermediate variables for Region 1

$$C_L + A \text{ Re } \cosh^{-1}[i\alpha\bar{R}_L/\varepsilon] \qquad \text{IV.25.2}$$

Take limit $\alpha \to 0$, $\bar{R}_L$ fixed

$$C_L + A[\ell n 2\alpha R_L - \ell n\varepsilon] \qquad \text{IV.25.3}$$

Now IV.24.3 and IV.25.3 must be equal, so we set $\phi_L = \phi_o(-1,0) + \phi_{so}(-1,0)$, $H_L = H(-1,0)$ and write

$$\phi_L + A[\ell n\bar{R}_L + \ell n\alpha - \ell n2 + H_L]$$

$$= C_L + A[\ell n\bar{R}_L + \ell n\alpha + \ell n2 - \ell n\varepsilon] \qquad \text{IV.26}$$

from which, by noting that the $\ell n\bar{R}_L$ and $\ell n\alpha$ terms cancel, as indeed they must, we arrive at the equation

$$\phi_L = C_L + A[2\ell n2 - \ell n\varepsilon - H_L] \qquad \text{IV.27}$$

We get similar equations in each of the four intermediate regions.

<u>Region 2</u>

Outer Solution

$$B + A[\ell n(r_R/r_L) + J(\vec{r})] \qquad \text{IV.28.1}$$

Write in intermediate coordinates for Region 2

$$B + A[\ell n(\frac{\alpha\bar{R}_R+2}{\alpha\bar{R}_L}) + J(\alpha\bar{X}_L-1,\alpha Y_L)] \qquad \text{IV.28.2}$$

Take limit $\alpha \to 0$, $\bar{R}_L$ fixed

$$B + A[\ell n2 - \ell n\alpha\bar{R}_L + J(-1,0)] \qquad \text{IV.28.3}$$

Inner solution written in intermediate variables

$$C_L + A \text{ Re } [\cosh^{-1}(i\alpha\bar{R}_L/\varepsilon] \qquad \text{IV.29.1}$$

Take limit $\alpha \to 0$, $\bar{R}_L$ fixed

$$C_L - A[\ln 2 - \ln\varepsilon + \ln\alpha\bar{R}_L] \qquad \text{IV.29.2}$$

Equating IV.28.3 and IV.29.2 yields

$$B = C_L + A[-2\ln 2 + \ln\varepsilon - J_L] \qquad \text{IV.30}$$

where $J_L = J(-1,0)$

Region 3

Outer solution written in intermediate variables for Region 3

$$B + A[\ln(\frac{\alpha R_R}{\alpha\bar{R}_L+2}) + J(\alpha\bar{X}_R+1, \alpha\bar{Y}_R)] \qquad \text{IV.31.1}$$

Take limit $\alpha \to 0$, $\bar{R}_R$ fixed

$$B + A[\ln\alpha\bar{R}_R - \ln 2 + J_R] \qquad \text{IV.31.2}$$

where $J_R = J(1,0)$

Inner solution written in intermediate variables

$$C_R + A \text{ Re } \cosh^{-1}(i\alpha\bar{R}_R/\varepsilon) \qquad \text{IV.32.1}$$

Take limit $\alpha \to 0$, $\bar{R}_R$ fixed

$$C_R + A[\ln 2 - \ln\varepsilon + \ln\alpha\bar{R}_R] \qquad \text{IV.32.3}$$

Equating IV.31.2 with IV.32.2, we obtain

$$B = C_R + A[2\ln 2 - \ln\varepsilon - J_R] \qquad \text{IV.33}$$

Region 4

Outer solution written in intermediate variables for Region 4

$$\phi_o(\alpha\bar{X}_R+1,\alpha\bar{Y}_R) + \phi_{so}(\alpha X_R+1,\alpha\bar{Y}_R)$$

$$+ A\ [\ln\ (\frac{\alpha\bar{R}_L+2}{\alpha\bar{R}_R}) + H(\alpha\bar{X}_R+1,\alpha\bar{Y}_R)] \qquad \text{IV.34.1}$$

Take limit $\alpha \to 0$, $\bar{R}_L$ fixed

$$\phi_R + A[\ln 2 - \ln\alpha\bar{R}_R + H_R] \qquad \text{IV.34.2}$$

where $\phi_R = \phi_o(1,0) + \phi_{so}(1,0)$

$H_R = H(1,0)$

Inner solution written in intermediate variables for Region 4

$$C_R + A\ \mathrm{Re}\ [\cosh^{-1}(i\alpha\bar{R}_R/\varepsilon)] \qquad \text{IV.35.1}$$

Take limit $\alpha \to 0$, $\bar{R}_L$ fixed

$$C_R - A[\ln 2 - \ln\varepsilon + \ln\alpha\bar{R}_R] \qquad \text{IV.35.2}$$

Setting IV.34.2 equal to IV.35.2 yields

$$\phi_R = C_R + A[-2\ln 2 + \ln\varepsilon - H_R] \qquad \text{IV.36}$$

From the above we extract four matching equations to find the unknown constants:

$$\phi_L = C_L + A[2\ln 2 - \ln\varepsilon - H_L] \qquad \text{IV.27}$$

$$B = C_L + A[-2\ln 2 + \ln\varepsilon - J_L] \qquad \text{IV.30}$$

$$B = C_R + A[2\ln 2 - \ln\varepsilon - J_R] \qquad \text{IV.33}$$

$$\phi_R = C_R + A[-2\ln 2 + \ln\varepsilon - H_R] \qquad \text{IV.36}$$

Solving these equations results in the following expressions for the unknowns. The algebra is simple, and is omitted here.

$$A = \frac{\phi_L - \phi_R}{8\ell n2 - 4\ell n\varepsilon + H_R - H_L + J_L - J_R} \qquad \text{IV.37}$$

$$B = \frac{\phi_L + \phi_R}{2} + \frac{A}{2}\,[H_L - J_L + H_R - J_R] \qquad \text{IV.38}$$

$$C_L = \frac{B + \phi_L + A[H_L + J_L]}{2} \qquad \text{IV.39}$$

$$C_R = \frac{B + \phi_R + A[H_R + J_R]}{2} \qquad \text{IV.40}$$

IV. 3 Discussion of Matching Results

These equations confirm the results of the previous section, i.e., that $A = 0(1/\ell n\varepsilon)$, as indeed it must in order for the matching to work. It is interesting to note that the value of A could be written in the form of an asymptotic expansion in $1/\ell n\varepsilon$.

$$A = \sum_{n=1}^{N} A_n/(\ell n\varepsilon)^n \qquad \text{IV.41}$$

where

$$A_n = (8\ell n2 + H_R - H_L + J_L - J_R)^{n-1}/4^n$$

This suggests that a step by step matching procedure could have been used to obtain the same results. Appendix A discusses the problem of a single slit in a vertical wall using both a step by step method and a "block" matching process (i.e., the heuristic method).

The constant B (eqn. IV.38) is of some interest. Although its value has no effect on the flow, either inside or outside of the cylinder, it represents a pulsating pressure which is felt throughout the inside region. It thus takes on a primary importance in the calculation of the vertical force on the cylinder.

Furthermore, since B takes on a first order value equal to $1/2(\phi_L + \phi_R)$, we are confronted with an apparent paradox. In the limit $\varepsilon \to 0$, B remains a fixed $0(1)$ constant implying $0(1)$ pressure fluxuations on the inside of the cylinder for no gap. For the original zero gap problem, however, we assume that there is no pressure fluctuation on the inside of the cylinder. This would indeed be the case for the idealized model, since there would be no explanation for the communication of pressure from the outside region to the inside region. The inside of the cylinder could not "know" what the behavior of the fluid was outside, or, indeed, whether there was any fluid on the outside whatsoever.

This behavior may be explained by considering the incident wave as the sum of two standing waves, a symmetric part and an asymmetric part. The first order pressures at the left (p_L) and the right (p_R) gaps due to the symmetric and asymmetric parts respectively may be written

$$p_L = p_{sym} \cos\,(\omega t+\alpha) + p_{asym} \sin\,(\omega t+\beta)$$

$$p_R = p_{sym} \cos\,(\omega t+\alpha) - p_{asym} \sin\,(\omega t+\beta)$$

The symmetric part of this pressure will not drive any flow through the gap. The inside pressure in phase with the symmetric outside pressures must therefore be simply p_{sym}. On the other hand, the asymmetric pressures will induce motion through the cylinder but will cause no constant pressure rise in the inside region.

The calculation of forces will be discussed in more detail in Chapter V. We will turn for the moment to another look at the matching.

IV.4 Uniqueness of Matched Solution

The present problem may be treated without resorting to the matching procedure. We could, for example, treat the cylinder as a two-dimensional body immersed in a moving fluid and calculate the scattering by an integral equation method (see, e.g., Wehausen and Laitone, p. 533).

By this method we would find that the cylinder could be represented by a vortex sheet coincident with the cylinder surface. The strength of the sheet would equal the difference in tangential velocities across the surface of the cylinder.

Unfortunately, no method exists for solving this integral equation exactly. If one did, we could in principle evaluate it for small ε by expanding about $\varepsilon = 0$ (where the vortex strength becomes proportional to the outside tangential velocity). As it is, the solution must be found numerically. A numerical solution would, however, become insensitive to small changes in ε for small gaps, and would not be practical for the range of gap widths of interest.

The formulation of the problem in terms of a body immersed in a fluid raises some theoretical questions about the matching scheme, however. In Chapters II and III we formulated the problem for three separate regions. Each region is simply connected, and the solutions formulated are unique.* The formulation of the problem as a body immersed in a single region represents flow in a multiply connected

*The proof of the uniqueness of the solution derived via Green's theorem is given in any book on partial differential equations (e.g., Garabedian). It should be noticed that the uniqueness property does not pertain to the eigen functions characterized by the singularities at the edges of the cylinder. The elimination of higher order singularities rests on energy arguments and on Van Dyke's "principle of least singularity".

region, however. Flow in a multiply connected region (such as flow past an air foil) cannot be uniquely specified by Laplace's equation and the boundary conditions. Such flow, satisfying all the boundary conditions, may contain an undetermined amount of "bound" vorticity (vorticity which does not travel with the fluid particles) which is manifested by a fixed circulation, Γ, about the body (cf. Lamb, §49).

In order to arrive at a solution in a multiply connected region the circulation Γ must be specified. The problem as put forth in Chapter II appears to be incomplete, therefore, since no value for Γ is determined, and since we have already seen that the problem is conceptually equivalent to a cylinder in a fluid region.

The resolution of this dilemma, and the justification for the matching scheme, rests on the fact that the total circulation about the cylinder has implicitly been set equal to zero by the matching itself, as can be seen from the following discussion.

The circulation, Γ, is defined as the integration of the tangential velocity around a closed loop.

$$\Gamma = \oint_C \vec{u} \cdot d\vec{\ell} \qquad \text{IV.42}$$

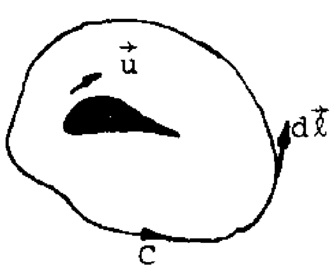

If the motion is irrotational and the loop C is drawn so that the region inside the loop is simply connected (i.e., free of any bodies), Γ must equal zero. If, on the other hand, the loop contains a body, the value of Γ cannot be determined from potential theory. (Its value for air foil problems is fixed by an empirical observation that the aft stagnation point moves to the trailing edge of the foil. This condition is called the Kutta condition - see L. Prandtl and O. G. Tienjtens, Figures 42-51.)

In order to fully specify the problem set up in Chapter II we must then specify the value of Γ as defined by IV.42 to be zero. The rationale for selecting this condition rather than involving the Kutta condition (saying the trailing edge is a stagnation point) is discussed in Chapter VI with regards to the experimental results.

Figure IV.3 shows the path of integration drawn about the cylinder a distance ε off the bottom.

The points 1, 2, 3, 4 are located in the "intermediate" regions. In order to perform the integration, split the loop C into four segments: C_{12}, C_{23}, C_{34} and C_{41}, where the segment referred to lies between the points designated by the subscripts. We may evaluate the integrals over each of these segments by noting that, for the line integral between points a and b,

$$\int_a^b \frac{\partial \phi}{\partial \ell}\, d\ell = \phi(b) - \phi(a)$$

We may therefore write

$$\oint \frac{\partial \phi}{\partial \ell} d\ell = \int_1^2 \frac{\partial \psi_L}{\partial \ell} d\ell + \int_2^3 \frac{\partial \tilde{\phi}}{\partial \ell} d\ell + \int_3^4 \frac{\partial \psi_R}{\partial \ell} d\ell + \int_4^1 \frac{\partial \overline{\phi}}{\partial \ell} d\ell$$

$$= \psi_{L2} - \psi_{L1} + \tilde{\phi}_3 - \tilde{\phi}_2 + \psi_{R4} - \psi_{R3} + \overline{\phi}_1 - \overline{\phi}_4 \qquad \text{IV.43}$$

where ψ_{L2}, ψ_{L1}, $\hat{\phi}_3$, etc. refer to the functions ψ_L, $\hat{\phi}$, etc. evaluated at the points 1, 2, 3 and 4 (Figure IV.4) respectively. We may designate these points in intermediate variables: $\overline{R}_1$, $\overline{R}_2$, $\overline{R}_3$ and R_4, and write, setting the expression for Γ equal to zero (eqn. IV.43),

$$0 = C_L + A \text{ Re } \cosh^{-1}(\frac{i\alpha\overline{R}_2}{\varepsilon}) - C_L - A \text{ Re } \cosh^{-1}(\frac{i\alpha\overline{R}_1}{\varepsilon}$$

$$+ B + A \ \ell n[\frac{\alpha\overline{R}_3}{2}] + J(1,0) - B - A \ \ell n[\frac{2}{\alpha\overline{R}_3}] - J(-1,0)$$

$$+ C_L + A \text{ Re } \cosh^{-1}(\frac{i\alpha\overline{R}_4}{\varepsilon}) - C_L - A \cosh^{-1}(\frac{i\alpha\overline{R}_3}{\varepsilon}$$

$$+ \phi_o(-1,0) + \phi_{so}(-1,0) + A \ [\ell n(\frac{\alpha\overline{R}_1}{2}) + H(-1,0)]$$

$$- \phi_o(1,0) - \phi_{so}(1,0) - A \ [\ell n(\frac{2}{\alpha\overline{R}_4}) + H(1,0)]$$

Here $\overline{R}_i$ is the radius measured in terms of the intermediate variables from the point (-1,0), for i = 1 and 2, and (1,0), for i = 3,4, to the point i. This expression becomes asymptotically valid for small gaps, so, as in the matching, it is appropriate to evaluate it in the lim $\alpha \to 0$ keeping

$\bar{R}_i$, $i = 1-4$, fixed. Taking this limit in the same manner as before we arrive at,

$$0 = A\left\{ -\ell n\left(\frac{2\alpha\bar{R}_2}{\varepsilon}\right) - \ell n\left(\frac{2\alpha\bar{R}_1}{\varepsilon}\right) + \ell n\left(\frac{\alpha\bar{R}_3}{R}\right) + J_R \right.$$

$$- \ell n\left(\frac{2}{\alpha\bar{R}_2}\right) - J_L - \ell n\left(\frac{2\alpha\bar{R}_4}{\varepsilon}\right) - \ell n\left(\frac{2\alpha\bar{R}_3}{\varepsilon}\right)$$

$$\left. + \ell n\left(\frac{\alpha\bar{R}_1}{2}\right) + H_L - \ell n\left(\frac{2}{\alpha\bar{R}_4}\right) - H_R \right\} + \phi_L - \phi_R$$

$$= A\left\{ 4\ell n\varepsilon - 8\ell n2 + H_2 - H_R + J_R - J_L \right\} + \phi_L - \phi_R$$

This yields the relationship

$$A = \frac{\phi_R - \phi_L}{4\ell n\varepsilon - 8\ell n2 + H_L - H_R + J_R - J_L} \qquad \text{IV.44}$$

which is precisely the same result as that found by matching (eqn. IV.37). If the circulation is specified Γ, the source strength becomes

$$A = \frac{\Gamma + \phi_R - \phi_L}{4\ell n\varepsilon - 8\ell n2 + H_L - H_R + J_R - J_L} \qquad \text{IV.45}$$

Thus the solution found by matching is indeed unique, and assumes a circulation of zero.

IV.5 Flow Impedance

The question may be raised as to what would be the effect of altering the gap geometry or the inside flow. The assumption that the cylinder wall has zero thickness, for example, is clearly violated in practice. The models used in the experimental tests had a wall thickness of 1/8", the same order as the gap width.

We may define for this purpose a gap "impedance" which will indicate the relative resistance of the gap to flow. In a direct analogy to electrical circuit theory, we can define this impedance as the potential difference across the gap required to induce a unit current (flow strength). If the point p_1 lies on one side of the gap and p_2 on the other, the impedance, I, may be defined as

$$I = \frac{\phi(p_2) - \phi(p_1)}{A} \qquad \text{IV.46}$$

If we consider the flow through a gap in a wall with zero thickness, for example, the impedance may easily be seen to equal

$$I_{gap} = \ln\frac{2r}{\varepsilon} + \ln\frac{2r}{\varepsilon} = 2\ln\frac{2r}{\varepsilon}$$

The im dance naturally increases with r (the distance from the ce r of the gap). The quantity of interest, however, is th part of the impedance which is independent of the distance We may term this the "characteristic" impedance of the gap, d may write from the above expression

$$I_{gap} = \text{characteristic impedance} = 2\ln\frac{2}{\varepsilon}$$

Any cha l exhibits a characteristic impedance. For example, the lculation of A in the preceding section may be thought of a n application of Kirchoff's law to the "circuit" circumscribing the cylinder (Figure IV.3) wherein the following impedances have been used:

Section	I^c
Outside Dome	$-2\ln 2 + H_L - H_R$
Inside Dome	$-2\ln 2 + J_R - J_L$
Gaps (2)	$-2\ln 2/\varepsilon$
Total	$4\ln \; - 8\ln 2 + H_L - H_R + J_R - J_L$

The first order potential across the cylinder $(\phi_R - \phi_L)$ may be thought of as a battery (a "current independent" voltage source) hooked into the loop pictured in Figure IV.4.

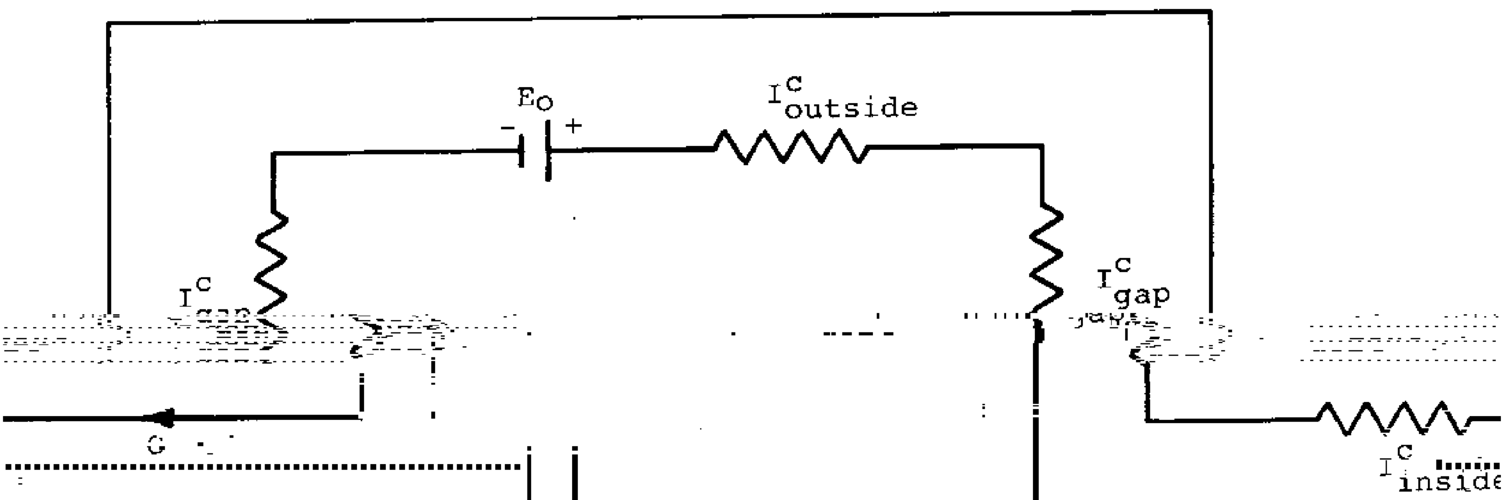

IV.4

THE CONTOUR INTEGRAL

FIGU

ELECTRICAL ANALOG

simple ohm's law for this case.

Kirchoff's law becomes

computed as

The current, C, may easily

$$\frac{E_o}{I^c_{inside} + 2I^c_{gap}} ,$$

$$C = \frac{}{I^c_{outsid}}$$

which is equivalent to eqn. IV.44. It should be noted that the introduction of a finite circulation is equivalent to stepping up the potential of E.

The purpose of elaborating here on the electrical analog is simply to aid in the conceptualization of the problem. It becomes easy to see now the effect of altering the geometry of the gap or the inside region.

For example, consider the problem of a cylinder of finite thickness. If the zero thickness cylinder represents the mean line of the finite thickness case, Figure IV.5 shows the situation.

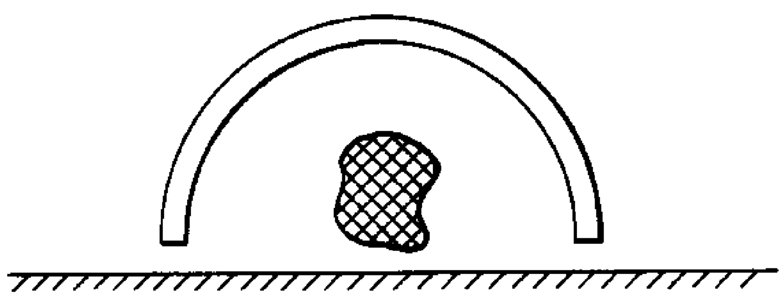

FIGURE IV.5

Provided the thickness of the cylinder wall is not too great, the main alteration of the previous result will appear in the characteristic impedance of the gaps.

I^c gap will be affected by a change in gap geometry. Whether it will increase or decrease depends on the exact nature of the inner flow, the type of singularities present at the edges, etc. Guincy (1971) has indicated that the extraordinary transmission properties of the submerged slit may be eliminated when finite thickness is taken into account. This suggests that I^c gap will indeed increase for realistic gaps.

The total impedance may also be increased by the presence of an obstacle in the inside region. Any obstruction to the flow will cause the streamlines to come closer together thus increasing the potential drop along a streamline needed to sustain a given flow.

impedance. If one of these impedances becomes infinite (complete flow obstruction), e source strength, A, becomes zero and the second order pe rbations disappear. If an obstruction blocks the flow thr gh the inside region, for example, we would have to consi r higher order terms to account for the gaps. The far fie solution for the inner problem suggests an $O(\varepsilon^2)$ dipole te

$$\lim_{\varepsilon \to 0} \mathrm{Re}\,[\mathrm{co} \ldots^{-1}(ir/\varepsilon)] = \ell n\left(\frac{2r}{\varepsilon}\right) - \frac{\varepsilon^2}{4r} + O(\varepsilon^4)$$

No attempt has een made to quantify the effect of the finite wall thickne . Photographs of the gap flow (Appendix F) indicate that ot r factors may be of overriding concern. These factors are d cussed in Chapter VI.

V. FORCES ON THE CYLINDER, REFLECTION COEFFICIENTS

Once the velocity potential both outside and inside the cylinder is known, the calculation of forces becomes straightforward. Bernoulli's equation for pressure in unsteady irrational flow may be linearized and written, noting the nondimensionalization introduced in chapter II (eqn. II. 4.4):

$$P(x,y,t) = -\frac{\partial\phi}{\partial t}(x,y,t)$$

$$= \mathrm{Re}[\ i\phi(x,y)] \qquad \text{V.1}$$

The total force on the cylinder will equal the integration of the net pressure over the cylinder's su face times the appropriate direction cosine. This neglects viscous influences.

Figure III. 1 (page) shows the cylinder and the coordinates system used. In the notation used before, we repeat the velocity potentials for the inside and outside regions respectively:

$$\tilde{\Phi}(\overline{r}) = B + A\ell n(r_L/r_R) \qquad \text{V.2.1}$$

$$\overline{\phi}(\overline{r}) = \phi_o(\vec{r}) + \phi_{so}(\vec{r}) + A[\ \ell n(r_L/r_R) + H(\vec{r})\ ] \qquad \text{V.2.2}$$

$J(\vec{r})$ has been set equal to zero, as it must for the semi-circular cylinder (Chapter III). A computer program has been written to compute $\phi_o(\vec{r})$, $\phi_{so}(\vec{r})$ and $H(\vec{r})$ on the surface of the cylinder.

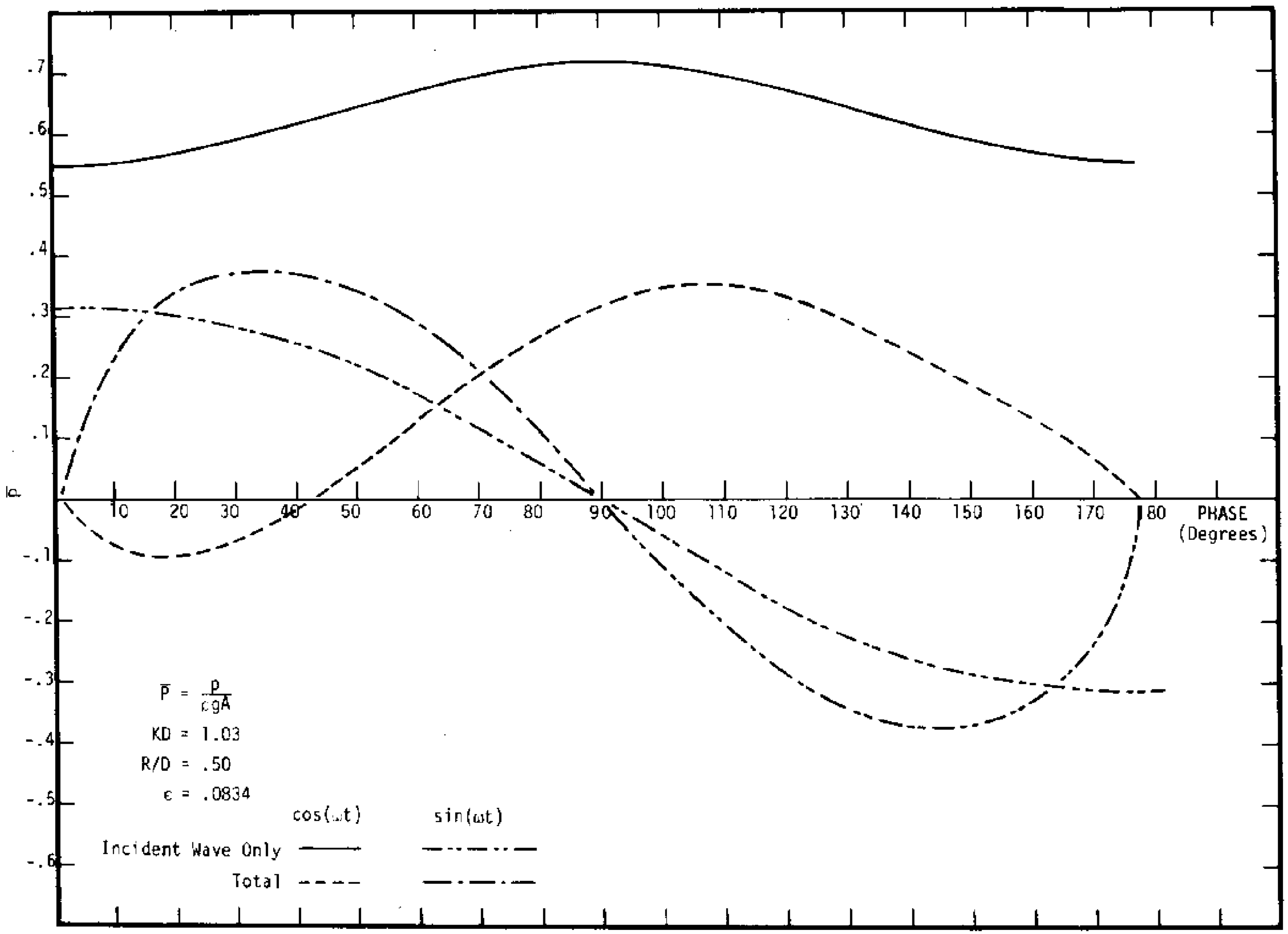

FIGURE V.1
TYPICAL COMPUTED PRESSURES

The net pressure on the cylinder is the difference of the pressure acting inside and that acting outside the cylinder. Thus, for a point (x_s,y_s) on the cylinder $(\vec{r}_s = x_s\hat{i} + y_s\hat{j})$, the net pressure becomes

$$p_{net}(x_s,y_s,t) = \text{Re } ie^{-i\omega t} [\ \tilde{\phi}(x_s,y_s) - \overline{\phi}(x_s,y_s)\ ]$$

or, writing in complex form

$$\tilde{\phi}(\overline{r}) = B + A\ln(r_R/r_L) \qquad \text{V.2.1}$$

$$\overline{\phi}(\overline{r}) = \phi_o(\vec{r}) + \phi_{so}(\vec{r}) + A[\ln(r_L/r_R) + H(\vec{r})] \qquad \text{V.2.2}$$

$J(\vec{r})$ has been set equal to zero, as it must for the semi-circular cylinder (Chapter III). A computer program has been written to compute $\phi_o(\vec{r})$, $\phi_{so}(\vec{r})$ and $H(\vec{r})$ on the surface of the cylinder.

The net pressure on the cylinder is the difference of the pressure acting inside and that acting outside the cylinder. Thus, for a point (x_s,y_s) on the cylinder $(\vec{r}_s = x_s\hat{i}+y_s\hat{j})$, the net pressure becomes

$$p_{net}(x_s,y_s,t) = \text{Re} \left[ie^{-i\omega t}\left(\tilde{\phi}(x_s,y_s) - \overline{\phi}(x\ ,y\ )\right)\right]$$

or, writing in complex form

$$p(x_s,y_s) = i\ [\tilde{\phi}(x_s,y_s) - \overline{\phi}(x_s,y_s)] \qquad \text{V.3}$$

The net pressure is taken positive in the direction away from the center of the cylinder. The horizontal and vertical forces on the cylinder may now be written as:

$$F_H = \frac{2i}{\pi}\int_0^{\pi}\cos\theta\left\{B - \phi_o(\vec{r}_s) - \phi_{so}(\vec{r}_s) + A[2\ln(r_{Rs}/r_{Ls}) - H(\vec{r}_s)]\right\}d\theta$$

V.4.1

$$F_V = \frac{2i}{\pi}\int_0^{\pi}\sin\theta\left\{B - \phi_o(\vec{r}_s) - \phi_{so}(\vec{r}_s) + A[2\ln(r_{Rs}/r_{Ls}) - H(\vec{r}_s)]\right\}d\theta$$

V.4.2

where $r_{Rs} = 2\sin\theta/2$

$r_{Ls} = 2\cos\theta/2$

The integrals in V.4 may be divided into those which must be evaluated numerically and those which can be evaluated analytically:

Numerically

$$\frac{2i}{\pi}\int_0^{\pi}\begin{Bmatrix}\cos\theta\\ \sin\theta\end{Bmatrix}[\phi_o(\vec{r}_s) + \phi_{so}(\vec{r}_s) + AH(\vec{r}_s)]\,d\theta$$

$$\simeq \frac{2i}{N}\sum_{n=1}^{N}\begin{Bmatrix}\cos\theta_n\\ \sin\theta_n\end{Bmatrix}\left\{\frac{\cosh(K\sin\theta_n)e^{i(K\cos\theta_n)}}{\cosh K_d} + \phi_{so_n} + AH_n\right\}$$

V.5.1

Analytically

$$\frac{2iB}{\pi}\int_0^{\pi}\begin{Bmatrix}\cos\theta\\ \sin\theta\end{Bmatrix}d\theta = \begin{Bmatrix}0\\ \frac{i2B}{\pi}\end{Bmatrix}$$

V.5.2

$$\frac{4iA}{\pi}\int_0^{\pi}\begin{Bmatrix}\cos\theta\\ \sin\theta\end{Bmatrix}\ln\left(\frac{r_{Rs}}{r_{Ls}}\right)d\theta = \frac{4iA}{\pi}\int_0^{\pi}\begin{Bmatrix}\cos\theta\\ \sin\theta\end{Bmatrix}$$

$\ldots$an$(\theta/2)\,d\theta$

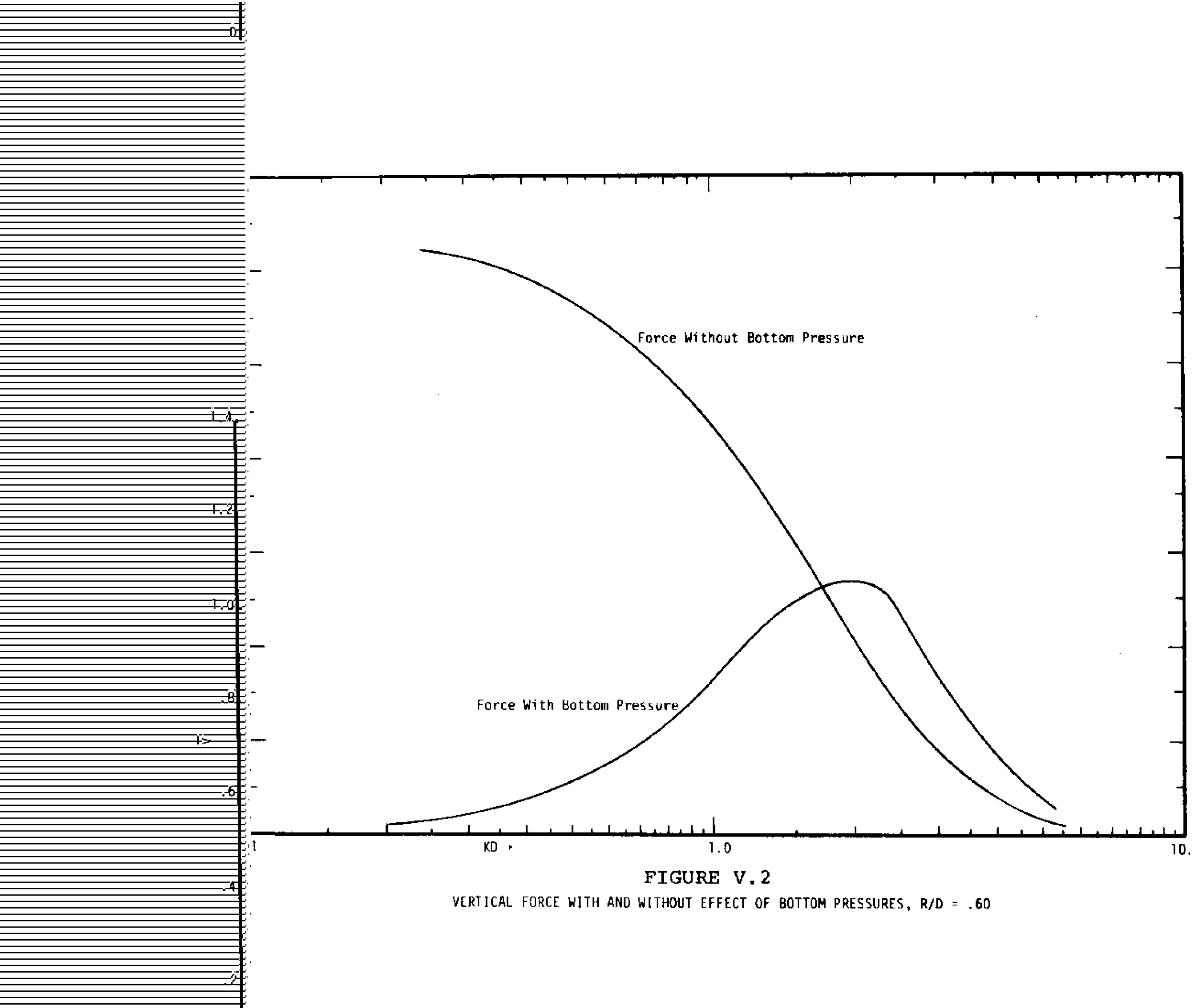

FIGURE V.2

VERTICAL FORCE WITH AND WITHOUT EFFECT OF BOTTOM PRESSURES, R/D = .60

$$= \left\{ \begin{matrix} 4iA \\ 0 \end{matrix} \right\} \qquad \text{V.5.3}$$

where

$$H_n = H(\cos\theta_n, \sin\theta_n)$$

$$\theta_n = \frac{\pi}{N}(n - 1/2)$$

$$n = 1, 2, \ldots, N-1, N$$

These expressions are evaluated in the computer program listed in Appendix F. It has been common practice among engineers calculating forces on ocean structures to use what is known as "Morison's formula" (Morison, 1951) to compute horizontal loads. By this formula, the (dimensional) horizontal force on an object is written (omitting the drag term):

$$F = \rho V C_M \frac{dU}{dt} \qquad \text{V.6}$$

where V = volume displaced by the object

C_M = a mass coefficient, a function of the geometry and period

dU/dt = acceleration of fluid particle at the center of the object when no scattering takes place (i.e., when the object is not there).

If the point (0,0) is taken as the center of the object,

$$\frac{dU}{dt} = -i \frac{gaK}{\cosh KD}$$

$V = \frac{\pi R^2}{2}$ (volume per unit length yielding force per unit length)

$$F = \frac{-i\rho gaK\pi R^2 C_M}{2 \cosh KD} \qquad \text{V.7}$$

Writing in non-dimensional form (eqn. II.4.5)

$$F_H = \frac{F}{\frac{\pi}{2}\rho g a R} = \frac{-iKRC_M}{\cosh KD} \tag{V.8}$$

The results of the horizontal force calculations are given in terms of C_M,

$$C_M = \frac{i\, F_H \cosh KD}{KR} \tag{V.9}$$

V.1 <u>A Simplified Theory</u>

Consider the case of $KD \ll 1$. In this case, the flow is uniform with depth, and we can replace the free surface (mathematically) by a rigid wall.

If, in addition, we stipulate that $R/D \ll 1$, the problem reduces to that of streaming flow past a cylinder with a slit (Figure V.3)

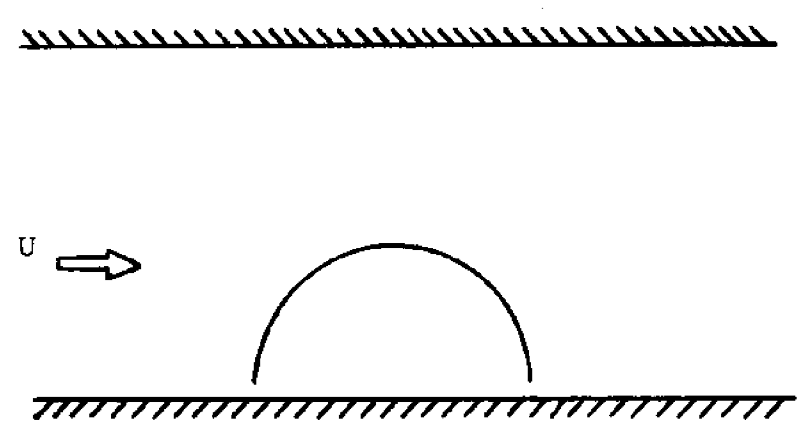

FIGURE V.3

FREE SURFACE REPLACED BY RIGID WALL

Now the incident flow is simply

$$\phi_o = U\ r\ \cos\ \theta,$$

where U is the maximum velocity.

As before we may write the total potential as

$$\text{outside cylinder:}\quad \phi^o = Ur\ \cos\ \theta(1 + R^2/r^2) + A\ln(r_L/r_R) \qquad \text{V.10}$$

$$\text{inside cylinder:}\quad \phi^i = A\ln(r_R/r_L) + B \qquad \text{V.11}$$

The exact first order flow is given by V.10. These solutions may be compared with those shown in Figure IV.3 (page). For this case, $H(\vec{r})$ is equal to zero since no wave terms exist. $J(\vec{r})$ is again zero, and we can apply IV.37 and IV.38 to find A and B.

where $Q(\theta)$ is found by comparing V.14 with V.10, V.11 and V.12:

$$Q(\theta) = 2R \cos\theta - \frac{8R\ln(r_R/r_L)}{4\ln\varepsilon - 8\ln 2} \qquad \text{V.15}$$

For zero gap, we get

$$F_H = 2\rho\pi R^2 \frac{dU}{dt} \qquad \text{V.16}$$

Comparing this with Morison's formula, eqn. V.6, we find $C_M = 2.0$. This is a classical result for a cylinder in unsteady motion.

The force with a finite gap will be

$$F_H = \rho R \frac{dU}{dt} \left\{ 2\pi R - \frac{8R}{4\ln\varepsilon - 8\ln 2} \int_0^{2\pi} \ln\left(\frac{r_R}{r_L}\right) \cos\theta \, d\theta \right\}$$

$$= \rho R \frac{dU}{dt} \left\{ 2\pi R + \frac{16\pi R}{4\ln\varepsilon - 8\ln 2} \right\} \qquad \text{V.17}$$

where use has been made of the relation

$$\ln(r_R/r_L) = \ln(\tan\theta/2)$$

and the integral has been integrated by parts.

From V.17 we can evaluate C_M for finite values of ε:

$$C_M = 2 - \frac{16}{4\ln\varepsilon - 8\ln 2} \qquad \text{V.18}$$

Table V.1 shows values of C_M computed for four values of ε. $C_M{}^*$ shown in the table is the value of C_M computed by the computer program (Appendix F) for

$$\bar{R} = \omega^2 R/g = .001$$

$$\bar{D} = \omega^2 D/g = .01$$

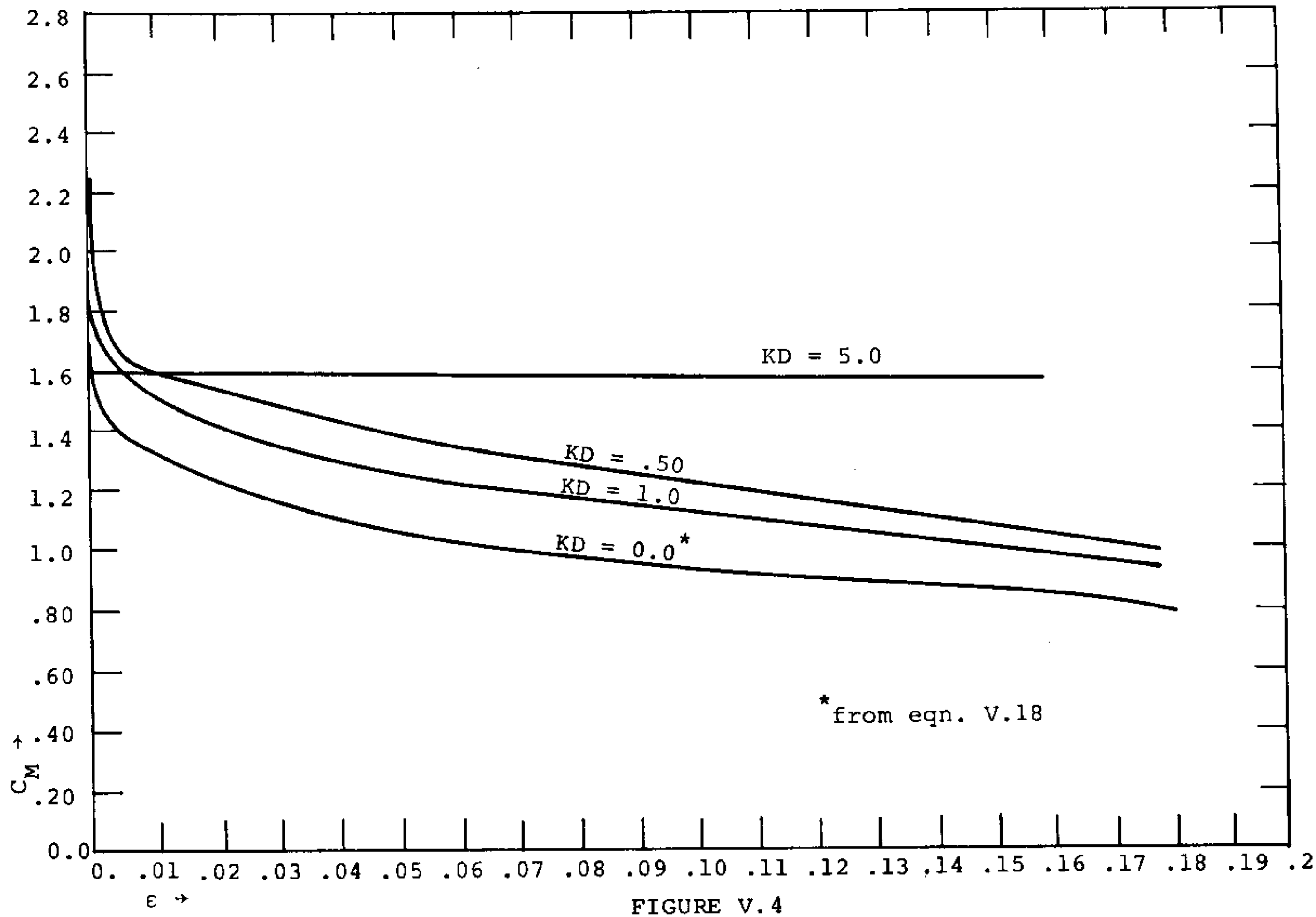

FIGURE V.4

MASS COEFFICIENT FOR DIFFERENT GAP WIDTHS, R/D = .5

TABLE V.1

C_M computed via eqn. V.18

C_M* computed by program

ε	C_M	C_M*
0.0	2.00	2.0
0.001	1.524	1.52
0.01	1.333	1.33
0.10	0.930	0.93

In addition to checking the calculations of the computer program, these results show the remarkable change in the added mass due to the gap. For an ε of only .001, the force coefficient is reduced 25% (the added mass by 50%!). This large drop will be discussed in more detail in the next chapter in conjunction with the experimental results.

The gaps do not affect the vertical force in this approximate theory. The source/sink potential is asymmetric, as is the first order potential. The vertical force, therefore, is zero for all values of ε, including $\varepsilon = 0$. A vertical force can only result when the free surface effect is included.

V.2 Reflection and Transmission Coefficient

Although the primary purpose of this thesis is to examine forces on a submerged object, the computation of transmission and reflection coefficients has also been carried out. These results may have direct engineering application in the design of breakwaters.

We have calculated the flow potential resulting from an incident wave from the left with a surface profile

$$\eta_o(x,t) = \cos(kx-\omega t)$$

or, if we separate the time dependence as in Chapter II, we may denote

$$\eta_o(x,t) = \mathrm{Re}\ [\eta_o(x)e^{-i\omega t}]$$

$$\eta_o(x) = e^{ikx} \qquad \text{II.6}$$

We may write the surface profile for downstream and for upstream from the cylinder as, respectively,

$$\eta_t(x) = \mathcal{T} e^{ikx} \qquad \text{V.19.1.}$$

$$\eta_r(x) = e^{ikx} + \mathcal{R}\ e^{-ikx} \qquad \text{V.19.2}$$

where $\mathcal{T}$ = transmission coefficient

$\mathcal{R}$ = reflection coefficient

To compute $\mathcal{T}$ and $\mathcal{R}$, the amplitude of the scattered wave for upstream and downstream must be computed. The surface elevation due to a potential, $\Phi(x,y,t)$ may be found from linear theory (cf. Newman, 1971, Chapter V)

$$\eta(x,t) = -\frac{1}{g}\,\frac{\partial\Phi(x,D,t)}{\partial t}$$

If $\overline{\Phi}(x,y)$ is the potential outside the cylinder in non-dimensional form and with the time dependence separated, we can write the non-dimensional surface elevation

$$\eta(x) = i\overline{\phi}(x,D) \qquad \text{V.20}$$

The reflection and transmission coefficients may then be written from V.19:

$$\mathcal{T} = ie^{-ikx} \left\{ \lim_{x\to\infty} \overline{\phi}(x,D) \right\} \qquad \text{V.21.1}$$

$$\mathcal{R} = e^{ikx} \left\{ \lim_{x\to-\infty} i\overline{\phi}(x,D) - e^{ikx} \right\} \qquad \text{V.21.2}$$

To evaluate $\lim\limits_{x\to\pm\infty} \overline{\phi}(x,h)$ we may once again utilize Green's theorem (eqn. III.7). If $\vec{\rho}$ is a point on the free surface (x,D), and $\vec{r}$ is a point on the cylinder surface (x_s,y_s), we may write

$$\overline{\phi}(\vec{\rho}) = \phi_o(\vec{\rho}) + A[\ell n(\rho_L/\rho_R) + H(\vec{\rho})]$$

$$- \frac{1}{2\pi} \int_C \phi_{so}(\vec{r}) \frac{\partial G}{\partial n} (\vec{\rho}|\vec{r})\, d\ell_r - \frac{1}{2\pi} \int_C G(\vec{\rho}|\vec{r}) \frac{\partial \phi_o(\vec{r})}{\partial n}\, d\ell_r$$

Taking the limit of both sides for $x \to \pm\infty$, we obtain

$$\lim_{x\to\pm\infty} \overline{\phi}(\vec{\rho}) = ie^{ikx} + A \lim_{x\to\pm\infty} H(x,D) \qquad \text{V.22}$$

$$- \frac{1}{2\pi} \int_C \phi_{so}(\vec{r}) \frac{\partial G^{\pm}}{\partial n} (\vec{\rho}|\vec{r})\, d\ell_r - \frac{1}{2\pi} \int_C G^{\pm}(\vec{\rho}|\vec{r}) \frac{\partial \phi_o(r)}{\partial n}\, d\ell_r$$

The asymptotic form of Green's function has been introduced:

$$G^{\pm}(\vec{\rho}|\vec{r}) = \lim_{x\to\pm\infty} G(\vec{\rho}|\vec{r}) \qquad \text{V.23}$$

$$= \frac{-i2\pi(K^2-\nu^2)\cosh Ky \cosh Ky_s\, e^{\pm iK(x-x_s)}}{K(K^2D - D + \nu)}$$

where $\nu = \omega^2 R/g$

The value of $\lim\limits_{x\to\pm\infty} H(x,D)$ may be found by setting, as we did in Chapter III,

$$\ln(\rho_L/\rho_R) + H(\vec{\rho}) = G(\vec{\rho}|\vec{\rho}_\ell) - G(\vec{\rho}|\vec{\rho}_r) + F(\vec{\rho}) \qquad \text{V.24}$$

$$\text{where} \quad \vec{\rho}_\ell = (-1,0)$$

$$\vec{\rho}_r = (1,0)$$

$F(\vec{\rho})$ is computed numerically over the surface of the cylinder (cf. Chapter III). Taking the limit of both sides of eqn. V.24 we find

$$\lim_{x\to\pm\infty} H(x,D) = \lim_{x\to\pm\infty} [G(x,D|-1,0) - G(x,D|1,0) + F(x,D)]$$

From V.23, taking $(x_s,y_s) = (\pm 1,0)$, we get, after some algebraic reduction,

$$\lim_{x\to\pm\infty} [G(x,D|-1,0) - G(x,D|1,0)]$$

$$= \frac{-4\pi(K^2-\nu)\cosh KD \sin 2K \, e^{\pm iKx}}{K(K^2D - D + \nu)} \qquad \text{V.25}$$

The limit of $F(\vec{\rho})$ must be found numerically from the values of $F(\vec{\rho})$ calculated in the determination of $H(\vec{\ })$.

Thus, we may write Green's theorem for $\lim\limits_{x\to\pm\infty} F(x,D)$ as

$$\lim_{x\to\pm\infty} F(x,D) = \frac{i(K^2-\nu^2)\cosh KD \, e^{\pm iKx}}{K^2D - D + \nu} \cdot \Big[(i \cosh Ky_s \cos\theta + \sinh Ky_s \sin \ F(x_s,y_s) + \frac{\cosh Ky_s}{K}\Big(\frac{\partial h_1(x_s,y_s)}{\partial n} + i\,\frac{\partial h_2(x_s,y}{\partial n} \ e^{\pm iKx_s} \Big] \, d\theta \qquad \text{V.26}$$

where

$$(x_s, y_s) = (\cos\theta, \sin\theta)$$

$$h_1(x_s, y_s) = \mathrm{Re}\,\{G(x_s, y_s|-1,0) - G(x_s, y_s|1,0)\}$$

$$h_2(x_s, y_s) = \mathrm{Im}\,\{G(x_s, y_s|-1,0) - G(x_s, y_s|1,0\ \}$$

$$\frac{\partial}{\partial n} = \cos\theta \frac{\partial}{\partial x_s} + \sin\theta \frac{\partial}{\partial y_s}$$

We may write the reflection coefficient in terms of integrals which must be evaluated numerically.

$$\mathcal{R} = \frac{(K^2-1)\cosh KD}{Q}\left\{\int_0^\pi e^{iKx_s}(i \cosh Ky_s \cos\theta + \sinh Ky_s)(\phi_{so}(\theta)\right.$$

$$+ e^{iKx_s} \frac{\cosh Ky_s}{\cosh KD})\, d\theta$$

$$+ iA\int_0^\pi e^{iKx_s} [(i \cosh Ky_s \cos\theta + \sinh KD \sin\theta)\, F(x_s, y_s)$$

$$\left. + A \frac{\cosh Kx_s}{K} \left(\frac{\partial h_1(x_s, y_s)}{\partial n} + i \frac{\partial h_2(x_s, y_s)}{\partial n}\right)]d\theta - \frac{4\pi \sin 2K}{K}\right\}$$

$$\text{where } Q = K\,D - D + \nu$$

The first term in brackets yields the reflection coefficient for the cylinder with no gap.

Values of $\mathcal{R}$ were computed by the same program used in the force computations (Appendix F). Figures V.4 and V.5 show the results of these computations along with the experimental points.

For the sake of comparison, the reflection coefficient is also computed using a formula derived by Mei (1969). Mei calculated the reflected wave by writing an integral equation similar to eqn. III.7 and solving it by means of a Born approximation (cf. Morse and Feshbach, V. II, p. 1073). This method utilizes as a first approximation to the flow the potential due to Rayleigh for waves over a gentle bottom slope. This potential is then inserted into the right-hand side of the integral equation to yield a second approximation.

A comparison of Mei's solution with the $\varepsilon = 0$ case (Figures V.5 and V.6) show the errors introduced in the assumption of small bottom slope for the case of a semi-circular cylinder.

The results of the reflection coefficient computations again reveal a remarkably large gap effect. The reflection coefficient is reduced by almost 50% (at $KD < 2.0$) for $\varepsilon = .0416$.

In the experiments, this corresponds to a gap width of 1/8" for a 3" cylinder. This result follows closely the results of Tuck in his solution to the transmission of water waves through a slit in a vertical wall (solved in Appendix A). Tuck's solution yielded transmission coefficients as high as .65 for a ratio of gap width to depth of submergence of 0.05 (Figure V.7).

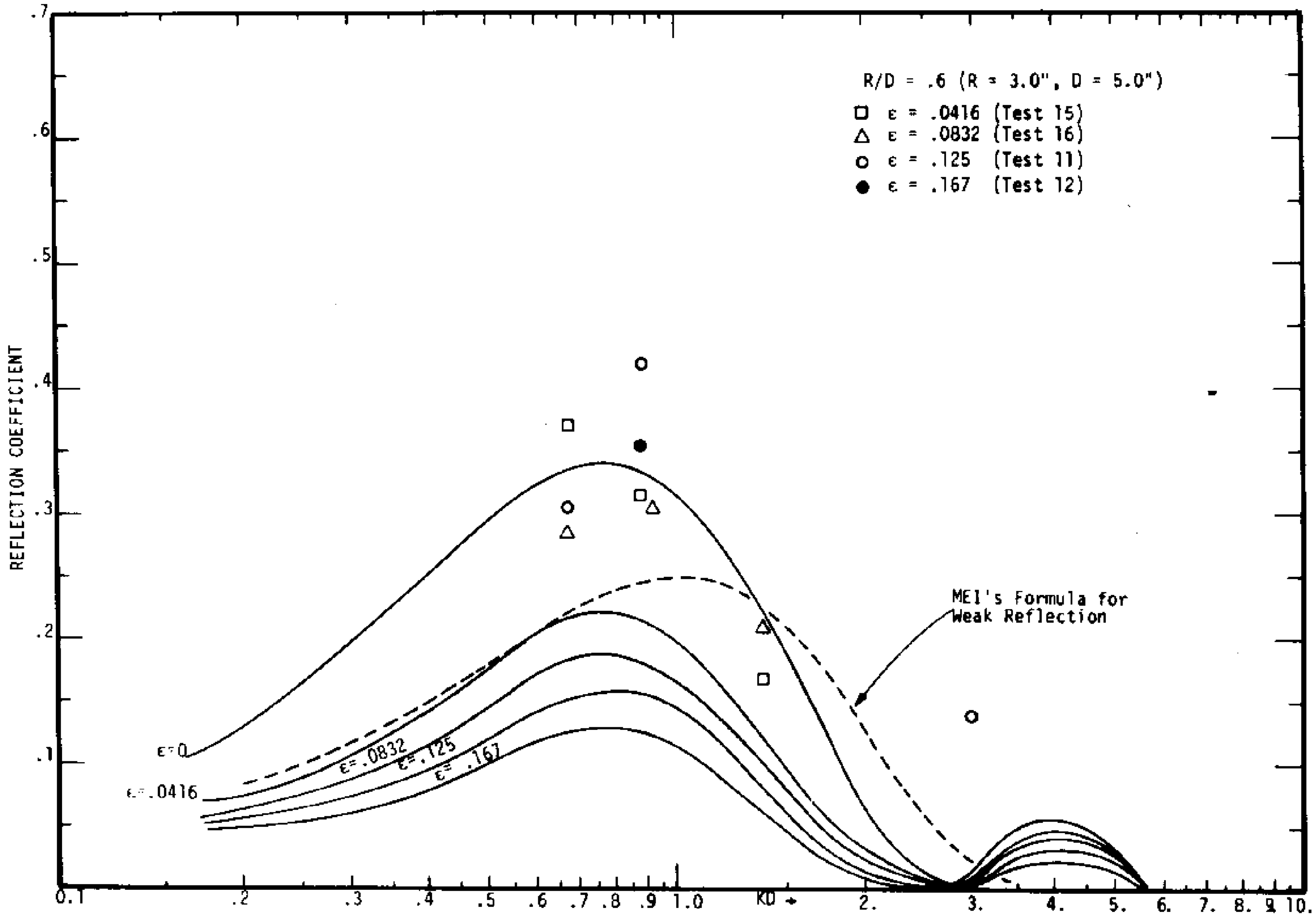

FIGURE V.5

REFLECTION COEFFICIENT FOR R/D = .60

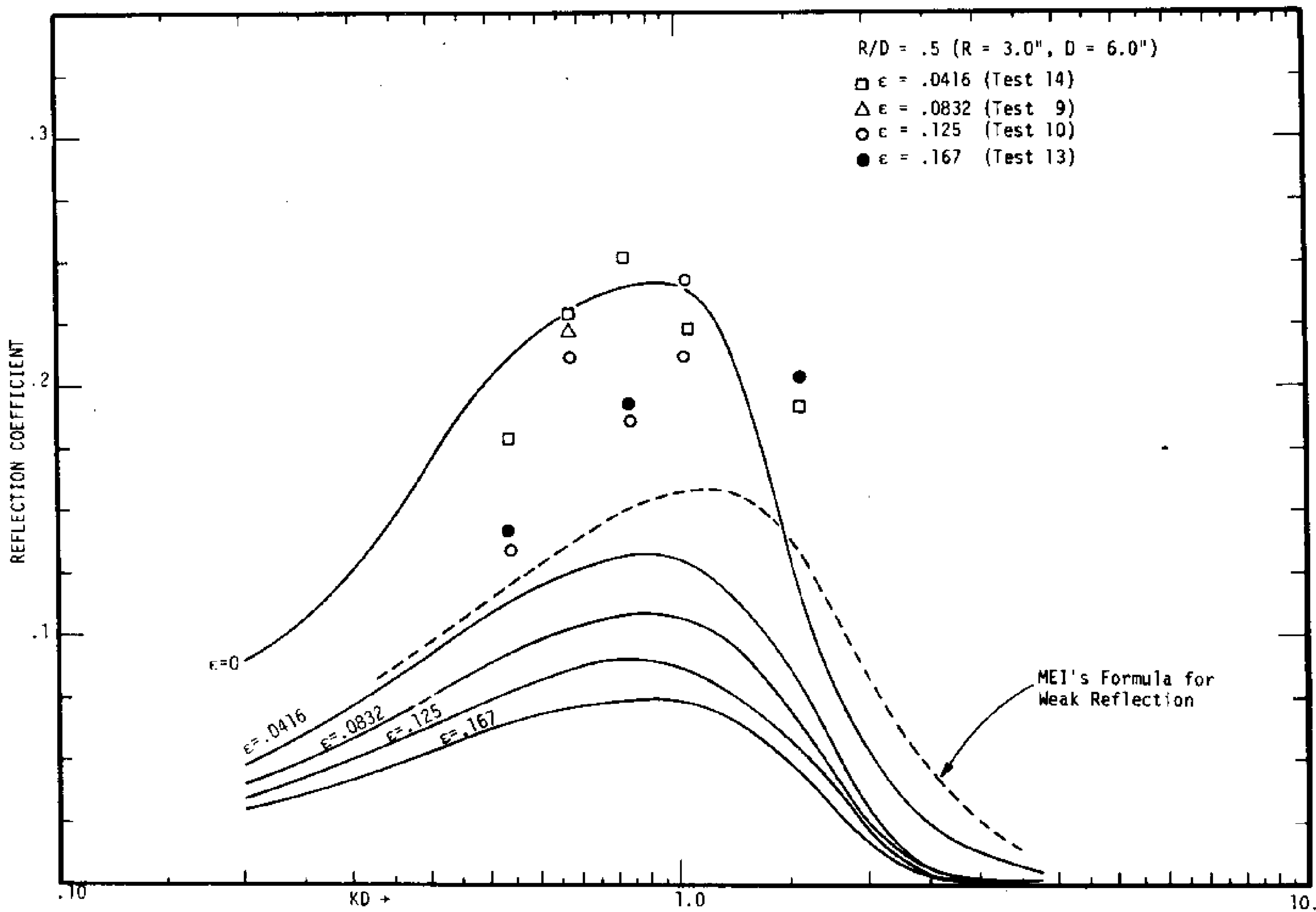

FIGURE V.6
REFLECTION COEFFICIENT FOR R/D = .5

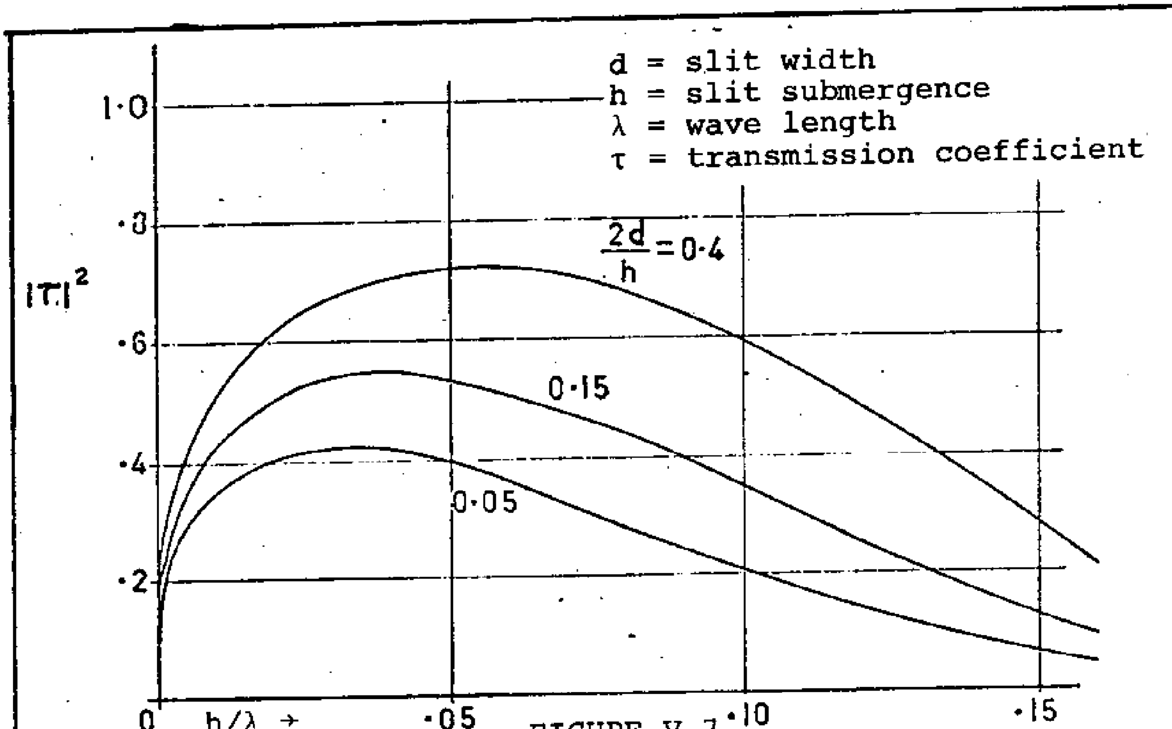

FIGURE V.7

TRANSMISSION OF WAVES THROUGH A SUBMERGED SLIT.
(from Tuck, 1971)

Tuck's results have been confirmed by the exact theory of Guiney (1971). The extraordinary transmission energy seems to be due largely to the unrealistic assumption of zero thickness.

In this thesis, an attempt is made to check the results experimentally. Figures V.5 and V.6 contain data points selected from some 60 test runs made at the M.I.T. Marine Hydrodynamics Laboratory (see Chapter VI). Considerable scatter in the data which appears to be linked to a faulty wave probe leave the reliability of the reflection coefficient data in doubt. There does, however, seem to be a definite trend for the data to take on higher values than those predicted by the present theory. This result would be expected if real fluid effects were considered since friction and flow separation would increas :he characteristic impedance of the gaps. Photographs of tl flow (Plates 7 through 12) do indeed show the creation of jet at the gaps, thus supporting the claim that real fluid ef cts are important at the gaps.

A further discussio of experimental results appears in Chapter VI.

V.3 Forces on Three-Di sional Structures

No attempt has bee ade here to solve the problem of flow past three-dimensi l objects (e.g., hemispheres). We may, however, draw so conclusions based on the results for the two-dimensional se reported herein.

It may be stated t, although no analytic solutions have been found, the nu ical solution to the first order "no gap" problem of flo ast submerged 3-dimensional shapes of arbitrary form is fa y well established (see e.g., Milgram and Halkyard, Garr n et al). These solutions arise out of a straightforwar umerical scheme for solving the Fredholm integral equat for the scattered wave. Where comparisons are possibl ith exact solutions, agreement has been excellent (Milgram d Halkyard calculated the added mass of a heaving sphere to within 3% of Havelock's value).

Such solutions are exactly equivalent to the first order, or "zero gap", solution found in Chapter III for the two-dimensional cylinder. There is no reason to believe that the qualitative effects of a gap about the base perimeter of a bottom mounted three-dimensional object would not be the same as those of the cylinder. We may therefore assume that the forces will be augmented by the effects of the ga n a manner similar to that found in the results of this the .

We have already noted (in Section IV.2) tha he inside region will experience a first order pressure in y case. This being true, we may make the following state ts about the forces on a three-dimensional object mounted ar the bottom.

1) The vertical force on the object will diffe rom that computed for no gap by an amount ranging fr zero to the full amount of the zero-gap force. Thi ugmenta-tion is mostly dependent on the wave period d is fairly insensitive to changes in the gap wi .

2) The horizontal force is augmented by an amo depen-dent on the wave period and the gap width. small gap will significantly affect the added mass of e object, but the effect may be less pronounced than t for the cylinder since the overall added mass (bloc e) of the three-dimensional object is less (.5 for a isphere vs. 1.0 for a cylinder).

Generally, therefore, the most crucial implication of this theory pertains to the vertical force. To examine this effect the Froude-Krylov force has been computed for a hemisphere with a radius of half the water depth. The Froude-Krylov force is that force computed assuming no scattered wave. The pressure is therefore

$$p(x,y,z) = \frac{e^{iKx} \cosh Ky}{\cosh KD}$$

which may be integrated over the surface of a hemisphere (times the respective direction cosine) to yield the total force.

F_r = non-dimensional force

$$= - \frac{2}{\pi \cosh KD} \int_0^{2\pi} d\theta \int_0^{\pi} d\phi [\sin \phi \cos \phi \, e^{iKx} \cosh Ky]$$

where $x = \cos \theta \sin \phi$

$y = \cos \phi$ V.28

The diffracted wave potential, and the resulting force, has also been computed for this case by Garrison. Both these forces are displayed in Figure V.7.

To account for the inside pressure the average of the outside pressures about the base of the hemisphere is computed:

$$\bar{p} = \frac{1}{2\pi} \int_0^{2\pi} p(x,0,z) \, d\theta = \frac{1}{2\pi \cosh KD} \int_0^{2\pi} e^{iK\cos\theta} \, d\theta$$

V.29

The total force, taking into account the inside pressure, may be calculated from V.28 and V.29:

$$F_{VT} = F_V + \pi\overline{p} \qquad \text{V.30}$$

(Note the non-dimensional radius is 1.0)

Garrison performed a series of experiments on a submerged hemisphere to check his diffraction theory. Garrison does not indicate the size of the hemisphere used in his tests, but he does state that it was supported a distance of 1/16" off the bottom of the wave tank. If the dome radius is taken to be 4" (a reasonable size in Garrison's wave tank), this corresponds to an ε of .0156.

In his tests, Garrison noted "As a consequence of the 1/16 inch clearance left between the model and channel floor the pressure inside the model did not remain constant but fluctuated as the waves passed."

In order to correlate his experimental results with the diffraction theory, Garrison measured the pressures at a point inside the dome. Under the assumption that the pressure throughout the interior of the dome is the same, the measured force was corrected by subtracting the effects of this internal pressure (i.e., eqn. V.30 solved for F_r). These corrected results are shown in Figure V.8.

Unfortunately, the uncorrected forces and the measured internal pressures are not available. Garrison has reported, however, that he has been successful in using the average pressure about the outside base of a tank to account for the inside pressure. Using this correction, he was able to show excellent agreement with experiments. Much of this data is proprietary.

It should be pointed out, however, that Garrison's experiment cannot be considered conclusive. Only one wave gage was used to measure the wave height. The gage was placed far enough upstream to be unaffected by the scattered wave, but any standing waves either from the beach or the tank walls would result in inaccurate wave height measurements. Also, in the case of horizontal forces, the load cells were connected to the dome with wire line diverted around a 5" ball bearing pulley. The pulley friction would adversely affect the force measurements.

Figure V.9 shows the results of Garrison's horizontal force measurements for two values of R/D (or, in Garrison's notation, h/a). The agreement with diffraction theory is excellent for this case, indicating that the effect of the gap is indeed small. The gap width for this case was a <u>nominal</u> 1/16". The dome was actually placed as close to the channel bottom as physically possible, so that these results may be considered a "zero-gap" result. Unfortunately, no data was taken for larger gaps.

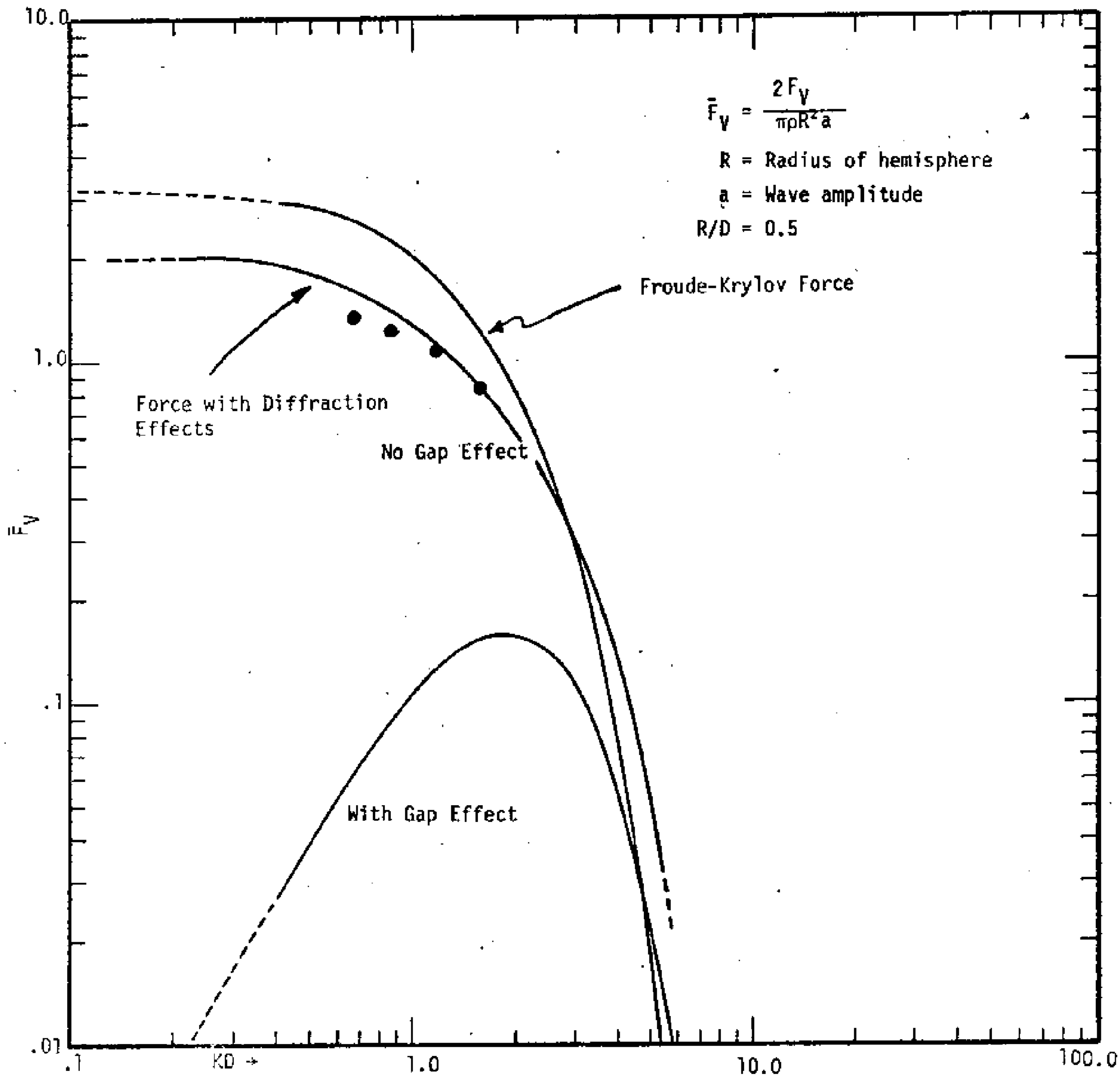

Figure V.8

VERTICAL FORCE ON HEMISPHERE WITH AND WITHOUT BOTTOM PRESSURES, INCLUDING DATA FROM GARRISON (1971)

Garrison's Experiments for
Submerged ... (Fro

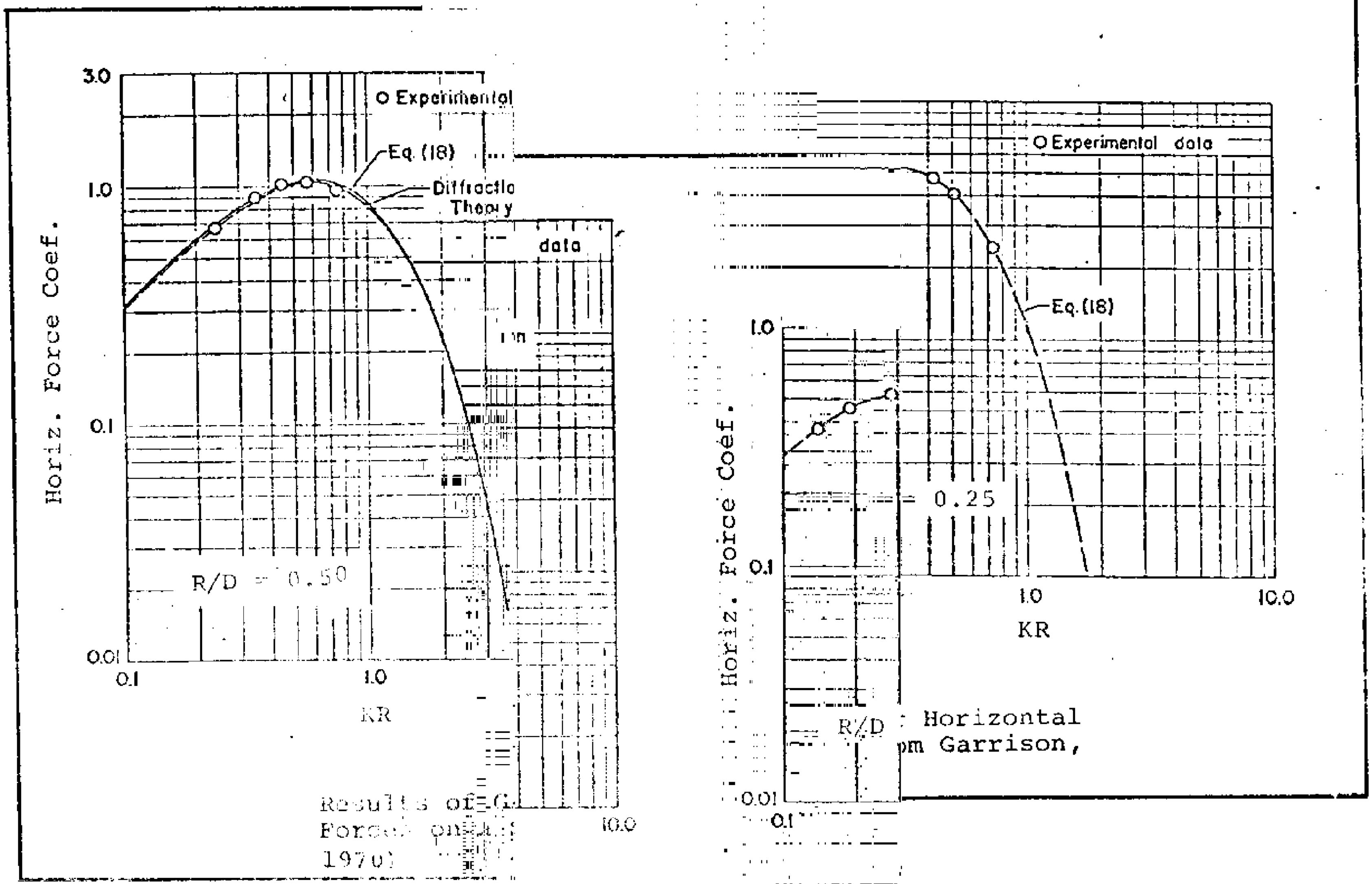

Results of G... Horizontal
Forces on ... om Garrison,
1970)

V.4 Experiments on Two-Dimensional Shapes

Herbich and Shank (1971) conducted an extensive series of experiments on various two-dimensional shapes, including a cylinder mounted close to the bottom. Their predicted forces based entirely on measured data are compared with forces predicted by the present theory in Figures V.10 and

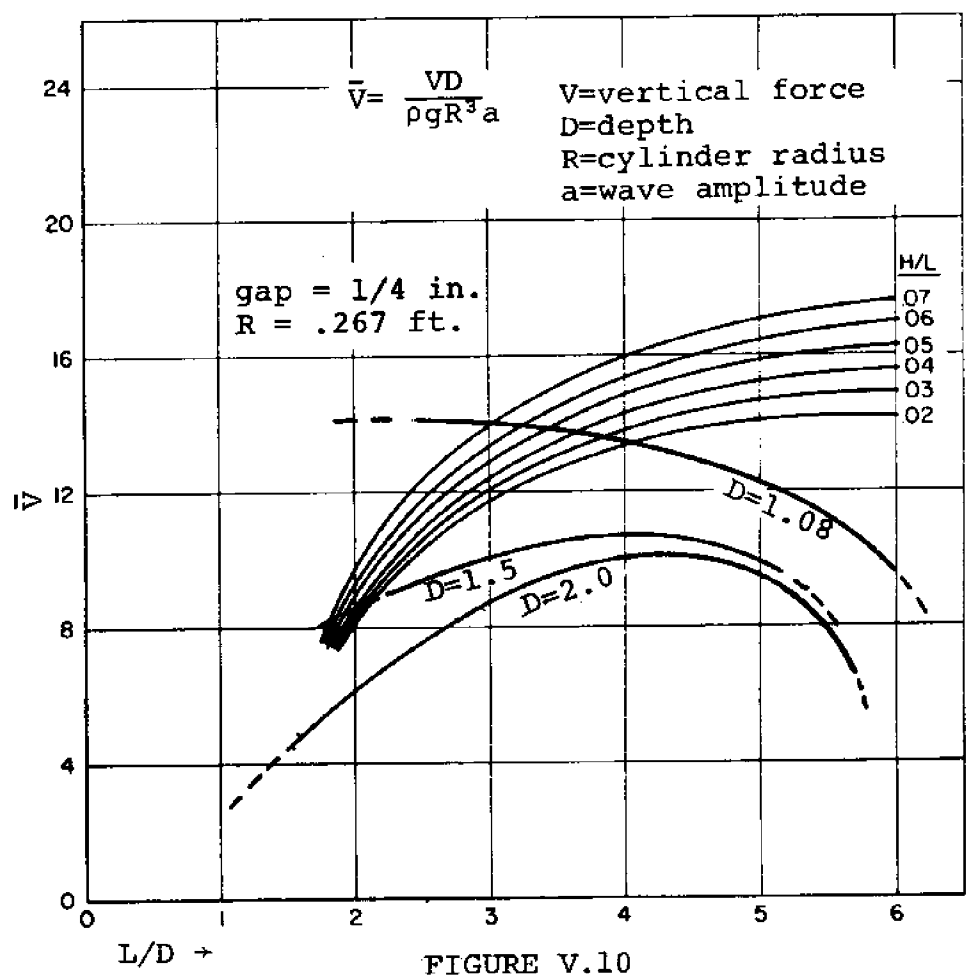

FIGURE V.10

COMPARISON OF VERTICAL FORCE COMPUTED FOR CYLINDER TO VALUES MEASURED BY HERBICH (FIG. 25) L = wave length, H = wave height, computed values marked with D.

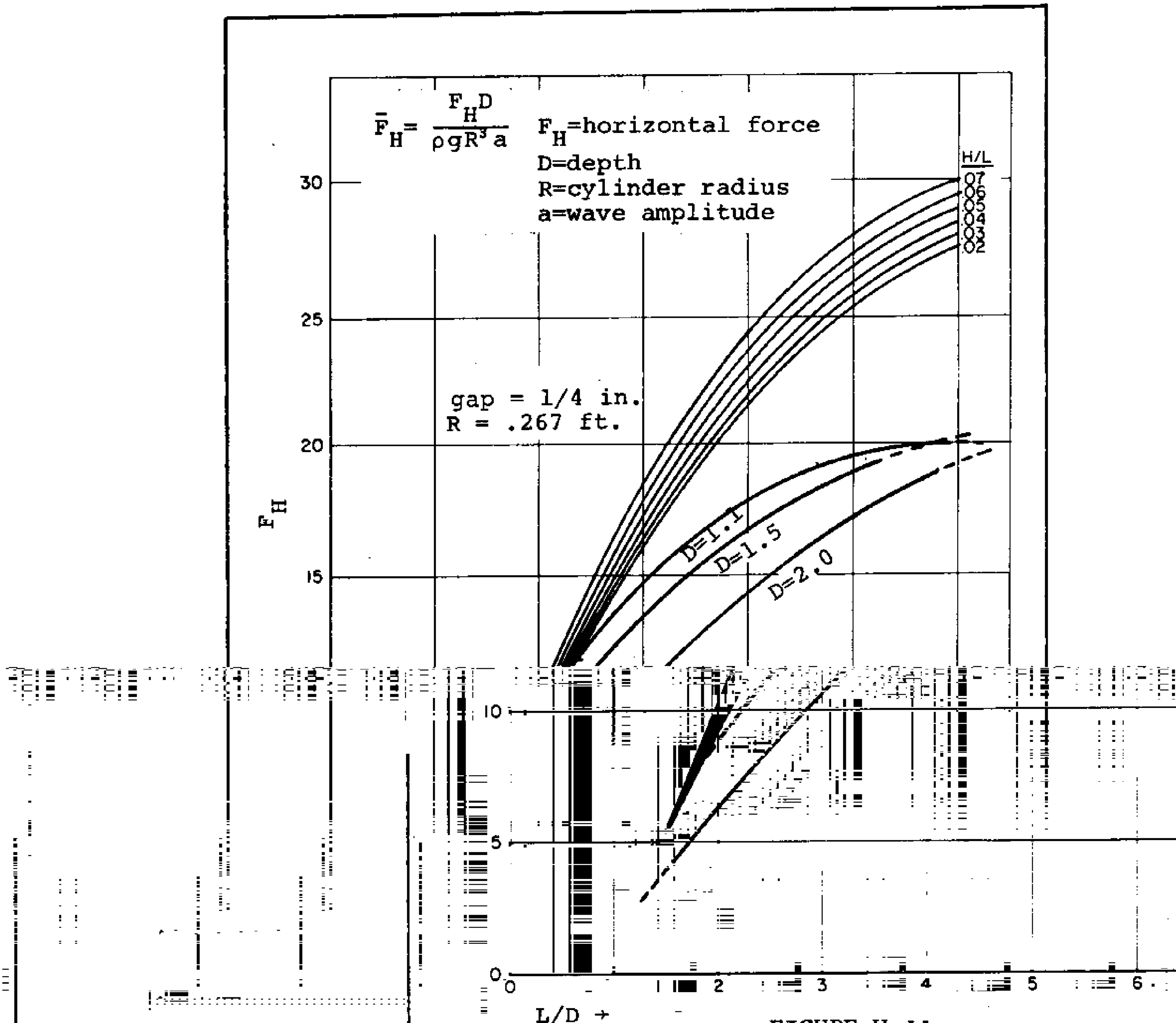

FIGURE V.11

COMPARISON OF HORIZONTAL FORCE COMPUTED FOR CYLINDER WITH VALUES MEASURED BY HERBICH (FIG. 24). L=wave length, H=wave height, computed values marked with D.

VI. EXPERIMENTAL INVESTIGATION

The theory presented in this thesis is predicated on the validity of the assumptions of linearized potential theory, namely, that viscous effects are negligible, that the flow is irrotational, that the fluid is incompressible, and that all the dependent variables are linearly dependent on the incident wave amplitude. In addition to these constraints, it should also be noted that the method used to derive the source/sink strength has not been rigorously justified, neither in this thesis nor in the literature, and may be open to question. The question arises, therefore, as to what exactly will be gained from model testing.

On the one hand, we may hope to duplicate the conditions in the test facility which most closely correspond to the assumptions of the theory, thus allowing us to judge from the test results the actual validity of the theory in the context of the given assumptions. On the other hand, we might choose to duplicate to whatever extent possible the actual conditions encountered during an engineering application (i.e., a full scale tank at sea) to observe the validity of the assumptions of linear theory themselves.

A scientist would select the first approach, and would scale his experiments accordingly. An average engineer might hope to perform the full scale tests so that he could have numbers to apply to his next design. A good engineer would take the first approach, while at the same time examining the phenomena excluded from the linear theory in order to determine the scale effects.

The problem with all this, of course, is that we are restricted to the budget and the test facilities at hand, and must be satisfied with that.

It should be noted, and we will discuss this in more detail in the following pages, that not all of the pitfalls of an experiment are connected with the hydrodynamic factors. The instruments and the methods of data reduction and analysis are wrought with dangers and must not be neglected in this discussion.

First we will turn to the hydrodynamic effects.

VI.1 Forces on Objects in a Real Fluid

The total force on an object in a moving fluid may be represented by the formula

$$F = \rho V C_M \frac{dU}{dt} + \frac{1}{2} \rho A_p C_D U|U| \qquad \text{VI.1}$$

where A_p is the area of the submerged object projected in the direction of the flow. This is the complete form of Morison's equation (Morison, et al, 1951), the first part of which was introduced in Chapter V (eqn. V.6).

The major failing of the Morison equation is that it does not take into account the variability of the coefficients C_M and C_D with time.

Some investigators have expressed the mass coefficient as a variable quantity. McNown and Wolf write F as

$$F = \rho V \left[\frac{d(kU)}{dt} + \frac{dU}{dt} \right] + \frac{1}{2} \rho C_D A_o U|U| \qquad \text{VI.2}$$

where k is the added mass.

This formulation agrees with the classic results of Stokes on the motion of pendulums in a liquid, namely, that the presence of viscosity and variable acceleration augment the mass coefficient.

Keulegan and Carpenter (1958) have justified Morison's formula by introducing a new coefficient, k', such that

$$\frac{d}{dt}(kU) = k' \frac{dU}{dt} \qquad \text{VI.3}$$

from which we get

$$C_M = 1 + k'$$

Clearly, the above expression (eqn. VI.3) is subject to doubt. Nevertheless, the Morison equation has been shown by experience to be useful in the prediction of forces, particularly in sinusoidal motion.

Keulegan and Carpenter attempted to answer the questions raised in this discussion by examining the forces on objects subjected to oscillatory motion.

A brief discussion of their approach is included here since their results lead to a justification of linear theory in relation to the present thesis.

Consider the forces on an object in a velocity field where U(t), the velocity, is

$$U(t) = -U_m \cos \omega t$$

If R is a characteristic length of the body (radius of a cylinder), the important physical parameters of the problem become

F	force (dependent variable)
ω	circular frequency of motion
R	length scale
U_m	velocity
ρ	fluid density
ν	fluid kinematic viscosity

Keulegan and Carpenter have arranged these parameters in non-dimensional units to arrive at the functional equation

$$\frac{F}{\rho U_m^2 R} = f\left(\theta, \frac{U_m T}{R}, \frac{U_m R}{\nu}\right) \qquad \text{VI.4}$$

where $\theta = \omega t$

$U_m T/R$ = "period parameter"

$U_m R/\nu$ = Reynolds number

Using the fact that F is periodic and that e flow from left to right is the reverse of that from right left [i.e., $F(\theta) = -F(\theta + \pi)$], the force may be written

$$\frac{F}{\rho U_m^2 R} = A_1 \sin \theta = A_3 \sin 3\theta + A_5 \sin 5\theta + B_1 \cos \theta + B_3 \cos 3\theta + \ldots \qquad \text{VI.5}$$

where the coefficients retain the dependence on $U_m T/R$ and $U_m R/\nu$ but are now constant in time.

Morison's equation may be written

$$\frac{F}{U_m^2 R} = \frac{VC_M \omega}{U_m R} \sin\theta - \frac{A_o C_D}{R} |\cos\theta| \cos\theta \qquad \text{VI.6}$$

This can be expanded by noting that

$$|\cos\theta| \cos\theta = a_o + a_1 \cos\theta + a_2 \cos 2\theta + \ldots$$

$$\text{where} \quad a_n = 0 \qquad n \text{ even}$$

$$a_n = (-1)^{n+1/2} \frac{8}{n(n^2-4)} \qquad n \text{ odd}$$

Then we have

$$\frac{F}{\rho U_m^2 R} = A_1 \sin\theta + A_3 \sin 3\theta + A_5 \sin 5\theta + \ldots$$

$$+ B_1' |\cos\theta| \cos\theta + B_3' \cos 3\theta + \ldots \qquad \text{VI.7}$$

$$\text{where} \quad B_1' = B_1/a_1$$

$$B_3' = B_3 - \frac{a_3}{a_1} B_1$$

Comparing VI.6 and VI.7, the following relationships may be established for C_M and C_D.

$$C_M(\theta) = \frac{U_m T}{\pi^2 R} [A_1 + A_3 + A_5 + 2(A_3+A_5) \cos 2\theta$$

$$+ 2A_5 \cos 4\theta + \ldots] \qquad \text{VI.8.1}$$

$$C_D(\theta) = -2B_1' + \frac{2}{|\cos\theta|}[2(B_3'-B_5') + 4(B_5'-B_3')\cos 2\theta$$

$$- 4B_5' \cos 4\theta + \ldots] \qquad \text{VI.8.2}$$

If C_M and C_D are constant, A_n and B_n' become zero for all $n > 1$. Keulegan and Carpenter used this fact to define the constant (or average) values of these coefficients to be

$$C_M^o = \frac{U_m T A_1}{\pi^2 R} \qquad \text{VI.9.1}$$

$$C_D^o = -2B_1' \qquad \text{VI.9.2}$$

They measured forces on cylinders in a slosh tank, Fourier analyzed the force output to obtain A_n, B_n from VI.5, and plotted C_M^o, C_D^o and the difference function

$$R = A_3 \sin 3\theta + A_5 \sin 5\theta + B_3' \cos 3\theta + B_5' \cos 5\theta \qquad \text{VI.10}$$

In this way Keulegan and Carpenter were able to assess the variability of C_M and C_D with time and determine the relative importance of Reynold's number and the period parameter on the coefficients A_n, B_n.

Working with cylinders ranging in diameter from .5 inches to 3.0 inches, they were able to conclude that the drag and inertial coefficients were effectively constant throughout the phase of the motion as long as $U_m T/R$ was sufficiently small. The actual variation in the values of C_M and C_D ...

$U_m T/R$ less than 20. There ... (VI.8) is negligible (<5%) fo

on Reynolds number. ... appears to be little dependen

This phenomenon can be explained by a simple physical explanation. The value $U_m T/R$ indicates the ratio of the distance traveled by a particle of fluid during a cycle to the radius of the cylinder:

$$U_m T/R = \pi \ell / R$$

where ℓ is the excursion distance of a fluid particle. Thus if $U_m T/R = 2\pi$, a fluid particle will just traverse the full diameter of the cylinder. Photographs of the flow indicate that no separation occurs for such small motion, and except for the effect of surface friction, one would expect potential theory (which predicts a constant C_M and $C_D \equiv 0$) to be valid.

It should be noted here that the results for a cylinder (as found by Keulegan and Carpenter) are not entirely sufficient to determine the relative real fluid effects for the submerged cylinder with a gap. First of all, no account was taken in Keulegan and Carpenter's work of the free surface effect (their models were placed in a deep tank). This will be discussed in the next section. Secondly, and most importantly, the flow through the gaps is more characteristic of the flow past a flat plate than flow past a cylinder. In this case the occurrence of ly shedding and flow separation is almost inevitable. In fa , photographs of flow past flat plates taken by Keulegan and ırpenter indicate that eddies form almost immediately upor ıe onset of motion. This is indeed the case for the gap flow as well, as may be observed from photographs of dye streaks in the area of the cylinder (Plates 7 through 10). Plate 10 shows the formation of an eddy for $U_mT/R = .092$.

The drag coefficient for plates is considerably larger than that for cylinders. C_D takes on values of greater than 10, for example, for a flat plate (flow incident) at small values of U_mT/R (R for the plate is taken as the plate length). We may be comforted by the fact, however, that even at such large values of C_D, the total drag force is still much less than the total inertial force. If, for example, (cf. Wiegel, 1964, Chapter 11)

$$\frac{C_M V}{C_D A_o a} = \frac{\pi C_M R}{2C_D a} >> 1$$

we may neglect drag forces entirely. Taking R = 3.0", a = 0.1", $C_M = 2.0$ and $C_D = 5.0$ we get

$$\frac{\pi C_M R}{2C_D a} = 19$$

This ratio is probably much larger since the selection of $C_D = 5.0$ seems unrealistically large. The results presented in Appendix G indicate that less than 10% of the total force comes from drag.

VI.2 Considerations in the Analysis of Test Data

We have stated that, for U_mT/R small, we may adopt the Morison equation for the description of forces on the submerged cylinder. This statement should be qualified for the case of our cylinder with a gap. Equation VI.6 cannot easily be applied to the vertical forces since fluid accelerations are so small in the vertical direction. In particular, the vertical force is due primarily to the hydrodynamic head associated with the wave crest passing over the object. It is difficult to calculate the "drag" in the vertical direction, although one interpretation might be that it consists of the force due to the $\frac{1}{2}\rho U^2$ pressure from Bernoulli's equation. In this case the "drag" would be in phase with the pressure force. At any rate, no attempt is made here to associate a mass coefficient with the vertical force.

We have already mentioned that the Morison equation, and Keulegan and Carpenter's analysis, did not account for the free surface effect. Specifically, it should be noted that a component of the inertial force will arise from the scattered waves. These waves are generated when a large amount of the flow from the incident waves is diverted, generating outwardly progressing waves. The scattered waves, therefore, produce pressures in phase with the incident wave velocity (since this is when the most fluid is diverted). A modification of Morison's formula to take this into account would appear as

$$F = C_1 \frac{dU}{dt} + \frac{1}{2} \rho A_o C_D U|U| + C_2 U \qquad \text{VI.11}$$

For our purposes, however, it is not necessary to use the expression in this form. Instead, we will treat C_M and U in Morison's equation as complex quantities and take the real part of the expression to obtain the phase of the inertial force, i.e.

$$\text{phase} = \tan^{-1} \left[\frac{C_2 U}{C_1 (dU/dt)} \right]$$

We also wish to non-dimensionalize with respect to the incident wave amplitude rather than the velocity. Write the incident wave

$$\eta_{in}(x,t) = \text{Re} \, [a_1 e^{iK_1 x} e^{-i\omega t}$$

$$+ a_2 e^{iK_2 x} e^{-i2\omega t} + a_3 e^{iK_3 x} e^{-i3\omega t} + \ldots] \qquad \text{VI.12}$$

where a_1 a_2, a_3 ... are complex numbers representing the wave amplitude of the respective Fourier component of the wave.

K_n is the wave number corresponding to the frequency $n\omega$, i.e., the solution to $K_n \tanh K_n D = n^2\omega^2/g$

In the following discussion, we shall adopt the notation used previously, i.e., $\theta = \omega t$. Also, as in the previous chapters the real part of the expressions will be assumed the physical quantity of interest.

The horizontal and vertical forces, and the moment on the object may be written respectively,

$$F_H = \sum_{n=1}^{N} H_n e^{-in\theta} \qquad \text{VI.13.1}$$

$$F_V = \sum_{n=1}^{N} V_n e^{-in\theta} \qquad \text{VI.13.2}$$

$$M = \sum_{n=1}^{N} M_n e^{-in\theta} \qquad \text{VI.13.3}$$

The reflection coefficient of the beach in the wave tank proved to reach values of .19. Thus it is necessary to account for waves impinging on the object from both directions. Figure VI.1 shows the situation. The incident waves

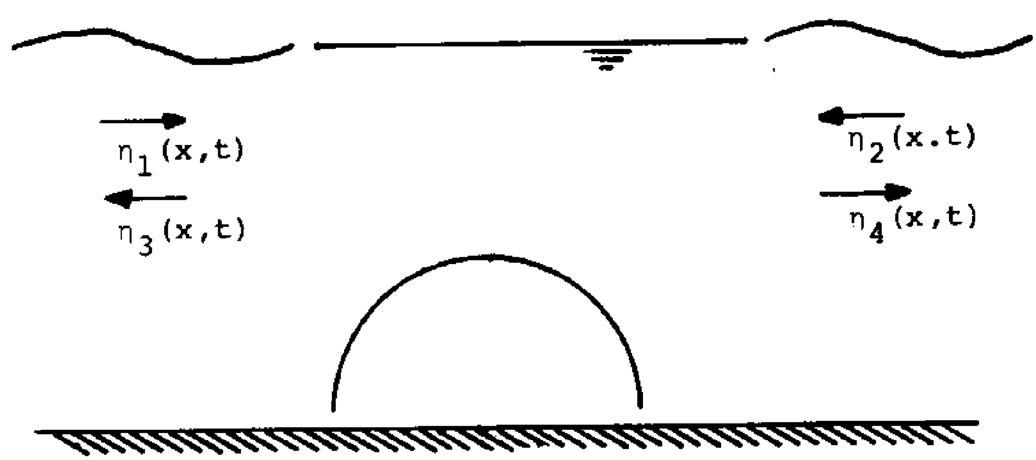

FIGURE VI.1
ASYMPTOTIC FORM OF WAVES IN TANK

coming from the left and the right are both reflected and transmitted by the cylinder. We may write

$$\eta_1(x,t) = \sum_{n=1}^{N} a_{1n}\, e^{iK_n x}\, e^{-in\theta} \qquad \text{VI.14.1}$$

$$\eta_2(x,t) = \sum_{n=1}^{N} a_{2n}\, e^{-iK_n x}\, e^{-in\theta} \qquad \text{VI.14.2}$$

$$\eta_3(x,t) = \sum_{n=1}^{N} a_{3n}\, e^{-kK_n x}\, e^{-in\theta} \qquad \text{VI.14.3}$$

$$\eta_4(x,t) = \sum_{n=1}^{N} a_{4n}\, e^{iK_n x}\, e^{-in\theta} \quad . \qquad \text{VI.14.4}$$

Let us define the respective reflection and transmission coefficients as

$$R_{Ln} = a_{3n}/a_{1n} \ (\text{with } a_{2n} = 0) \qquad \text{VI.15.1}$$

$$T_{Ln} = a_{4n}/a_{1n} \ (\text{with } a_{2n} = 0) \qquad \text{VI.15.2}$$

$$R_{Rn} = a_{4n}/a_{2n} \ (\text{with } a_{1n} = 0) \qquad \text{VI.15.3}$$

$$T_{Rn} = a_{3n}/a_{2n} \ (\text{with } a_{1n} = 0) \qquad \text{VI.15.4}$$

These definitions are consistent with linear theory, which assumes no harmonic generation by the obstacle or through shallow water effects (see, e.g., remarks by C. C. Mei at the M.I.T. Hydrodynamics Laboratory seminar of September 27, 1971). It should be pointed out that some nonlinearities are to be expected, particularly for the high frequency waves which are quite steep. In these cases the representation of the coefficients above would have to include cross-reflection and cross-transmission coefficients, for example,

$$R_{Lmn} = a_{3m}/a_{1n}$$

$$(\text{with } \eta_2(x,t) = 0,\ a_{1i} = 0,\ i \neq n)$$

The generation (or amplification) of certain harmonics was observed in a few cases. This appeared as 2nd harmonic "noise" superposed on the long waves downstream from the object. No attempt has been made to analyze this harmonic distortion, but the complete record of wave harmonics is included in Appendix G for the use of anyone interested in pursuing that study.

In the context of linear theory, therefore, we take note of the fact that

$$R_{Rn} = \bar{R}_{Ln} \qquad \text{VI.16.1}$$

$$T_{Ln} = T_{Rn} \qquad \text{VI.16.2}$$

where $\bar{R}_{Ln}$ denotes the complex conjugate of R_{Ln}.

The proof of VI.16 is given by Newman (1965) following the method of Kreisel (1949).

VI.2.1 <u>Horizontal Forces</u>

Given the incident waves $\eta_1(x,t)$ and $\eta_2(x,t)$ from VI.14, the velocity potential may be written (in dimensional form):

$$\Phi(x,y,t) = \Phi_1(x,y,t) + \Phi_2(x,y,t)$$

$$= -\frac{ig}{\omega} \sum_{n=1}^{N} \frac{[a_{1n}e^{iK_nx} + a_{2n}e^{-iK_nx}]}{\cosh K_nD} \cosh K_ny e^{-in\theta} \qquad \text{VI.17}$$

In Morison's formula, take U to be the horizontal velocity at the sea bed (the axis of the cylinder) so that

$$U(t) = \frac{\partial}{\partial x} \Phi(0,0,t)$$

$$= \frac{g}{\omega} \sum_{n=1}^{N} \frac{[a_{1n} - a_{2n}]}{\cosh K_n D} K_n e^{-in\theta} \qquad \text{VI.18}$$

from which we may identify

$$U_n = \frac{gK_n(a_{1n} - a_{2n})}{\omega \cosh K_nD}$$

The acceleration may similarly be written

$$\frac{dU(t)}{dt} = \sum_{n=1}^{N} \frac{dU_n}{dt} e^{-in\theta} \qquad \text{VI.19}$$

$$\frac{dU_n}{dt} = - in\omega U_n$$

Now Morison's equation may be written

$$F_H(t) = -\frac{i\rho g\pi R^2}{2}\sum_{n=1}^{N}\frac{nC_{Mn}K_n(a_{1n}-a_{2n})e^{-in\theta}}{\cosh K_nD}$$

$$+\frac{\rho g^2K}{\omega^2}\left|\sum_{n=1}^{N}\frac{C_{Dn}K_n(a_{1n}-a_{2n})e^{-in\theta}}{\cosh K_nD}\right|\sum_{n=1}^{N}\frac{C_{Dn}K_n(a_{1n}-a_{2n})e^{-in\theta}}{\cosh K_nD}$$

$$\simeq \sum_{n=1}^{N}\left(\frac{-i\rho g\pi R^2}{2}\right)\left[\frac{nC_{Mn}K_n(a_{1n}-a_{2n})}{\cosh K_nD}\right]e^{-in\theta} \qquad \text{VI.20}$$

where the drag coefficient has been assumed to be zero, as it should for

$$\frac{U_mT}{R} = \frac{2\pi g}{\omega^2R}\sqrt{\sum_{n=1}^{N}\frac{K_n^2(a_{1n}-a_{2n})^2}{\cosh^2K_nD}} < 5.$$

An examination of the test records, Appendix , reveals that this is indeed the case.

Turning to VI.20 we can identify the terms of VI.13 as

$$H_n = \frac{-g\ R}{2}\left[\frac{nC_{Mn}K_n(a_{1n}-a_{2n})}{\cosh K_nD}\right]$$

from which

$$C_{Mn} = \frac{i2H_n}{\rho g\pi R^2nK_n(a_{1n}-a_{2n})} \qquad \text{VI.21}$$

This value of C_{Mn} is computed from the reduced test data. Its value and phase for $n = 1$ is given for tests 9-17 in Table VI.5. Other harmonic values may be found in the analysis program output listed in Appendix G.

VI.2.2 Vertical Forces

The measured values of the vertical force were normalized with respect to the superposed incident wave amplitudes over the center of the cylinder. Using the normalization of II.4.5, the normalized force may be written

$$\bar{F}_V = \sum_{n=1}^{N} \bar{V}_n e^{-in\theta}$$

$$\bar{V}_n = \frac{2V_n}{\pi\rho g R(a_{1n}+a_{2n})} \qquad \text{VI.23}$$

These values are reproduced for the first harmonic in Table VI.4 for higher harmonics in the computer listings, Appendix G.

VI.2.3 Moments

The theoretical value of the moment about the axis of the cylinder, for linear theory, is zero. This is the case since all pressures act normal to the cylinder surface and therefore act along a radius line. All forces are directed through the axis of the cylinder which therefore cannot experience a moment.

Figure VI.2 shows the schematic configuration of the cylinder, its supporting struts and the load cells.

The moment about the point at which the line of action of the horizontal force intersects the vertical centerline is

$$M = (F_1+F_2)(y_1-\Delta) + F_4(y_2-\Delta) \qquad \text{VI.23}$$

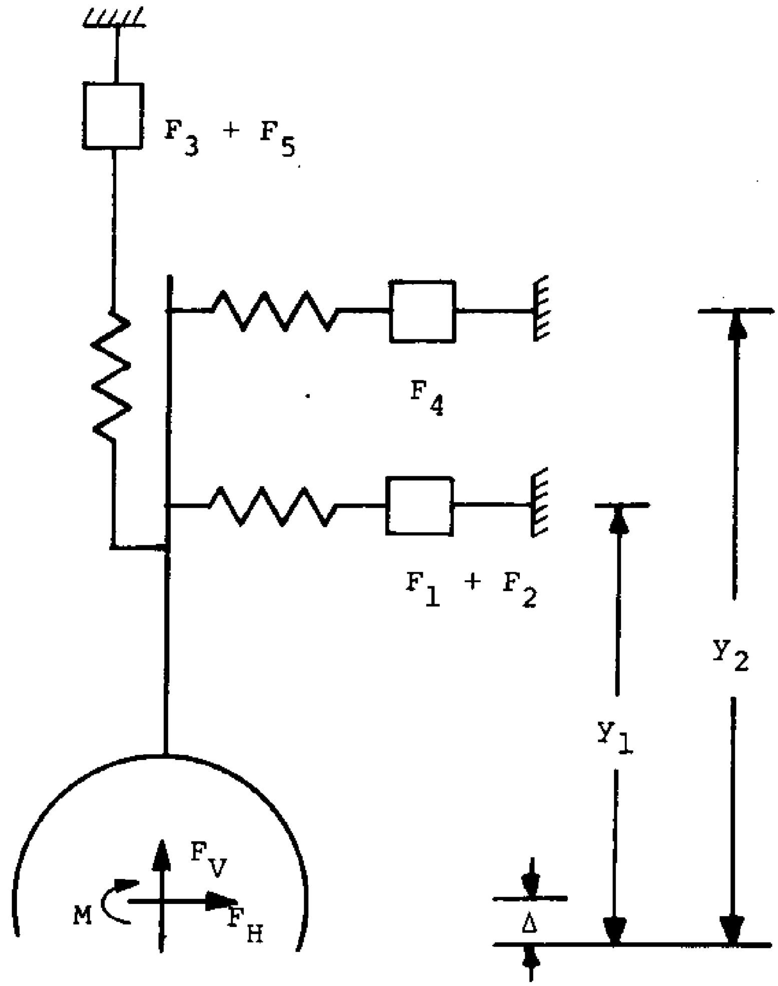

FIGURE VI.2

SCHEMATIC OF CYLINDER AND LOAD CELLS

where Δ = the distance above the bottom through which the horizontal force acts.

Notice that the two terms of VI.23 will generally be of opposite sign but nearly equal magnitude. M is expected to be relatively small (theoretically zero) so the percentage error in M for small errors in F_1, F_2 and F_4 will be large. Taking the moment about the point $(0,y_1)$ yields

$$M = F_4(y_2-y_1) + F_H(y_1-\Delta) \qquad \text{VI.24}$$

In this case we have less sensitivity of M to numerical errors in the terms on the right.

The moment is normalized with respect to the incident wave from the left:

$$\bar{M}_n = \frac{M_n}{\frac{1}{4}\rho\pi R^2 a_{1n}} \qquad \text{VI.25}$$

The calculation of these quantities from the test data will be discussed in Section VI.4.

VI.3 Experimental Test Setup

Figure VI.3 shows a schematic drawing of the test facilities including the wave paddle, wave probes, dynamometer and cylindrical model. Plate 1 shows the entire test setup, including the instrumentation rack. Plate 2 shows the model in position for a test. Plate 3 shows the cylinder out of water. Plate 4 shows a closeup of the dynamometer, including force blocks 3 and 5 (in the foreground), the load carrying members and the stiffening strip for force block #1 (in the lower right). Plate 5 is a view of the wavemaker from above, and Plate 6 shows a view of the waterline of the tank looking upstream from the position of the model.

The equipment for this test is described in a thesis by Kern (1971). The following will describe the main features of the equipment.

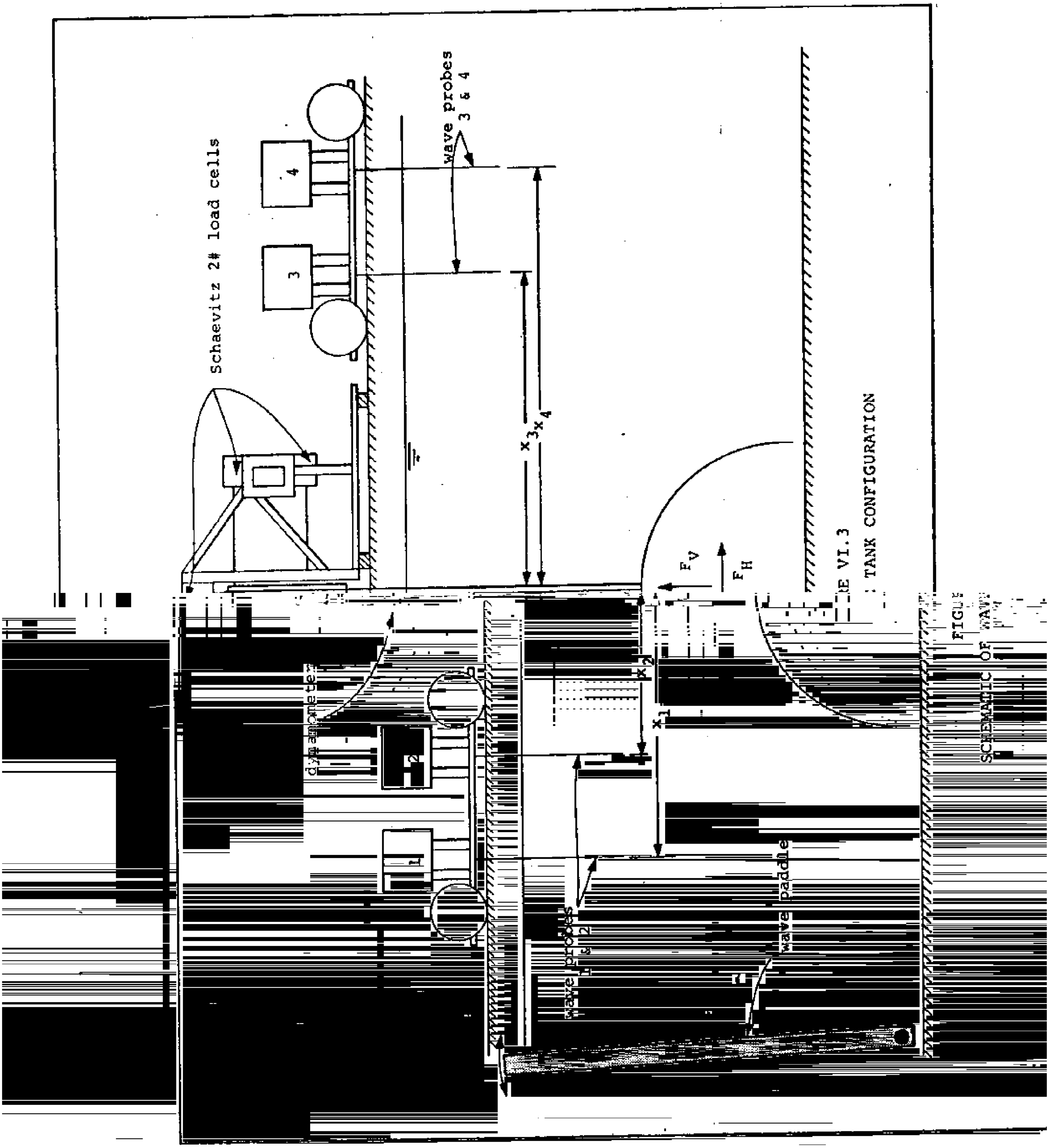

FIGURE VI.3 SCHEMATIC OF WAVE TANK CONFIGURATION

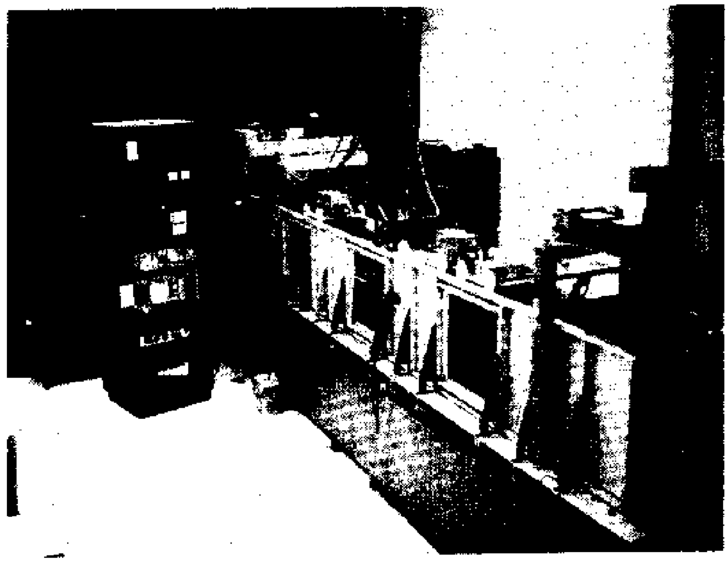

PLATE 1
EXPERIMENTAL SET UP INCLUDING WAVE TANK AND INSTRUMENTATION

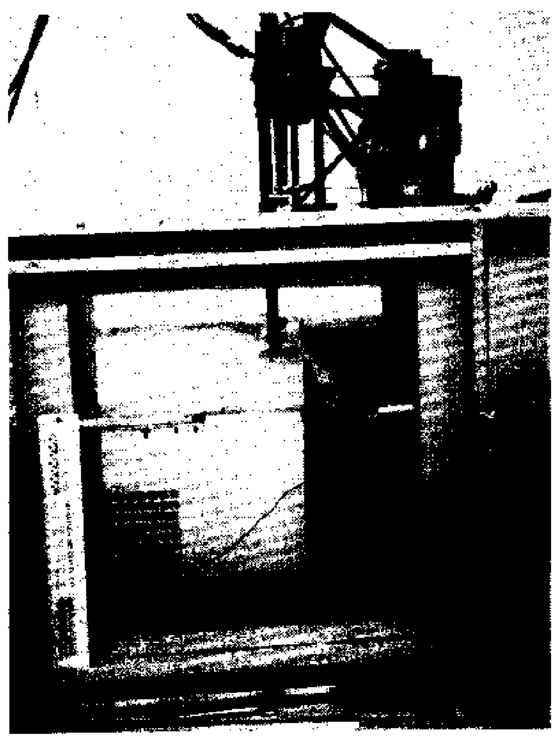

PLATE 2
SEMI-CIRCULAR CYLINDER SHOWN IN TEST POSITION

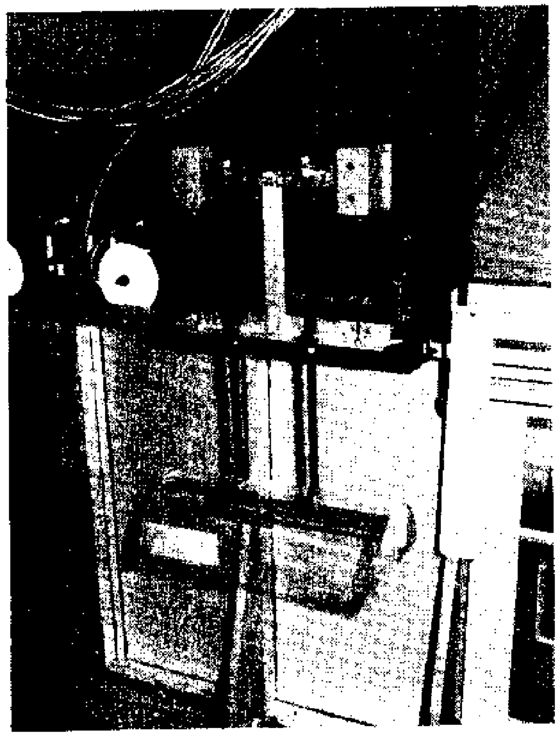

PLATE 3
CYLINDER SHOWN ATTACHED TO
3-COMPONENT DYNAMOMETER

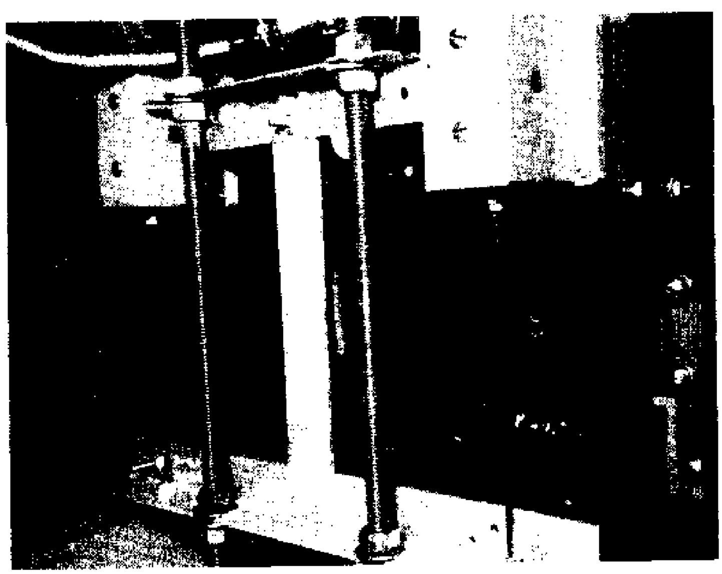

PLATE 4
CLOSE-UP OF DYNAMOMETER

VI.3.1 The Wave Tank

The wave tank was designed by Mr. Dean Lewis of the Marine Hydrodynamics Laboratory under the direction of Professor Jerome Milgram. It is constructed of aluminum and measures sixteen feet long by one foot wide by two feet deep. Windows in the sides of the tank aid in flow visualization (Plate 2). The side walls of the tank are parallel to within .01 inch.

Since the two-foot depth made tests on bottom structures in shallow and intermediate depth waves difficult, a special aluminum platform was constructed to act as a ground plane raising the effective bottom of the tank 14 inches. This platform extends the entire length of the wave tank (excluding the beach). It is constructed by bolting two 1/4" aluminum plates together with 1/4" plywood sandwiched between and extending 1/16" beyond the side edges (to protect the anodized surface of the wave tank). Plexiglass legs support the structure of this bottom. The legs were milled in order to insure a level surface.

A 12" × 12" × 3/4" aluminum plate pivoting about the raised bottom was installed in the tank to act as the wave paddle.

VI.3.2 The Wave Absorbing Beach

The final 5 feet of the wave tank is filled with tightly compressed rubberized horse hair mattress material. The intersection of the beach with the water line has a gradual slope falling off sharply below the water line. The reflection coefficient from the beach is highly dependent on the wave number. Figure VI.4 shows values of the reflection coefficients calculated as $|a_{11}|/|a_{21}|$ for a number of tests. The coefficient peaks at about .20 for KD ≈ .90. The wavelength corresponding to KD = .90 of 2.9 feet corresponds roughly to the distance between the cylinder and the beach, indicating that resonance might possibly be the source of the large reflection coefficients for these wavelengths.

VI.3.3 <u>The Dynamometer</u>

Forces on the cylinder are measured by means of five 2 lb. Schaevitz inductance type load cells connected by rigid wires to a frame onto which are attached the supporting struts for the cylinder. The load cells are attached to a rigid frame which is clamped to the wave tank during testing. The configuration of the load cells, the rigid connecting wire rods, and the cylinder support frame is such that the horizontal and vertical loads are transmitted separately to load cells 1, 2, 4 (horizontal) and 3, 5 (vertical). Figure VI.1 shows this schematically.

A force acting along the axis of any load cell causes the ferrite core of an inductor to deflect slightly, altering the inductance in an LC circuit and thus the frequency in a high frequency oscillator circuit. These high frequency

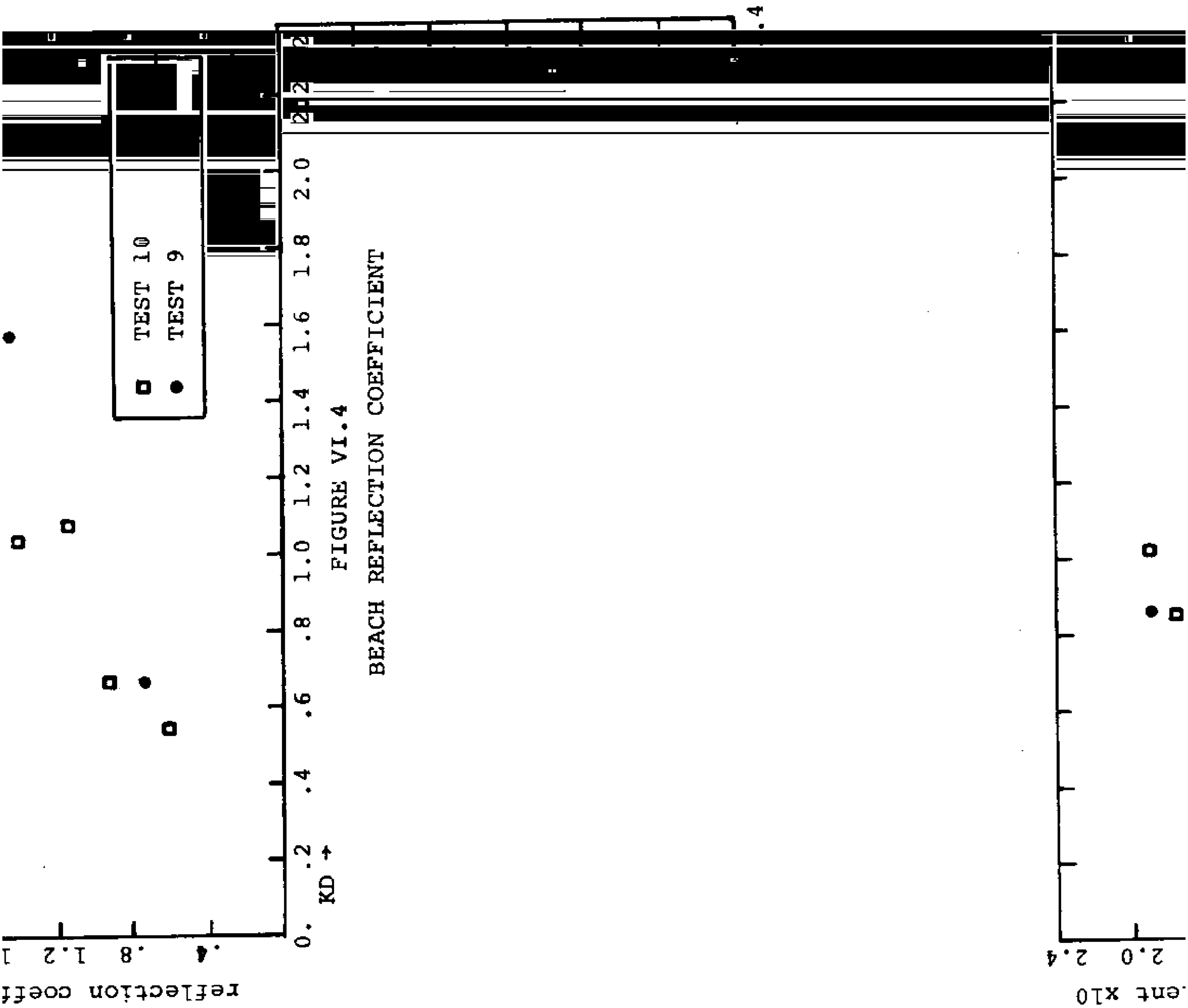

FIGURE VI.4
BEACH REFLECTION COEFFICIENT

signal fluctuations are converted to dc voltages for data acquisition. The output of the signal conditioning equipment is a dc voltage linearly proportional to the force acting on the load cell up to approximately 2 pounds of force.

The cylinder, its supporting frame, and the load cells comprise a linear mass spring system (neglecting non-linear hydrodynamic drag). A horizontal force of 1 lb. at the center of the cylinder caused a net deflection of the cylinder of approximately .20 inches. To minimize this deflection, steel cantilevered deflection arms were rigged to stiffen the load cells measuring horizontal forces (load cells 1, 2 and 4 - see Plates 2, 3 and 4). With the stiffened load cells the deflection of the cylinder was reduced to .06 inches/lb.

Under typical conditions, the cylinder would experience forces of .3-.5 lbs. The velocity of the cylinder under these conditions would reach a maximum of $(2\pi \times .03) =$ .188 inch/sec. as compared with the maximum particle velocity of the water of approximately 2.0 inch/sec.

The natural period of vibration of the cylinder out of water was observed to be .0575 sec. for horizontal motion. The vertical motion was critically damped.

VI.3.4 The Wave Probes

Four distinct wave components exist in the far field (away from the cylinder, the beach or the wavemaker):

$\eta_1(x,t)$, $\eta_2(x,t)$, $\eta_3(x,t)$ and $\eta_4(x,t)$. To establish the height and phase of each component four simultaneous measurements at different positions are necessary. To accomplish this, four capacitance type wave height sensors were placed in the tank, two upstream and two downstream. The sensors consist of a conducting wire surrounded by plastic insulation vertically immersed in the liquid. The water acts as a grounded surface, so that a capacitance is set up between it and the conducting wire which is connected in an L-C oscillator circuit. The frequency of the L-C circuit comprising the wave probe capacitance modulates a known fixed frequency signal. The resultant FM signal is demodulated to give a dc signal output which is linearly proportional to the wave height.

Normally the resolution of the wave probes is reduced by the effects of surface tension. A miniscus layer of water attaches itself to the probe as the waves travel over, thus distorting the true reading of the probe. To diminish this effect, each probe is mounted on the cone of a small radio loud speaker which is driven by a 60 Hz. signal from a power supply. The probes are then vibrated vertically with an amplitude of approximately 1/16", or roughly the amplitude of the miniscus, which will alternately ride up and down the wave probe 60 times a second. Taking the average of the 60 Hz. signal on the output thus yields the correct wave height measurement.

The wave probes proved sensitive to the proximity of metal objects. In the tank, the capacitance between the wave probes and the side of the tank itself proved a bothersome component, since the output would vary depending on the relative position of the probe to the windows. Care was taken to calibrate the probes in their actual test position so that no calibration errors would result from a zero-shift.

Another problem was encountered with the oscillator circuits. In particular, one circuit became unstable during the testing and caused severe jumps in the output for one wave probe. After some unsuccessful attempts to interchange the bad oscillator, the experiments were run with the questionable wave probe in position 3 (see Figure VI.2) where it would have the least effect on the incident wave measurements. With the exception of this probe, the calibration of the wave probes proved repeatable to within 5%, which figure may be taken as the accuracy of the incident wave amplitude measurements.

VI.3.5 Analog Signal Processing

If the calibration coefficient of the i^{th} force block is k_i lb./volt, we may write the forces and moment on the cylinder as

$$F_H = k_1v_1 + k_2v_2 + k_4v_4 \qquad \text{VI.26.1}$$

$$F_V = k_3v_3 + k_5v_5 \qquad \text{VI.26.2}$$

$$M = k_4V_4(y_2-y_1) + F_H(y_1-\Delta) \qquad \text{VI.26.3}$$

where v_i represents the voltage output of the i^{th} signal conditioner. In order to utilize these signals, the signals are filtered and added by means of separate operational amplifier circuits. These circuits are shown schematically in Figure VI.5. The inputs are the voltages v_1, v_2, v_3, v_4 and v_5 respectively. The outputs correspond (in volts) to the quantities $C_H F_H$, $C_V F_V$ and $C_m[M - F_H(y_1-\Delta)]$ respectively. C_H, C_V and C_m may be adjusted by altering the gain of the operational amplifier circuits. The outputs of each circuit may be written

$$V_H = \frac{R_{11}R_7(1-iR_7\omega C_1)}{R_{10}(1+R_7^2\omega^2 C_1{}^2)} \left[\frac{v_1}{R_1} + \frac{v_2}{R_2} + \frac{v_4}{R_4}\right] \qquad \text{VI.27.1}$$

$$V_V = \frac{R_8(1-iR_8\omega C_2)}{1 + R_8^2\omega^2 C_2^2} \left[\frac{v_3}{R_3} + \frac{v_5}{R_5}\right] \qquad \text{VI.27.2}$$

$$V_M = \frac{v_4 R_9 R_{13}(1-iR_9\omega C_3)(1-iR_{13}\omega C_4)}{R_6(1+R_9^2\omega^2 C_3^2)(1+R_{13}^2\omega^2 C_4^2)} \qquad \text{VI.27.3}$$

where the signals are considered to be monochromatically oscillatory:

$$v_i = |v_i|e^{-i\omega t}$$

For the case of a general periodic signal, each Fourier component will experience a different gain. From VI.26 we note that the resistances R_1-R_5 must be selected so that

$$\frac{v_1}{R_1} + \frac{v_2}{R_2} + \frac{v_4}{R_4} \simeq k_1 v_1 + k_2 v_2 + k_4 v_4 \qquad \text{and}$$

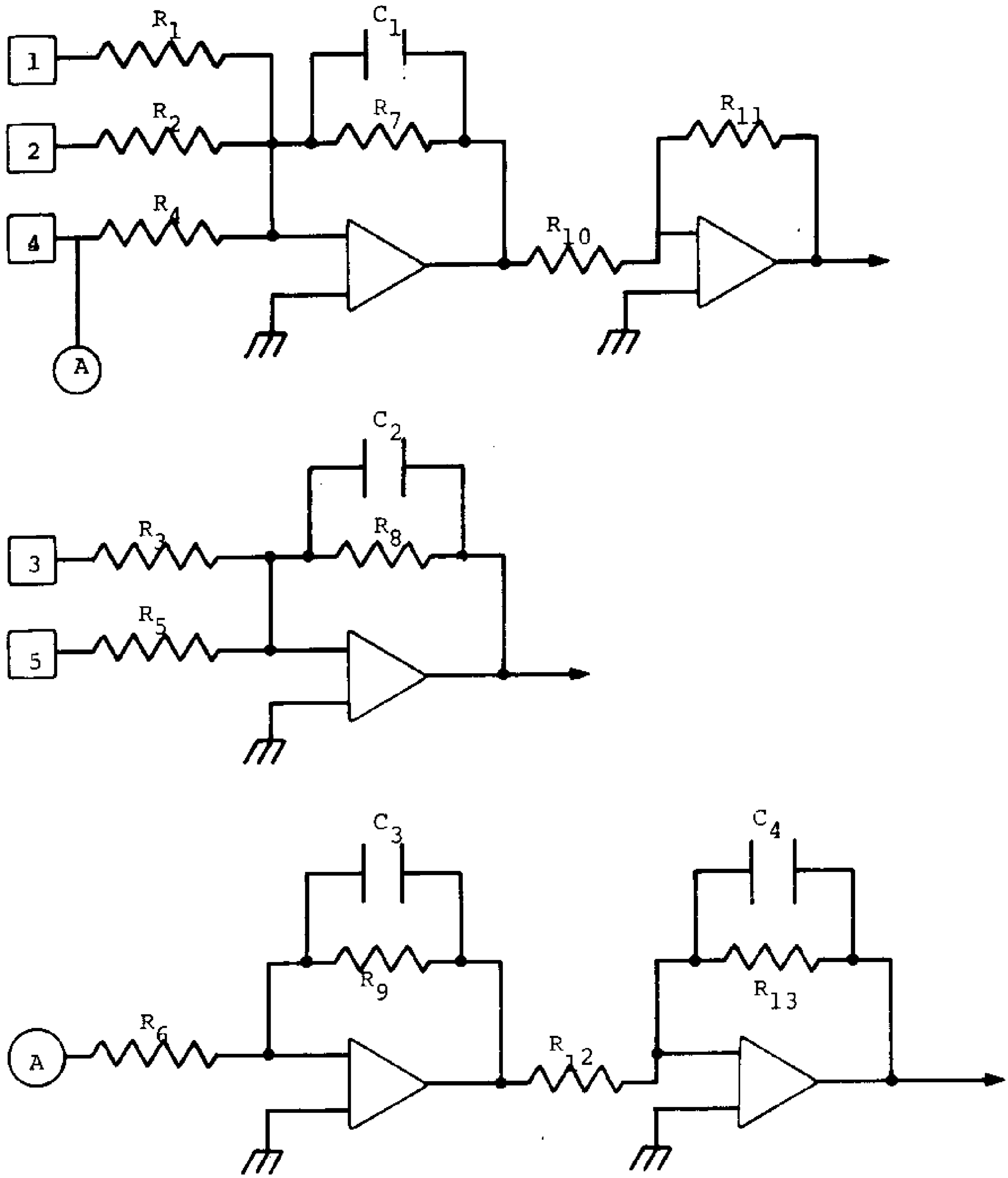

Figure VI.5

ANALOG PROCESSING CIRCUITS FOR FORCES AND MOMENT

$$\frac{v_3}{R_3} + \frac{v_5}{R_5} \simeq k_3 v_3 + k_5 v_5 \ .$$

The RC circuits served as an initial low pass filter for the signals from the instruments. Values of RC were chosen to attenuate effectively all signals over 120 Hz. For a typical value of RC = .045, the attenuation at 60 Hz. is 60%, at 120 Hz. 99%. Similar circuits for amplifying the wave probes were designed to give similar attenuation.

The output of the Op. Amp. was fed into a hybrid EAI 680 analog/IBM 1130 digital computer system at the M.I.T. Mechanical Engineering Computer Facility. An existing program, ADCNV, was used to sample the signals at a fixed sample rate, place the sampled (digitized) data on the 1130's disk memory and punch the stored data on IBM cards for further processing.

All tests were digitized using a sample rate of 250 Hz. This prevented aliasing of signals up to 125 Hz. (signals above 120 Hz. are filtered in the Op. Amp. circuits). Digital filtering will be discussed in VI.7.

VI.3.6 <u>The Test Section</u>

The cylinders were fabricated from 1/8" thick plexiglass tubing 4" and 6" in diameter. To connect the cylinder (half-tube) to the dynamometer frame two 3/8" holes were tapped in the upper surface and 3/8" rods inserted to serve as struts (see Plates 3 and 4). The force on the 3/8" rods is negligible compared to the force on the cylinder (tests showed the force on the rods less than 0.5% of the cylinder forces).

The 3" radius cylinder was used in tests 9-16, 18 and 19. The 2" cylinder was used in test 17.

VI.4 Instrument Calibration

Calibration was performed by applying a known physical input to each sensor and recording the output (in volts) of the appropriate circuit. The voltage readings were taken on a Hewlett-Packard two-channel recording oscillograph. Periodic checks were made to insure that the voltages read by the oscillograph were equal to those reaching the digitizing system at the Mechanical Engineering Computer.

VI.4.1 Wave Probe Calibration

The wave probes were calibrated by adjusting the output for the probes in still water to be zero and raising the probe carriages on metal strips of 1/8" and 1/4" dimensions. The voltage change recorded indicated the calibration coefficient for each probe.

Tables VI.1 and VI.2 summarize the overall calibration coefficients and positions of the wave probes for the 10 runs.

All probe signals were amplified in operational amplifier circuits possessing the following transfer function:

$$V_{out} = \frac{R_{out} V_{in} (1 - iR_{out} \omega C)}{R_{in} (1 + R_{out}^2 \omega^2 C^2)} \qquad \text{VI.28}$$

Table VI.1

WAVE PROBE POSITION

Run	x_1 (inches)	x_2 (inches)	x_3 (inches)	x_4 (inches)
9	-42.250	-36.875	23.375	28.125
10	"	"	"	"
11	"	"	"	"
12	"	"	28.125	32.875
13	"	"	23.375	28.125
14	"	"	"	"
15	"	"	"	"
16	"	"	28.125	32.875
17	"	"	"	"
18	-	-	-	-
19	-	-	-	-

Table VI.2

WAVE PROBE CALIBRATION

Calibration Coefficients (volts per inch):

Runs	9-17	18,19
C_{w1}	-21.6	-20.8
C_{w2}	-26.0	-16.8
C_{w3}	-17.2	-50.0
C_{w4}	030.4	-30.3

If A_i is the amplitude of a wave of frequency ω at probe i, from VI.28 we can see that its value may be written

$$A_i = \frac{V_{out}}{C_{wi}} (1 + i\ R_{out}\omega C) \qquad \text{VI.29}$$

For probes 1, 2 and 4

$$R_{out}C = .022$$

and for probe 3

$$R_{out}C = .044.$$

VI.4.2 Dynamometer Calibration

Each force block was calibrated individually by applying calibration weights of .5 lb. and 1 lb. The gain of the signal conditioning equipment was adjusted so that load cells 1, 2 and 4 (horizontal load) each yielded (as close as possible) 1 volt/lb. Load cells 3 and 5 were adjusted to give 5 volts/lb. With the precise coefficients determined for each load cell, the values of R_1, R_2, R_3, R_4 and R_5 were determined. For all tests, the following values were set:

R_1 = 20,000 Ω	R_{10} = 50,000 Ω
R_2 = 19,500 Ω	R_{12} = 15,500 Ω
R_3 = 20,000 Ω	R_{13} = 100,000 Ω
R_4 = 50,000 Ω	
R_5 = 50,000 Ω	C_1 = .22 μfd
R_6 = 100,000 Ω	C_2 = .22 μfd
R_7 = (see Table VI.3)	C_3 = .22 μfd
R_8 = 500,000 Ω*	C_4 = .22 μfd
R_9 = 150,000 Ω	

*R_8 = 200,000 Ω for test 9.1

R_{11} was adjusted for various test runs to maintain an acceptable signal level. Table VI.3 shows the values of R_7 and C_H for each test run. The values of C_V and C_m were

$$C_V = 20.0 \text{ volts/lb. (test 9.1)}$$

$$= 50.0 \text{ volts/lb. (all other tests)}$$

$$C_m = -1.50 \text{ volts/ft. lb. (all tests)}$$

Table VI.3

HORIZONTAL FORCE CALIBRATION DATA

Run	$R_7(\Omega \times 10^{-3})$	C_H(volts/lb.)
9.1	200	-20.0
9.2	200	-20.0
9.3	400	-40.0
9.4	400	-40.0
9.5	400	-40.0
9.6	400	-40.0
9.7	400	-40.0
10.2	200	-20.0
10.3	200	-20.0
10.4	400	-40.0
10.5	400	-40.0
10.6	400	-40.0
10.7	400	-40.0
10.8	200	-20.0
11.1	200	-20.0
11.2	200	-20.0
11.3	200	-20.0
11.4	400	-40.0
12.1	200	-20.0
12.2	200	-20.0
12.3	200	-20.0
12.4	400	-40.0
13.1	200	-20.0
13.2	200	-20.0
13.3	200	-20.0
13.4	400	-40.0
13.5	400	-40.0
14.1	200	-20.0
14.2	200	-20.0
14.3	200	-20.0
14.4	200	-20.0
14.5	400	-40.0

Run	$R_7(\Omega \times 10^{-3})$	C_H(volts/lb.)
15.1	200	-20.0
15.2	200	-20.0
15.3	200	-20.0
15.4	200	-20.0
16.1	200	-20.0
16.2	200	-20.0
16.3	200	-20.0
16.4	400	-40.0
17.1	400	-40.0
17.2	400	-40.0
17.3	400	-40.0
17.4	400	-40.0
17.5	600	-60.0
17.6	600	-60.0
18.1	200	-20.0
18.2	200	-20.0
18.3	200	-20.0
18.4	200	-20.0
18.5	200	-20.0
18.6	200	-20.0
18.7	200	-20.0
19.1	200	-20.0
19.2	200	-20.0
19.3	200	-20.0
19.4	200	-20.0
19.5	200	-20.0
19.6	200	-20.0

VI.5 Signal Processing and Analysis

Once the signals have passed through the analog circuits the EAI/IBM digitizing system and finally punched on cards, the problem remains to determine the non-dimensionalized forces, moment, reflection coefficients and any other parameters of interest. In order to find all the desired information the digitized data must be Fourier analyzed to determine the amplitudes of the first several Fourier components. The digitized data contains frequency components up to 120 Hz. Since the highest frequency water wave we will investigate has a fundamental frequency of approximately 2 Hz., we may ignore all frequencies above 10 Hz. (5th harmonic) or so. In order to avoid aliasing, the Fourier analysis must use very small (less than 1/240 sec. to eliminate 120 Hz. aliasing) time steps for integration, or, as an alternative, the digital data may be put through a digital low pass filter. This latter approach was used here (see Appendix F for details of the numerical filter).

After passing through the low pass filter, the data may be Fourier analyzed using relatively large time steps. The filtered data is in the form of a matrix, y_{ij}, with i corresponding to a time coordinate. j=0 is arbitrarily taken to correspond to t=0, j=N to t=T. The channels are numbered as follows:

Channel

1	Output for wave probe 1
2	Output for wave probe 2
3	Output for wave probe 3
4	Output for wave probe 4
5	Output for F_H (horizontal force)
6	Output for M (moment)
7	Output for F_V (vertical force)

Given the filtered data y_{ij} and the fundamental frequency $\omega_1 = 2\pi/T$, the Fourier components of the signals may easily be computed:

$$S_{in} \simeq \frac{\Delta\tau}{T} \sum_{m=1}^{N_T} y_{im} \exp(inm\omega\Delta\tau) \qquad \text{VI.28}$$

The Fourier components must still be converted to physical units. In order to reproduce the original physical quantities, it is not only necessary to utilize the static calibration coefficients C_1 C_2, etc., but it is also necessary to recognize that the anlog filters and amplifiers contain frequency dependent characteristics. To retrieve the initial input, therefore, it is necessary to correct for the effect of the operational amplifier circuits on the signal.

Equation VI.7 shows this correction for the wave probe channels:

$$A_{in} = \frac{S_{in}}{C_{wi}} (1 + iR_{out}n\omega_1 D) \qquad \text{VI.29}$$

$$i = 1 - 4$$

The equivalent expressions for the forces and moment follow from VI.27

$$A_{5n} = \frac{S_{5n}}{C_H}(1 + iR_7 n\omega C_1) \qquad \text{VI.30.1}$$

$$A_{6n} = \frac{S_{6n}}{C_m}(1 + iR_9 n\omega C_3)(1 + iR_{13}\omega C_4) \qquad \text{VI.30.2}$$

$$A_{7n} = \frac{S_{7n}}{C_V}(1 + iR_8 n\omega C_2) \qquad \text{VI.30.3}$$

where A_{in} represents the n^{th} Fourier component of the i^{th} channel output (in correct units) corrected for the analog filtering.

VI.5.1 Dynamic Effects

We have seen that the dynamometer system with the cylinder attached represents a linear mass/spring system. Figure VI.6 shows a typical response curve for an impulsive loading applied to the cylinder in a horizontal direction. The

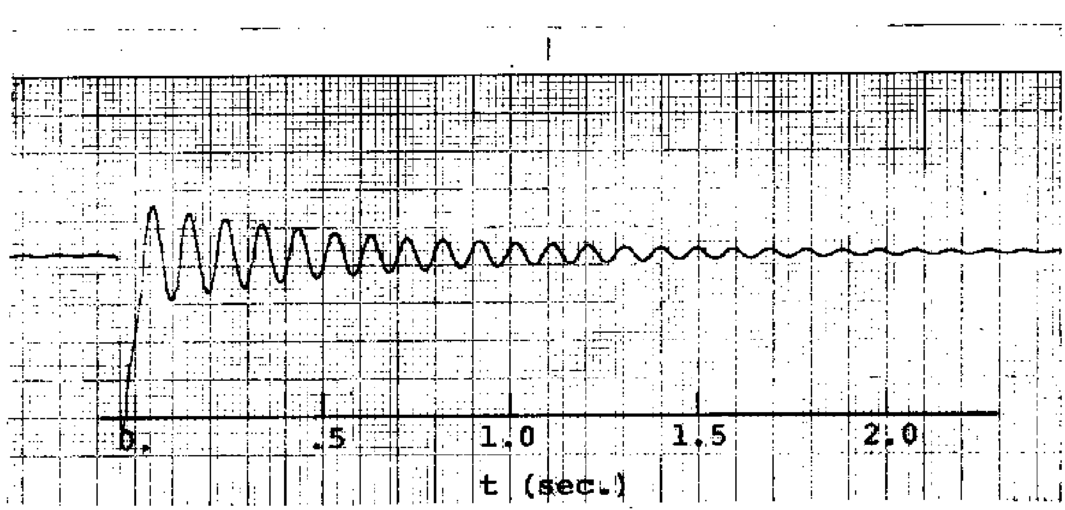

FIGURE VI.6

F_H RESPONSE FOR IMPULSIVE LOAD

amplitude of the deflection of the load cells is therefore influenced by the resonant interaction of the cylinder/ dynamometer system with the periodic (unknown) forcing function. Ideally this effect would be eliminated by making the system infinitely stiff. Unfortunately, an infinitely stiff system would not deflect at all, and no voltages would be read.

The compromise reached here consisted of the inclusion of the stiffening bars on load cells 1, 2 and 4 to reduce the natural period of the horizontal motion to .2 sec. (see Section VI.5). From the theory of single degree of freedom linear system response, the amplitude of the output signal for a given sinusoidal input may be written (Den Hartog, 1956)

$$y(t) = Y\, e^{-i\omega t}$$

$$Y = \frac{(X/k_o)\, e^{-ix}}{\sqrt{(1-\beta^2)^2 + (2\zeta\beta)^2}}$$

where X is the input amplitude (complex)

$$B_{in} = A_{in}\, e^{i\psi_{in}} \sqrt{(1-\beta_{in}^2)^2 + (2\zeta_i\beta_{in})^2} \qquad \text{VI.31}$$

where B_{in} = the n^{th} Fourier component of the i^{th} channel signal (in physical units) corrected for analog filtering and for the dynamic response of the dynamometer system

$\beta_{in} = n\omega_1/\omega_{ni}$

ω_{ni} = natural circular frequency of motion for the cylinder in the i^{th} channel mode

ζ_i = damping ratio in the i^{th} channel mode

$\psi_{in} = \tan^{-1}\left[\dfrac{2\zeta_i\beta_{in}}{1-\beta_{in}^2}\right]$

B_{in} represents the Fourier component of the physical quantity of interest. We may write, for example,

$$\eta_1(x_1,t) + \eta_2(x_1,t) = \mathrm{Re}\left\{\sum_{n=1}^{5} B_{in}e^{-in\omega t}\right\} \qquad \text{VI.32}$$

where only the first five harmonics have been included.

VI.5.2 Added Mass Computations from System Vibrations

Before turning to the computations for the incident and reflected waves, we will look at the vibrations of the system from the standpoint of calculating the added mass of the cylinder.

As was mentioned in Section VI.5, the natural period of the system was increased from .0575 sec. for the cylinder out of water to approximately .2 sec. when the cylinder is immersed (considering only the horizontal motion).

It is possible to calculate the added mass based on these observations. The following discussion will treat m as the effective mass of the cylinder and k as the effective spring constant of the cylinder. Thus,

$$T_n = 2\pi \sqrt{m/k}. \qquad \text{VI.33}$$

For the cylinder out of water,

$$T_n = .0575 \text{ sec.}$$
$$k = 200 \text{ lb./ft. (measured)}$$

therefore

$$m = .0168 \text{ lb.}$$

We have used VI.33 under the assumption that the damping ratio is zero. Figure VI.5 shows a typical curve of the free vibrations of the cylinder. This case is typical of the vibrations, and as can be seen, is quite lightly damped. The largest damping ratio observed during the tests was .0285. We may continue this discussion based on an undamped oscillator, keeping in mind only the fact that the damping must be included for forced motion near resonance.

Continuing with the discussion of the added mass, we may write for the cylinder immersed in water

$$T_n = 2\pi \sqrt{(m+m')/k} \qquad \text{VI.34}$$

where m' = displaced plus added mass of cylinder due to motion of the water and wave generation.

From VI.34

$$m' = k(T_n/2\pi)^2 - m \qquad \text{VI.35}$$

In order to compute m' it is necessary to compute the gap flow problem for the case of an oscillating cylinder. This problem is related to the wave force problem via the Haskind's relations. For the solution to the radiation problem, see Appendix E.

The trend of the data may be seen from the following tabulations by gap width:

D = 6.0 inches

ε(inches)	m'(meas.)	m(comp.)
1/8	.287	.218
1/4	.244	.172
3/8	-	-
1/2	.228	.162

D = 5.0 inches

ε(inches)	m'(meas.)	m(comp.)
1/8	.275	.168
1/4	.240	-
3/8	-	-
1/2	.152	.152

The calculations of the added mass correlate with the trend of the data, but appear to be lower by approximately 25%. This fact could easily be attributed to an error in the measurement of the spring constant k (the value of k was arrived at by measuring a .06" deflection with a ruler!).

As a check on the computer program, the damping coefficients computed for the oscillating cylinder were used to calculate C_M for the same frequency using equation E.18. C_M was also calculated by the wave force method of program MAIN (Appendix F) and the two values compared. In all cases checked these values agreed to within 5%.

Test	D (in.)	R (in.)	ε (in.)	T_V	ζ_V	T_H	ζ_H	m' (Meas.)	m' (Comp.)
9	6.0	3.0	1/4	.1620	.0208	.2270	.0195	1.18	.172
10	6.0	3.0	3/8	-	-	-	-	-	-
11	5.0	3.0	3/8	-	-	-	-	-	-
12	5.0	3.0	1/2	.1475	.0159	.2140	.0159	1.08	.152
13	6.0	3.0	1/2	.1500	.0240	.2200	.0159	1.15	.162
14	6.0	3.0	1/8	.1875	.0350	.2450	.0230	1.44	.218
15	5.0	3.0	1/8	.1850	.0390	.2400	.0285	1.40	.168
16	5.0	3.0	1/4	.1670	.0250	.2250	.0210	1.17	-
17(a)	6.0	2.0	1/8	.1275	.0326	.1740	.0180	1.61	-
17(b)	6.0	2.0	1/4	.1125	.0220	.1638	.0192	1.36	-
17(c)	6.0	2.0	3/8	.1060	.0165	.1600	.0220	1.28	-

TABLE VI.4

Results for Cylinder Vibration Tests

VI.5.3 Force Computations

Given B_{in}, $i = 1\text{-}4$, we may now calculate the four wave functions a_{in}, $i = 1\text{-}4$. To do this, write the wave amplitude for each of the four positions as the sum of the respective components (referring to equations VI.14):

$$\eta(x_1,t) = \eta_1(x_1,t) + \eta_3(x_1,t)$$

$$= \sum_{n=1}^{5} B_{1n} e^{-in\omega t}$$

$$= \sum_{n=1}^{5} [a_{1n} e^{iK_n x_1} + a_{3n} e^{-iK_n x_1}] e^{-in\omega t}$$

where $\omega = 2\pi/T$

This yields

$$B_{1n} = a_{1n} e^{iK_n x_1} + a_{2n} e^{-iK_n x_1} \qquad \text{VI.37.1}$$

Similar equations for each position yield

$$B_{2n} = a_{1n} e^{iK_n x_2} + a_{3n} e^{-iK_n x_2} \qquad \text{VI.37.2}$$

$$B_{3n} = a_{4n} e^{iK_n x_3} + a_{2n} e^{-iK_n x_3} \qquad \text{VI.37.3}$$

$$B_{4n} = a_{4n} e^{iK_n x_4} + a_{2n} e^{-iK_n x_4} \qquad \text{VI.37.4}$$

Solving VI.37 for a_{1n}, a_{2n}, a_{3n} and a_{4n} by straight-forward algebraic means yields the following solution:

$$a_{1n} = \frac{i(B_{1n} e^{-iK_n x_2} - B_{2n} e^{-iK_n x_1})}{2 \sin K_n \Delta_1} \qquad \text{VI.38.1}$$

$$a_{3n} = \frac{i(B_{2n}e^{iK_nx_1} - B_{1n}e^{iK_nx_2})}{2 \sin K_n\Delta_1} \qquad \text{VI.38.2}$$

$$a_{2n} = \frac{i(B_{3n}e^{-iK_nx_4} - B_{4n}e^{-iK_nx_3})}{2 \sin K_n\Delta_2} \qquad \text{VI.38.3}$$

$$a_{4n} = \frac{i(B_{4n}e^{iK_nx_3} - B_{3n}e^{iK_nx_4})}{2 \sin K_n\Delta_2} \qquad \text{VI.38.4}$$

where $\Delta_1 = x_2 - x_1$

$\Delta_2 = x_4 - x_3$

The normalized forces may now be determined directly. From VI.21, write

$$C_{Mn} = \frac{i2B_{5n}}{\rho g\pi R^2 nK_n(a_{12} - a_{2n}} \qquad \text{VI.39}$$

From VI.22, obtain

$$\bar{V}_n = \frac{2B_{7n}}{\pi\rho gR(a_{1n} + a_{2n})} \qquad \text{VI.40}$$

And from VI.25,

$$\bar{M}_n = \frac{2B_{6n}}{\rho\pi R^2 a_{1n}} \qquad \text{VI.41}$$

VI.5.4 Reflection and Transmission Coefficients

Noting the relationships for the reflection and transmission coefficients, eqns. VI.15 and VI.16, we may write

$$a_{3n} = R_{Ln}\ a_{1n} + T_{Rn}\ a_{2n}$$

$$a_{4n} = T_{Ln}\ a_{1n} + R_{Ln}\ a_{2n}$$

Setting $\tau_n = T_{Ln} = T_{Rn}$ and $R_n = R_{Ln} = \bar{R}_{Rn}$,

$$a_{3n} = R_n a_{1n} + \tau_n a_{2n} \qquad \text{VI.42.1}$$

$$a_{4n} = \tau_n a_{1n} + \bar{R}_n a_{2n} \qquad \text{VI.42.2}$$

In the following we will drop the R subscript, it being understood that the equations apply to each harmonic.

Let the reflection coefficient be

$$R = r_1 + ir_2$$

and the transmission coefficient

$$= t_1 + it_2$$

where r_1, r_2, t_1 and t_2 are real quantities.

Also, let

$$a_i = p_i + iq_i$$

where p_i and q_i are real numbers.

Equations VI.42 may then be written

$$p_3 = r_1 p_1 - r_2 q_1 + t_1 p_2 - t_2 q_2$$

$$q_3 = r_1 q_1 + r_2 p_1 + t_1 q_2 + t_2 p_2$$

$$p_4 = r_1 p_2 + r_2 q_2 + t_1 p_1 - t_2 q_1$$

$$q_4 = r_1 q_2 - r_2 p_2 + t_1 q_1 + t_2 p_1$$

The unknowns may easily be solved algebraically.

$$r_1 = D_1/\text{Det} \qquad \text{VI.43.1}$$

$$r_2 = D_2/\text{Det} \qquad \text{VI.43.2}$$

$$t_1 = D_3/\text{Det} \qquad \text{VI.43.3}$$

$$t_2 = D_4/\text{Det} \qquad \text{VI.43.4}$$

where

$$\text{Det} = \begin{vmatrix} p_1 & q_1 & p_2 & -q_2 \\ q_1 & p_1 & q_2 & p_2 \\ p_2 & q_2 & p_1 & -q_1 \\ q_2 & -p_2 & q_1 & p_1 \end{vmatrix}$$

D_i = Det with i^{th} column replaced by (p_3, q_3, p_4, q_4)

This operation must be carried out for each of the five harmonics in order to obtain the respective reflection and transmission coefficients.

VI.6 Presentation of Results

A total of 19 tests were conducted, each test consisting of several runs corresponding to different wave periods. The results of the first eight tests are not reported here since the calibration coefficients of the wave probes were in doubt and the results meaningless. These early tests served mainly the purpose of working out experimental techniques.

The numbering sequence is retained here, however, since it is more convenient in referring to the computer output which is numbered by the original sequence.

Table II.4 summarizes the parameters for tests 9-17. All these tests were run with the cylinder a measured distance above the bottom. Runs were made with gap widths of 1/8", 1/4" 3/8" and 1/2". The results for the first harmonic quantities are summarized in Table VI.5. Notice that all tests, with the exception of 17, were run using the 3" radius cylinder.

Figures VI. through VI. show these results graphically. Figures VI. and VI. show the phases of the horizontal and vertical forces for a number of cases. The theoretical values are plotted for each case.

After conducting these tests it became apparent that the experimental scatter made it difficult to assess the exact effect of the gap as presented by the theory. The difference in vertical forces was negligible for the gap widths tested and, while the general trend of the data appears correct, the mass coefficient could not really be resolved close enough to correlate with the logarithmic dependence or ε predicted.

To obtain a better verification of the variation of C_M with ε, test 18 was conducted in an attempt to simulate the zero-gap case. Plates 11 and 12 show the cylinder setup for this test. In order to block the flow through the gaps as much as possible, a plate in the raised bottom of the tank was removed and the cylinder set in the slot. Plate 12 shows a closeup of this area with dye injected during the passing of a wave. While the flow is not completely blocked, a comparison with Plates 7, 8 and 9 shows a marked reduction.

The results for test 18 are shown in Figure VI. The mass coefficient has been significantly increased over the finite ε cases.

Computer Output of Results

Program DATA reduced and analyzed the data for each test run. Appendices G and H of this thesis present a complete record of the program output for tests 9 through 19.

The output in Appendix G shows the Fourier coefficients of the filtered data, the calculated wave parameters, the non-dimensional forces, and parameters concerning the test. Calibration data has been presented elsewhere in this chapter. (Tables VI.

The first part of this output, the complex Fourier coefficients of the data, corresponds to the values B_{in} discussed in the last chapter. The physical quantity corresponding to the output of channel m may be written as

$$x_m(t) = \mathrm{Re}\left\{\sum_{n=1}^{5} B_{mn}e^{-in\omega t}\right\} = \sum_{n=1}^{5} [c_{mn}\cos n\omega t + d_{mn}\sin \omega t] \qquad \text{VI.44}$$

The value of c_{mn} and d_{mn} are listed for each channel under the columns marked "cos" and "sin" respectively. The values for the first 5 harmonics are given.

The next section of output lists wave parameters. These may be defined as follows:

FREQUENCY = $n\omega$, n being the harmonic number.

WAVE LENGTH = wave length in feet.

WAVE FM. LEFT:

AMP = magnitude of a_{1n} with units of inches.

PHASE = phase of a_{1n} in degrees.

WAVE FM. RIGHT:

AMP = magnitude of a_{2n} with units of inches.

PHASE = phase of a_{2n} in degrees.

REF. COEF:

AMP = magnitude of R_n. This is a dimensionless quantity, the designation "(in.)" in the program is an error.

PHASE = phase of R_n in degrees.

TRANS COEF:

AMP = magnitude of τ_n, also a dimensionless quantity regardless of the program specification.

PHASE = phase of τ_n in degrees.

QRT = value of $|R_n|^2 + |\tau_n|^2$, theoretically equal to 1.0 for conservation of energy.

The output marked "NON-DIMENSIONAL FORCES" gives the following results for each harmonic:

FREQUENCY = $(n\omega)^2 D/g$, non-dimensional depth.

FH = magnitude of C_{mn} (eqn. VI.39)

AH = phase of C_{mn} in degrees.

FV = magnitude of $\bar{V}_n$ (eqn. VI.40)

AV = phase of $\bar{V}_n$ in degrees

FM = magnitude of $\bar{M}_n$ (eqn. VI.41)

AM = phase of $\bar{M}_n$ in degrees

KD = wave number times depth

KA = wave number times magnitude of a_{1n}

FACTOR= coefficient used to compute non-dimensional forces. This is of no interest here.

The test parameters listed at the bottom of the output include the depth in feet, the ratio R/D, the gap width given in feet, the cylinder radius in feet and the wave period in seconds. The three factors labeled "ADF", "ADV" and "ACTOR" are of no interest.

Tests 18 and 19 were conducted without the use of the digitizer. For these runs, wave amplitudes and phases were visually picked directly off the oscillograph records. The analysis is therefore made for only the first harmonic. An error in the input of a calibration coefficient caused the values of FH printed for these tests to be off by a factor of 1/2. To obtain the correct values of FH, multiply those given for tests 18 and 19 by two.

Appendix H lists the time history of the signals over one period for each channel. These are the values after passing through the high pass filter (Appendix D) but before any Fourier analysis. A plot of these points would duplicate the signal received from the signal conditioning equipment. Tests 11, 12 and 13 are not available in this form.

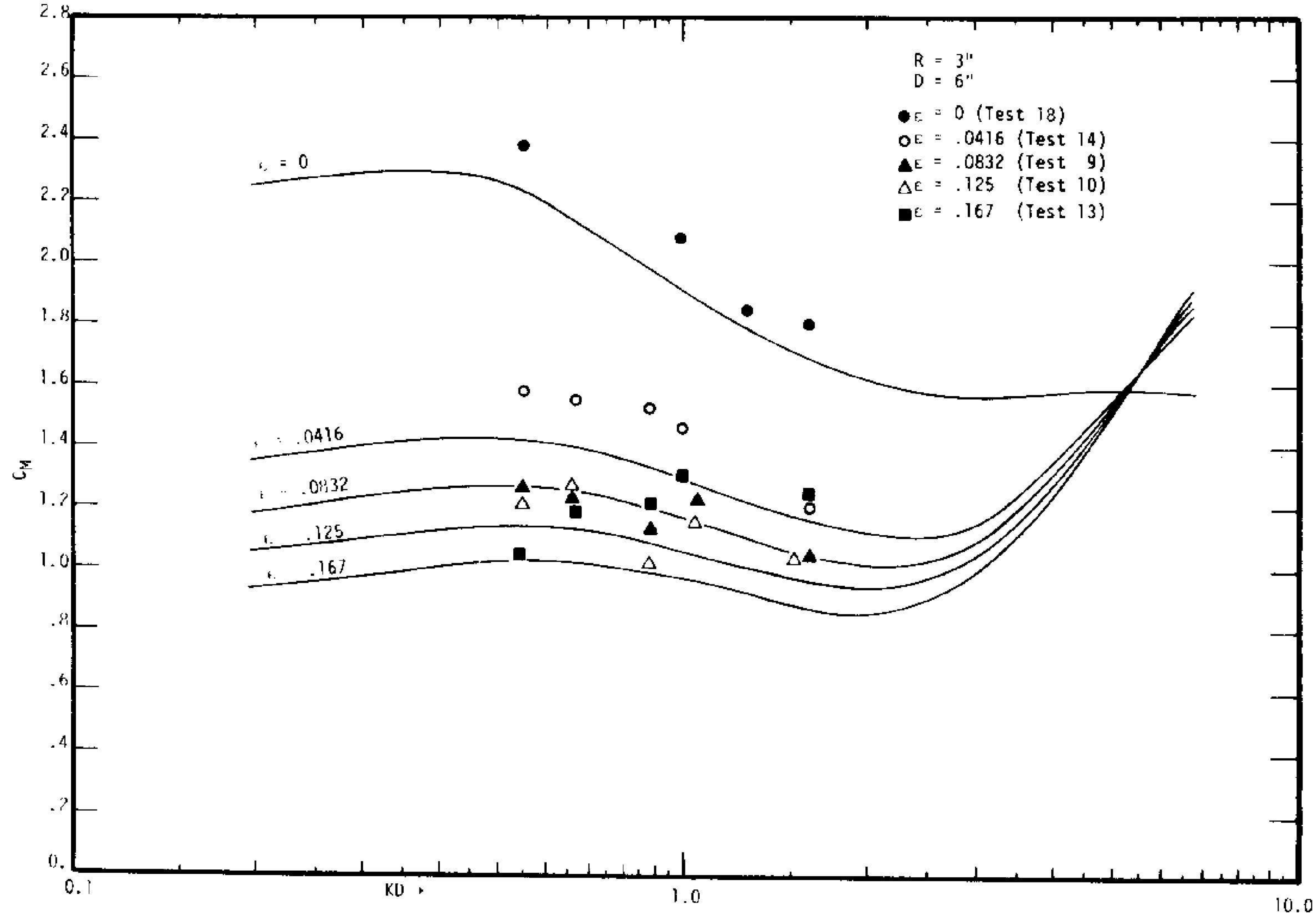

Figure VI.7
HORIZONTAL FORCE COEFFICIENT FOR R/D = .5

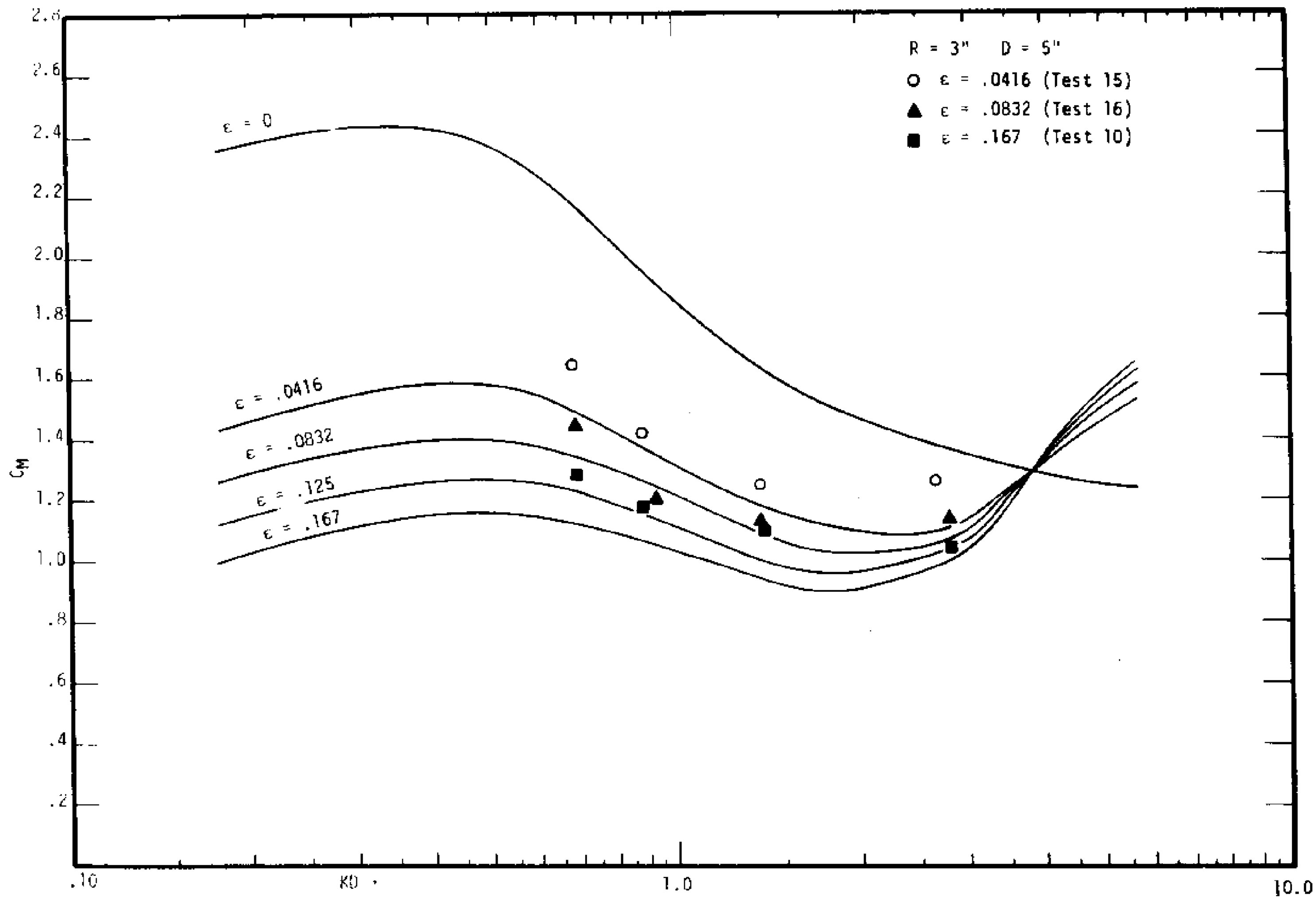

Figure VI.8
HORIZONTAL FORCE COEFFICIENT FOR R/D = .60

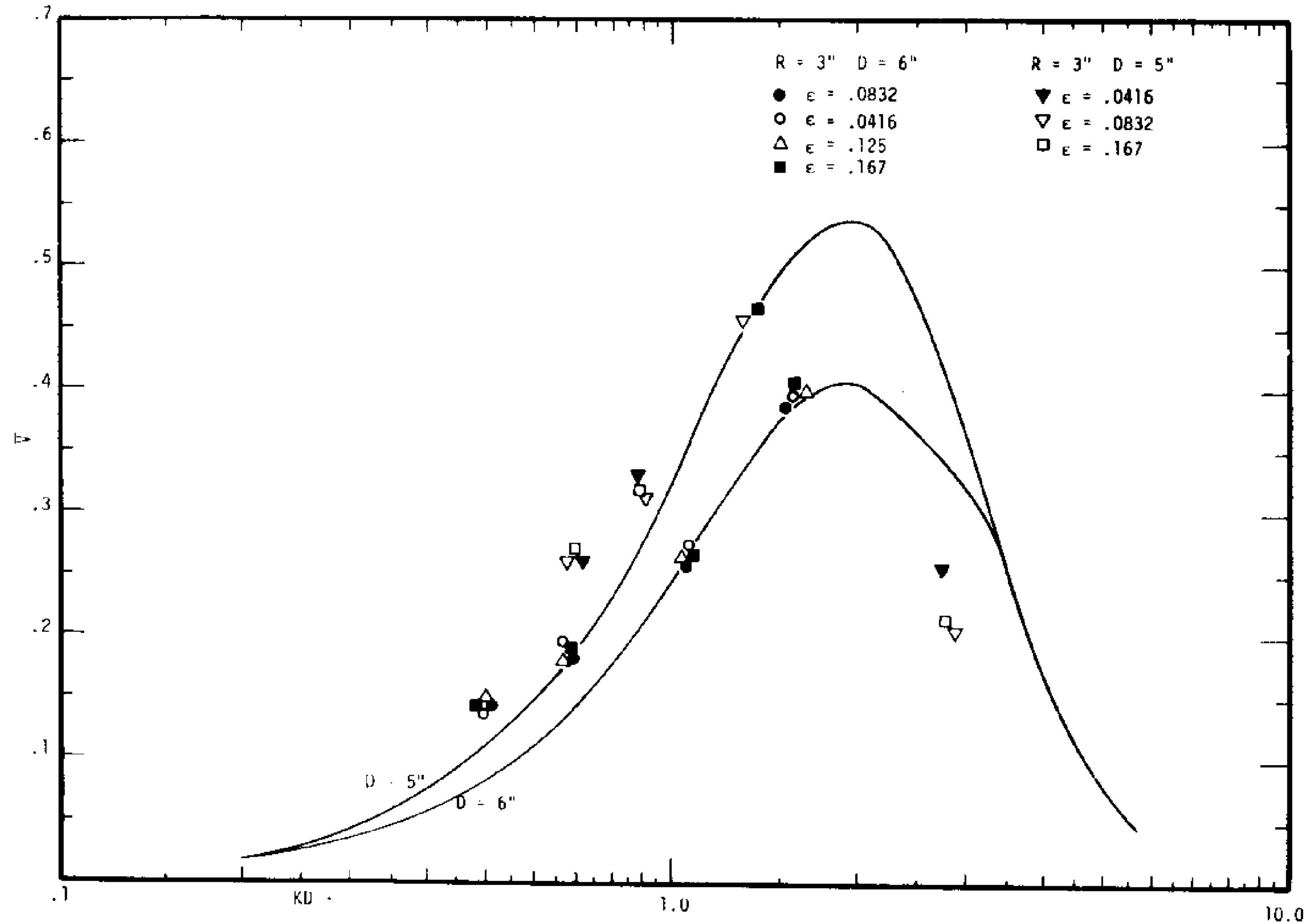

Figure VI.9
VERTICAL FORCE COEFFICIENT FOR R/D = .5 AND R/D = .6

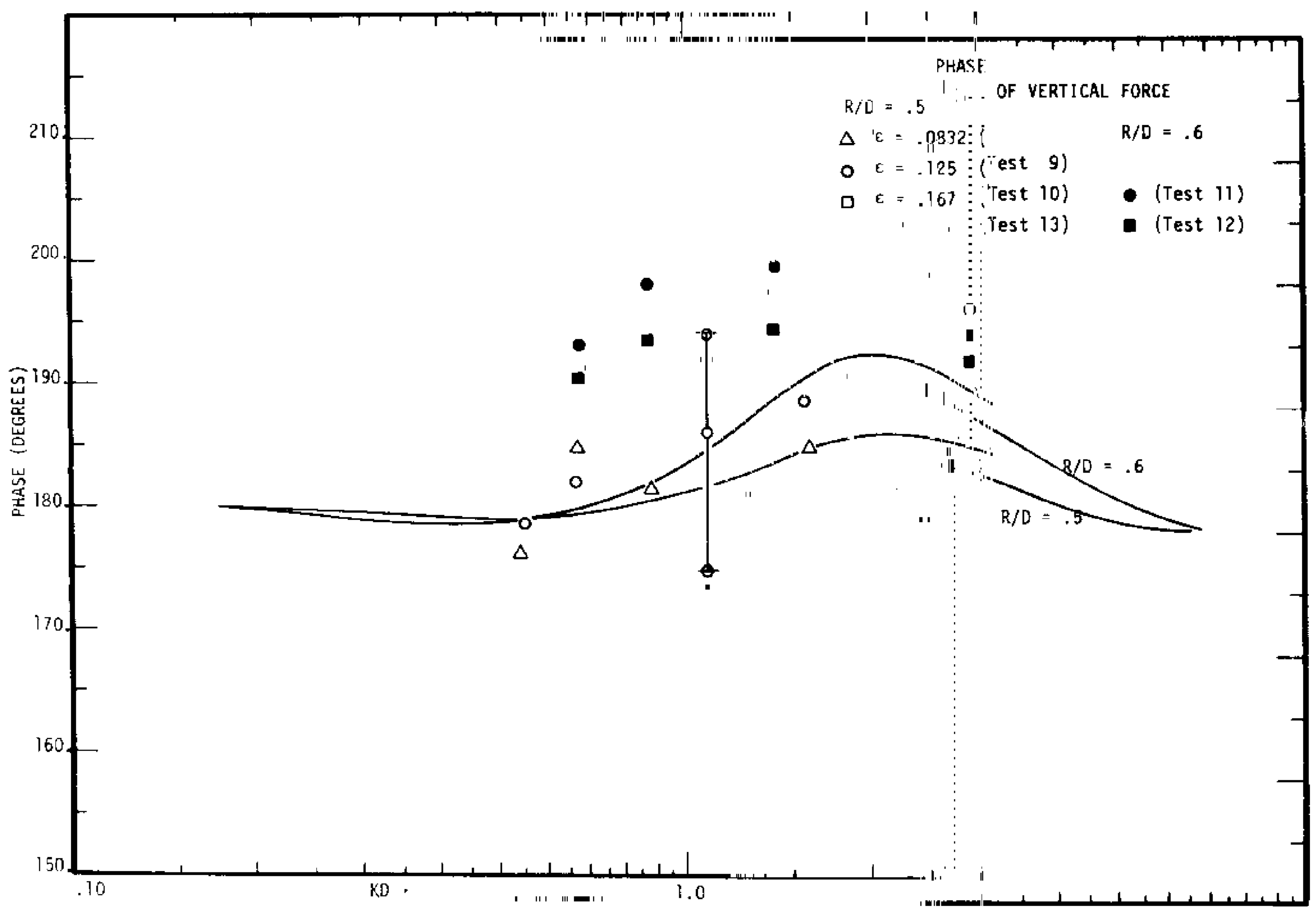

Figure VI.10

COMPUTED AND MEASURED PHASE OF VERTICAL FORCE FOR R/D = .5 AND R/D = .6

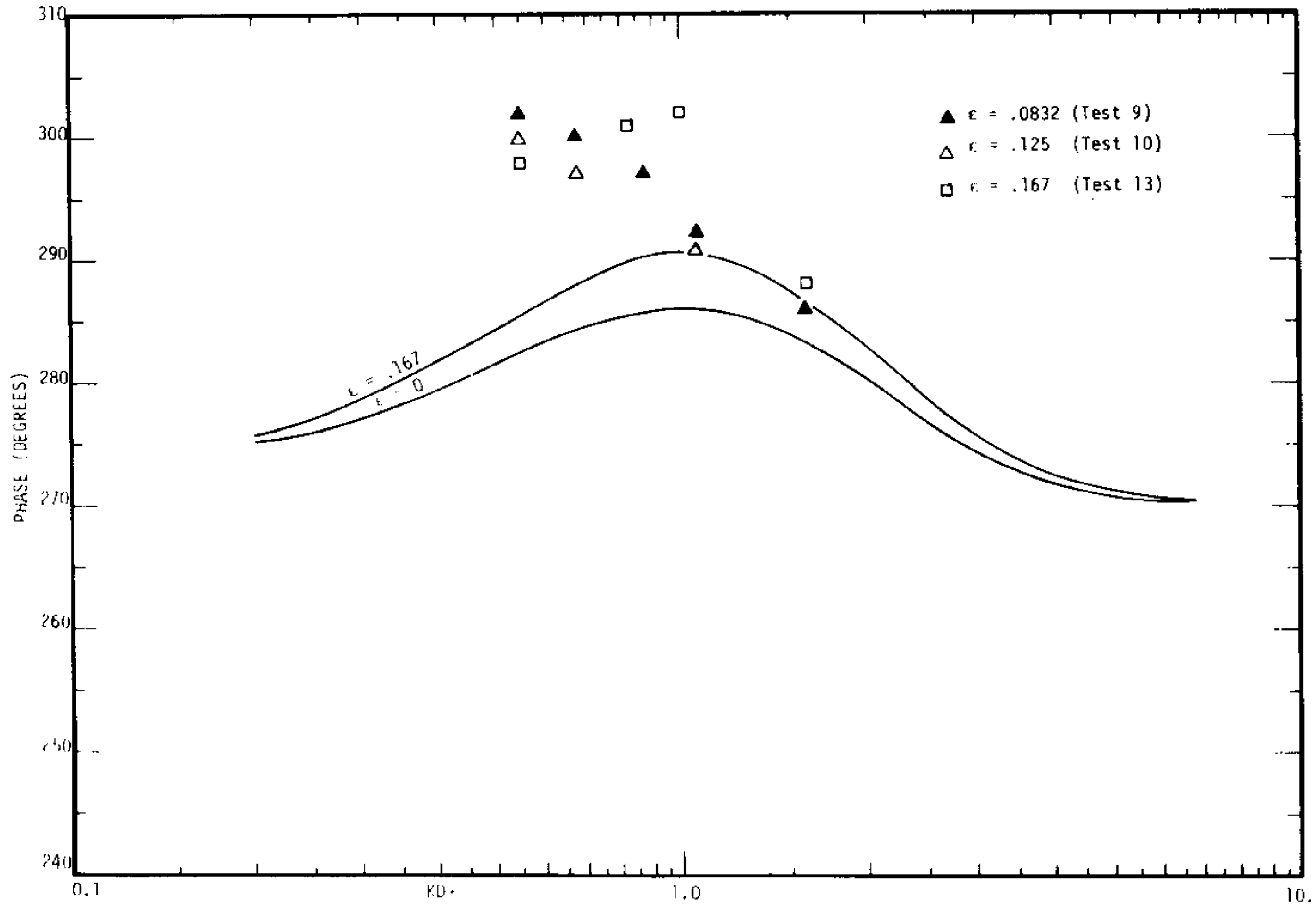

Figure VI.11

COMPUTED AND MEASURED PHASE OF HORIZONTAL FORCE FOR R/D = .5

RUN	T(sec.)	KD	KA_L	A_L(in)	A_R(in)	R	τ	C_M	α	F_V	α_V	M	D(in.)	ε(in)
9.1	.840	1.091	.039	.213	.023	.102	.922	1.110	33.9	.265	171.	.114	6.0	1/4
9.2	.853	1.069	.030	.167	.020	.084	.940	1.077	30.8	.246	169.	.122	6.0	1/4
9.3	1.493	.550	.008	.091	.007	.265	.882	1.381	40.7	.148	175.8	.100	6.0	1/4
9.4	1.00	.873	.021	.141	.025	.151	.952	1.349	35.5	.192	186.8	.037	6.0	1/4
9.5	.875	1.034	.014	.082	.017	.108	.964	1.058	34.3	.240	200.8	.116	6.0	1/4
9.6	.645	1.600	.037	.138	.020	.134	.934	1.163	30.1	.216	190.8	.079	6.0	1/4
9.7	1.250	.671	.012	.107	.012	.196	.906	1.210	44.7	.178	185.0	.126	6.0	1/4
10.2	.844	1.08	.036	.199	.023	.096	.900	1.078	31.0	.283	175.0	.124	6.0	3/8
10.3	.874	1.036	.027	.156	.022	.086	.950	1.080	34.0	.262	179.0	.139	6.0	3/8
10.4	1.487	.552	.076	.083	.005	.238	.841	1.328	33.5	.144	176.0	.115	6.0	3/8
10.5	1.250	.671	.011	.099	.009	.191	.900	1.227	39.0	.187	186.0	.146	6.0	3/8
10.6	1.015	.857	.019	.131	.023	.142	.959	1.221	35.0	.195	190.0	.041	6.0	3/8
10.7	.880	1.026	.015	.088	.017	.107	.922	.957	35.0	.257	204.0	.060	6.0	3/8
10.8	.660	1.540	.037	.145	.022	.160	.932	1.428	46.0	.221	207.0	.288	6.0	3/8
11.1	.421	2.902	.292	.503	.027	.689	.313	.496	12.6	.050	191.0	.095	5.0	3/8
11.2	.642	1.407	.059	.208	.027	.088	.990	1.146	24.4	.278	204.0	.220	5.0	3/8
11.3	.916	.869	.017	.096	.013	.246	.962	1.447	52.5	.287	196.0	.223	5.0	3/8
11.4	1.137	.673	.013	.094	.029	.136	1.090	1.115	15.5	.269	210.0	.044	5.0	3/8
12.1	.427	2.822	.135	.238	.031	.644	.615	.916	45.0	.106	238.0	.177	5.0	1/2
12.2	.650	1.375	.055	.200	.014	.182	.944	1.241	40.3	.317	216.5	.340	5.0	1/2
12.3	.909	.878	.017	.097	.032	.237	1.070	1.462	61.0	.369	194.4	.305	5.0	1/2
12.4	1.130	.678	.013	.093	.031	.287	1.185	1.484	16.7	.229	200.7	.103	5.0	1/2
13.1	550	1.588	.034	.130	.021	.140	.902	1.280	30.2	.402	174.3	.493	6.0	1/2
13.2	.860	1.057	.027	.153	.024	.096	.928	1.320	43.3	.133	238.0	.167	6.0	1/2
13.3	.995	.878	.019	.132	.026	.145	.927	1.230	39.5	.350	239.0	.207	6.0	1/2
13.4	1.239	.678	.011	.101	.021	.188	.952	1.230	42.5	.139	187.0	.139	6.0	1/2
13.5	1.475	.557	.079	.086	.006	.268	.878	1.164	33.2	.154	157.5	1.09	6.0	1/2
14.1	.650	1.580	.035	.133	.019	.169	.893	1.197	38.1	.208	174.9	.212	6.0	1/8
14.2	.900	.997	.026	.158	.026	.135	.907	1.490	52.4	.108	183.6	.123	6.0	1/8
14.3	1.000	.873	.020	.136	.026	.208	.897	1.539	38.5	.218	166.0	.182	6.0	1/8
14.4	1.240	.677	.011	.094	.006	.242	.893	1.547	39.6	.191	188.6	.134	6.0	1/8
14.5	1.500	.547	.008	.085	.004	.256	.826	1.586	43.6	.168	167.2	.112	6.0	1/8
15.1	.650	1.375	.062	.224	.023	.168	.930	1.255	45.0	.278	190.8	.172	5.0	1/8
15.2	.905	.882	.017	.099	.015	.314	.898	1.429	44.5	.170	221.7	.217	5.0	1/8
15.3	1.125	.682	.013	.097	.030	.068	1.027	1.640	26.1	.263	197.8	.116	5.0	1/8
15.4	.438	2.690	.102	.189	.036	.778	.757	1.270	88.9	.348	-50.0	.211	5.0	1/8
16.1	.432	2.762	.130	.236	.054	.498	.690	1.149	72.7	.085	254.0	.160	5.0	1/4
16.2	.650	1.375	.060	.217	.011	.209	.939	1.140	46.6	.271	229.0	.246	5.0	1/4
16.3	.875	.920	.017	.092	.022	.250	1.034	1.198	25.8	.473	227.4	.209	5.0	1/4
16.4	1.125	.682	.013	.095	.026	.185	1.070	1.435	35.1	.264	175.3	.058	5.0	1/4
17.1	1.495	.549	.009	.096	.008	.196	.924	1.850	40.1	.050	165.9	.136	6.0	1/8
17.2	1.785	.453	.005	.067	.004	.215	.859	1.750	32.8	.025	156.6	.115	6.0	1/8
17.3	1.465	.562	.009	.098	.005	.154	.888	1.486	37.6	.048	163.2	.174	6.0	1/4
17.4	1.788	.453	.005	.069	.003	.178	.825	1.411	31.8	.028	139.9	.088	6.0	1/4
17.5	1.450	.567	.009	.099	.003	.170	.874	1.450	27.6	.122	167.0	.151	6.0	3/8
17.6	1.750	.463	.005	.068	.003	.158	.822	1.446	27.3	.026	147.7	.111	6.0	3/8

Table VI.5

RESULTS OF TEST RUNS 9-17

VI.7 Real Flow Through Gaps

The inner solution for flow through the gaps indicates that the velocity reaches infinity at the edges. Real flow cannot attain infinite velocity, so it can be expected that this theory may be invalid in the regions adjacent to the cylinder edges.

In order to examine the flow, photographs of dye motion about the edges during the passage of various waves were taken. Plates 7-10 show this flow for the values of $U_m T/R$ (the Keulegan-Carpenter parameter), KA and T indicated (A in the plates indicates the amplitudes of the incident wave from the left).

As indicated in these plates, the flow through the gaps does not conform to the inner flow sketched in Figure III.2. The streamlines separate from the cylinder and form a jet, ending with a single eddy at some distance from the edge. The strength of the jet is dependent on the relative wave height, or, more precisely, on the Keulegan-Carpenter parameter.

The effect of this diversion from the assumed flow may be approximated by considering the free streamline flow through an orifice (cf. Milne-Thompson, Sec. 12.32). Qualitatively, it may be expected that the effect of the gap will be less in the case of real fluid flow than in the idealized model, since the inertial pressure drop across the gap will be less in the separated flow than in the attached case. On the other hand, the drag component of the force can be expected to be higher in the real fluid. This effect would tend to shift the phase angle of the horizontal force, as indeed appears to be the case from Figures VI.10 and VI.11.

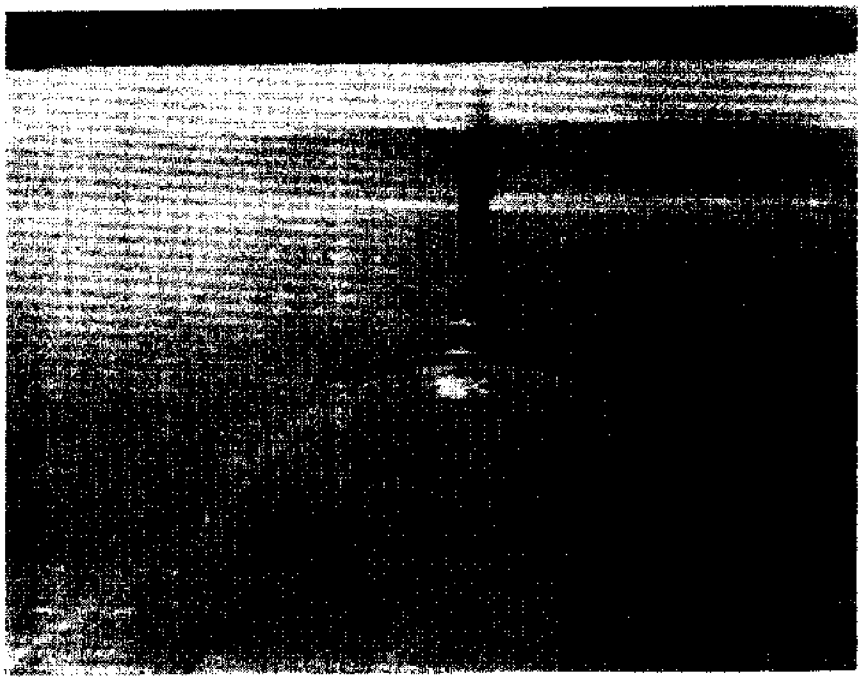

PLATE 7

$T = .90$, $KA = .158$, $U_m T/R = 1.60$

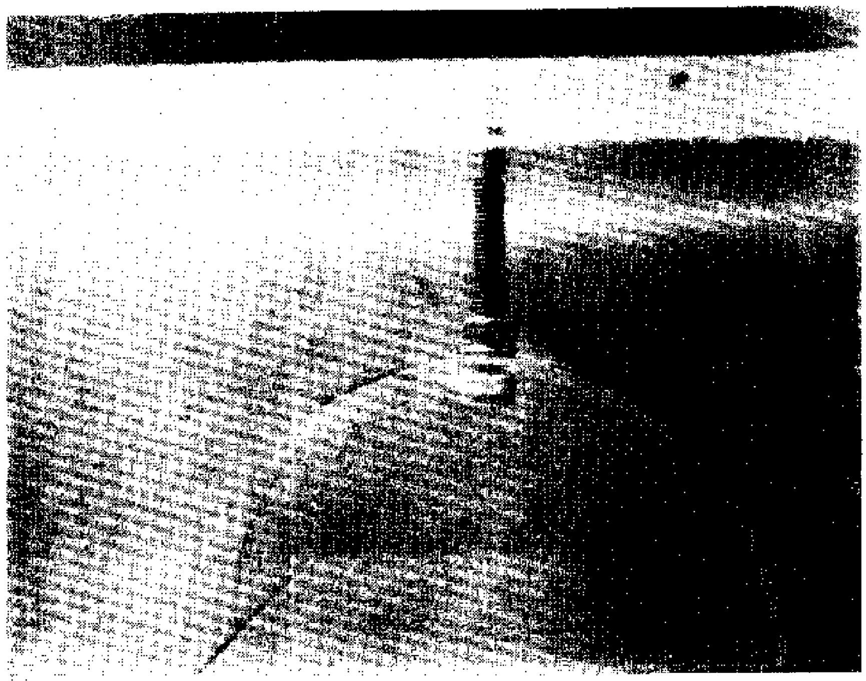

PLATE 8

$T = 1.30$, $KA = .045$, $U_m T/R = 1.20$

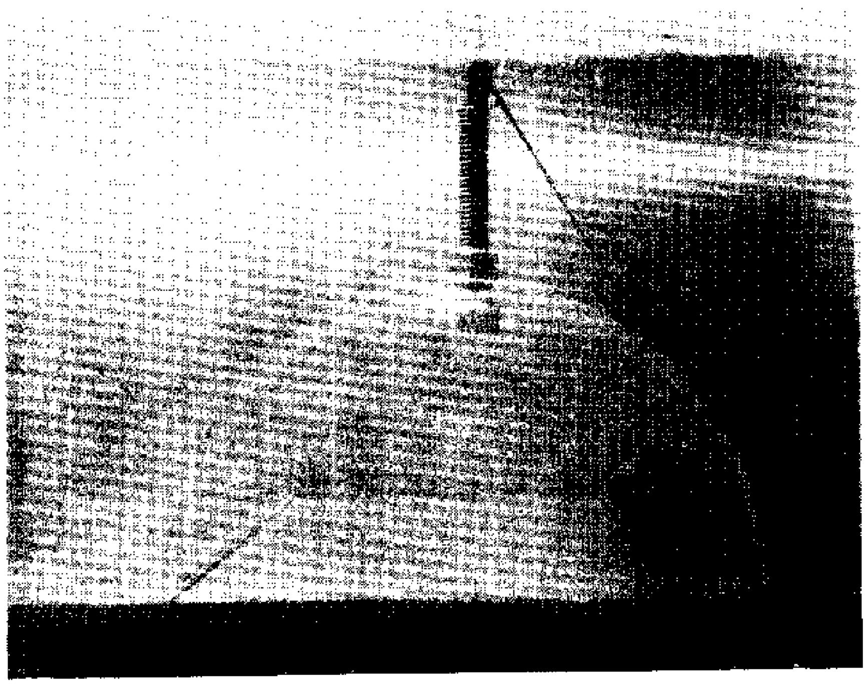

PLATE 9

$T = 1.15$, $KA = .042$, $U_m T/R = .96$

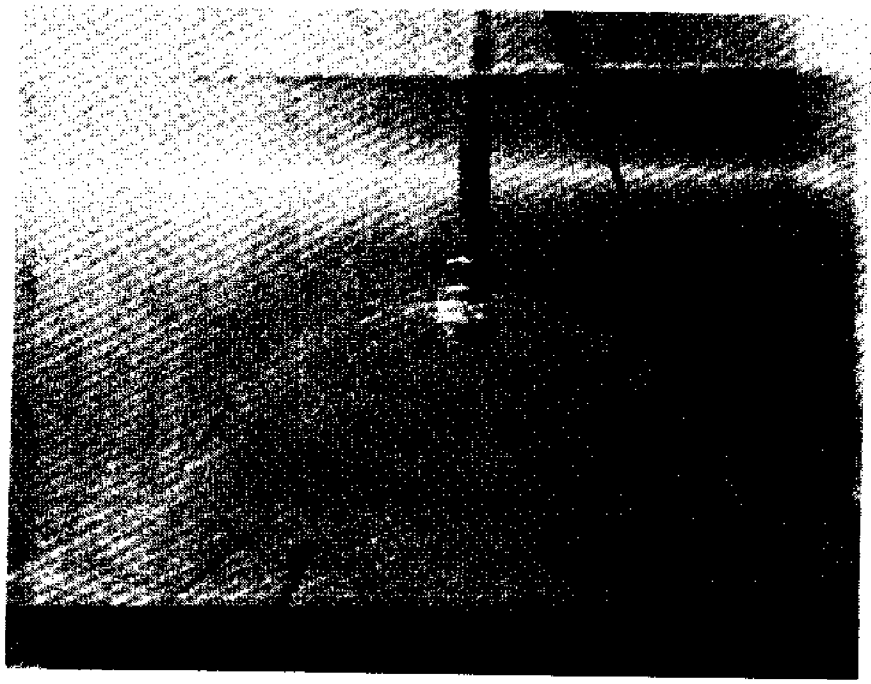

PLATE 10

$T = 1.30$, $KA = .0034$, $U_m\ T/R = .092$

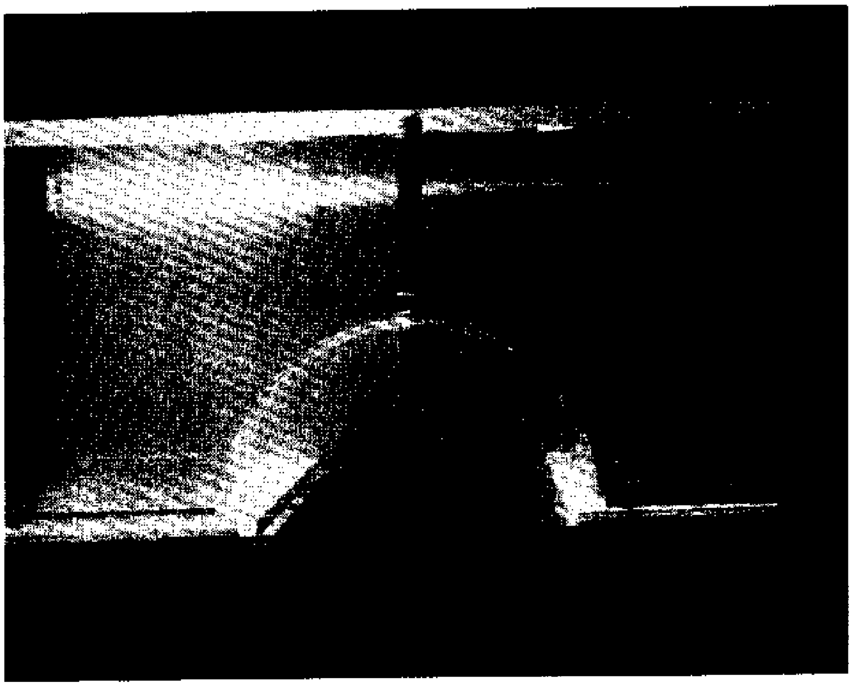

PLATE II

CYLINDER IN POSITION FOR "ZERO-GAP" TESTS

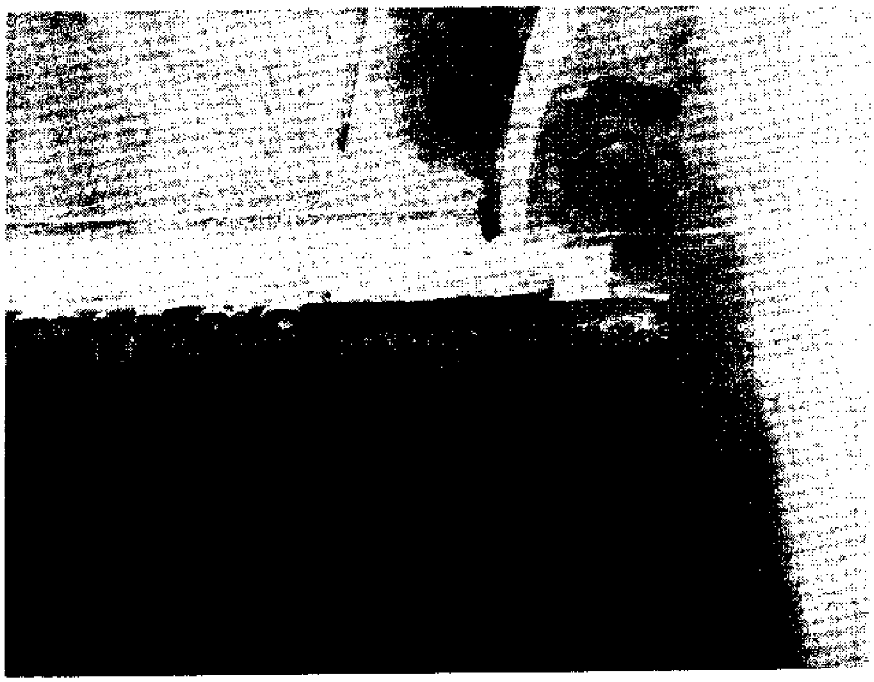

PLATE 12

FLOW THROUGH GAP DURING "ZERO-GAP" TESTS

VII. CONCLUSIONS

The solution derived herein provides an adequate theory for predicting the forces on a submerged cylinder, as is apparent from the correlation of the theory with experiment. In particular, and of significant engineering importance, is the conclusion that the inside region experiences a constant pulsating pressure equal to the average of the pressures acting around the base.

The applicability of this conclusion to the practical problem of forces on a three-dimensional object has not been proven, but intuitive reasoning indicates that it is plausible. If the pressure inside of a "dome", for example, did not exhibit a first order variation, the pressure drop across the gap would be a first order parameter, and thus the flow would be first order. For very small gaps this seems unrealistic.

The effect on the horizontal force, for the cylinder, is the same order as the gap flow. This has less significant implications with regard to the three-dimensional case. Since in practice flow will be restricted either by design or by nature (through erosion), the effect of flow through the bottom may be less pronounced. It might be noted, however, that a poorly designed experiment on three-dimensional models could give erroneous horizontal force measurements. In particular, if a model is suspended above the bottom in order to provide a clearance for vertical motion, horizontal forces will be less than in a more realistic setup with no clearance. The error can be expected, on the basis of this thesis, to be of the order $1/\ell n \varepsilon$.

With regards to both the vertical and the horizontal forces, the values computed on the basis of no gap appear to represent a conservative upper limit on the actual forces.

A more thorough investigation of the three-dimensional problem has not been carried out in this thesis. The same method could in principle be applied, however. To do this, the potential about a dome would have to be broken into its

APPENDICES

APPENDIX A

AN ALTERNATE MATCHING SCHEME

The semi-intuitive matching procedure used in Chapter III may be shown to be equivalent to a more formal expansion procedure. To show this, we will consider the problem of a single slit in a vertical wall. The slit is a distance h below the free surface, and waves are incident from the left (see Figure A.1). This problem has been solved by Tuck (1969), and will be examined here only to illustrate the equivalence of two alternate matching schemes.

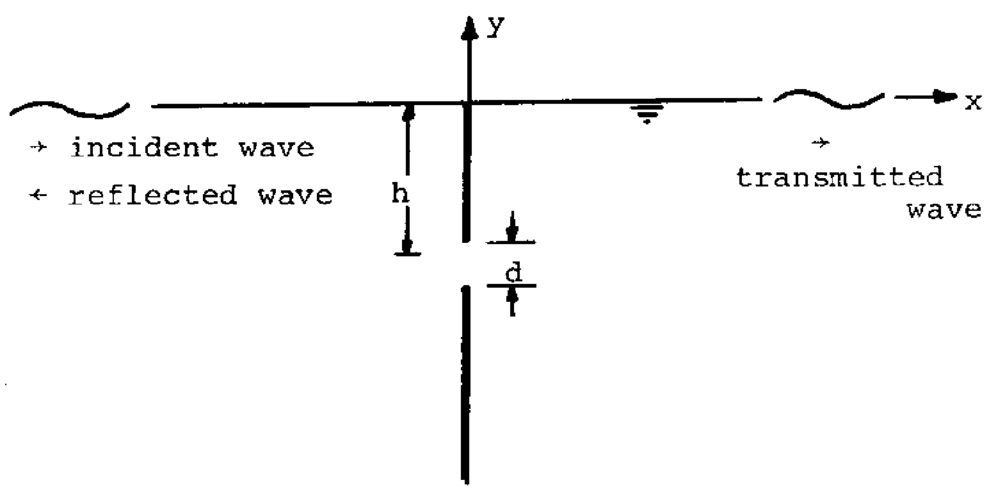

FIGURE A.1

TRANSMISSION THROUGH A SLIT

The vertical wall extends to an infinite depth. The transmission coefficient depends on the slit width (d) and the depth of submergence (h). We will thus assume that the perturbation parameter may be written as

$$\varepsilon = d/h, \qquad \text{A.1}$$

and that the transmission coefficient, τ, goes asymptotically to zero for small ε.

Now we may represent the velocity potentials on either side of the barrier as follows:

$$\text{left of wall:}\quad \phi^{\ell}(x,y,\varepsilon) = \phi_o^{\ell}(x,y) + \alpha_1(\varepsilon)\phi_1^{\ell}(x,y) + \alpha_2(\varepsilon)\phi_2^{\ell}(x,y) + \ldots \qquad \text{A.2.1}$$

$$\text{right of wall:}\quad \phi^{r}(x,y,\varepsilon) = \phi_o^{r}(x,y) + \alpha_1(\varepsilon)\phi_1^{r}(x,y) + \alpha_2(\varepsilon)\phi_2^{r}\ (x,y) + \ldots \qquad \text{A.2.2}$$

where $(x,y) = (\hat{x},\hat{y})/h$

$\hat{x}$ and $\hat{y}$ are dimensional variables

$$\lim_{\varepsilon\to 0} \frac{\alpha_{n+1}}{\alpha_n} = 0$$

$$\lim_{\varepsilon\to 0} \alpha_1 = 0$$

The boundary value problem satisfied by ϕ^{ℓ} and ϕ^{r} is as follows:

$$\nabla^2\phi^{\ell,r}(x,y) = 0 \qquad \text{A.3.1}$$

$$\frac{\partial\phi^{\ell,r}}{\partial x}(0,y) = 0 \qquad y > -1+\varepsilon;\ y < -1-\varepsilon \qquad \text{A.3.2}$$

$$\frac{\partial\phi^{\ell,r}}{\partial y} - \frac{\omega^2 h}{g}\phi^{\ell,r}(x,0) = 0 \qquad \text{A.3.3}$$

$$\phi^{\ell}(x,y) - ie^{-Ky}e^{-iKx} \simeq e^{iKx} \qquad x \to -\infty \qquad \text{A.3.4}$$

$$\phi^{r}(x,y) \simeq e^{-iKx} \qquad x \to +\infty \qquad \text{A.3.5}$$

Equations A.3 are valid to any order. By virtue of the linearity of these equations, all of the functions ϕ_i^{ℓ} and ϕ_i^{r},

$i = 0, 1, \ldots, N$, satisfy A.3. We may simplify A.3.2 by writing

$$\frac{\partial\phi^{\ell,r}}{\partial x}(0,y) = 0 \qquad y \neq -1,$$

and noting that the approximation is valid to $0(\varepsilon)$.

The potentials ϕ^{ℓ} and ϕ^{r} are assumed valid only at distances far removed from the slit. Using dimensionless notation (Chapter II), and assuming linear theory, the asymptotic form of ϕ_o^{ℓ} or $x \to -\infty$ and the complete ϕ_o^{r} may be written immediately:

$$\phi_o^{\ell}(x,y) = 2ie^{ky} \cos kx \qquad \text{A.4}$$

$$\phi_o^{r}(x,y) = 0 \qquad \text{A.5}$$

These are the solutions for a vertical barrier with no gap and no "breaking" at the point $(0^-, 0)$. The introduction of a small gap at a finite depth introduces a perturbation as indicated by A.2. The representations A.2 are called the "outer expansion" of the flow, and they represent the perturbed flow far from the slit (further than some radius δ). The perturbation potentials, ϕ_1, ϕ_2, etc., may thus be represented by multipole expansions at (0, -1). We will assume, and matching will show, that the correct perturbation is a simple source (or sink) placed at (0, -1). This will be shown to be valid to $0(\varepsilon^2)$.

We may thus write, tentatively,

$$\phi_n^{\ell,r}(x,y) = \pm A_n[\ell nr + H(\vec{r})] \qquad \text{A.6}$$

where $\vec{r} = (x,y+1)$

$r^2 = x^2 + (y+1)^2$

$H(\vec{r})$ is a regular function of F.

We take the source strength to be $+A_n$ on the left and $-A_n$ on the right, as must be the case from continuity. The value of A_n can only be found by matching the outer solution to an inner solution (Chapter III). The function $\ell n r + H(\vec{r})$ is obviously simply the Green's function for a simple source at (0,-1), thus $H(\vec{r})$ is known. The region of non-uniformity is determined by a radius δ_n within which the perturbation $\alpha_n A_n \ell n r$ is no longer small. This implies

$$\delta_n = 0(e^{-1/\alpha_n}) \qquad \text{A.7}$$

Inner Problem

We may proceed as in Chapter III to solve the inner problem by stretching coordinates.

$$\bar{x} = x/\varepsilon \qquad \text{A.8.1}$$

$$\bar{y} = \frac{y+1}{\varepsilon} \qquad \text{A.8.2}$$

We may represent the inner flow as an asymptotic expansion

$$\psi(x,y,\varepsilon) = C + \beta_1(\varepsilon)\psi_1(x,y) + \beta_2(\varepsilon)\psi_2(x,y) + \ldots \qquad \text{A.9}$$

where the β's play the same role as the α's in A.3. As is usually the case, $\beta_n = \alpha_n$ for this problem, but they will be designated separately since they are not necessarily equal. Since the boundary conditions remain linear and independent of the order, we may write

$$\psi_n(\bar{x},\bar{y}) = Q_n R_e \cosh^{-1}\bar{z} + q_n \qquad \text{A.10}$$

where $\bar{z} = \bar{x} + i\bar{y}$

We have made use of the derivation of the flow through a slit in an infinite wall from Chapter III.

Matching

We shall find the values of A_n, Q_n, C and q_n through the application of Van Dyke's matching principle (Van Dyke, 1964, p. 89). Specifically, we will use the "asymptotic matching principle":

> The m-term inner expansion of (the n-term outer expansion) = the n-term inner expansion of (the m-term outer expansion).

This matching is accomplished by the following procedure:

1. Choose m=n or n+1.
2. Write first n terms of the outer expansion (A.2) in terms of the inner variables $(\bar{x},\bar{y})$.
3. Expand this for small ε, include first m terms of expansion.
4. Write first m terms of the inner expansion (A.9) in terms of the outer variables (s,y).
5. Expand this for small ε, include first n terms.
6. Convert both expansions (from steps 3 and 5) into the same coordinates.
7. Equate the two expansions and determine the unknowns.

Now, choose m=2, n=1, to get:

1. 2 term outer expansion:

$$\phi^{\ell} \simeq 2ie^{Ky}\cos Kx + \alpha_1(\varepsilon)A_1[\ell n r + H(\vec{r})]$$

$$\phi^{r} \simeq -\alpha_1(\varepsilon)A_1[\ell n r + H(\vec{r})]$$

2. Rewritten in inner variables:

$$\phi^{\ell} \simeq 2ie^{K(\bar{y}\varepsilon - h)}\cos K\bar{x}\varepsilon + \alpha_1(\varepsilon)A_1[\ell n \varepsilon \bar{r} + H(\varepsilon\vec{\bar{r}})]$$

$$\phi^{r} \simeq -\alpha_1(\varepsilon)A_1[\ell n \varepsilon \bar{r} + H(\varepsilon\vec{\bar{r}})]$$

3. Expand for small ε (keeping $\bar{x},\bar{y}$ fixed):

$$\phi^{\ell} \simeq 2ie^{-Kh} + \alpha_1 A_1 \ell n \varepsilon$$

$$\phi^{r} \simeq -\alpha_1 A_1 \ell n \varepsilon$$

4. 1 term inner expansion:

$$\psi(\bar{x},\bar{y}) \simeq C$$

5. Rewrite in outer coordinates:

$$\psi(x,y) \simeq C$$

6. Expand for small ε, (x,y) fixed:

$$\psi(x,y) \simeq C$$

In order to obtain a solution, we must set $\alpha_1(\varepsilon) = 0(1/\ell n \varepsilon)$. Setting

$$\alpha_1(\varepsilon) = 1/\ell n \varepsilon,$$

we obtain, by equating the expressions obtained at step 3 to C:

$$2ie^{-kh} + A_1 = C$$

$$-A_1 = C$$

Thus, we obtain:

$$C = -A_1 = ie^{-kh} \qquad \text{A.11}$$

To find higher order terms, repeat this procedure for, say, m=3, n=2, etc. ad nauseum. We will perform one more iteration here:

1. 3 term outer expansion:

$$\phi^{\ell} \simeq 2ie^{-ky}\cos kx - \frac{ie^{-kh}}{\ell n\varepsilon}[\ell nr+H(\vec{r})] + \alpha_2 A_2[\ell nr+H(\vec{r})]$$

$$\phi^{r} \simeq \frac{ie^{-kh}}{\ell n\varepsilon}[\ell nr+H(\vec{r})] - \alpha_2 A_2[\ell nr+H(\vec{r})]$$

2. Rewrite in inner variables:

$$\phi^{\ell} \simeq 2ie^{-k(\bar{y}\varepsilon-h)}\cos k\bar{x}\varepsilon - \frac{ie^{-kh}}{\ell n\varepsilon}[\ell n(\bar{r}\varepsilon)+H(\varepsilon\vec{\bar{r}})]$$

$$+ \alpha_2 A_2[\ell n\bar{r} + H(\varepsilon\vec{\bar{r}})]$$

$$\phi^{r} \simeq \frac{ie^{-kh}}{\ell n\varepsilon}[\ell n\bar{r} + H(\bar{r}\varepsilon)] - \alpha_2 A_2[\ell n\bar{r} + H(\varepsilon\vec{\bar{r}})]$$

3. Expand for small ε, ($\bar{x},\bar{y}$ fixed)

$$\phi^{\ell} \simeq ie^{-kh} - \frac{ie^{kh}}{\ell n\varepsilon}[\ell n\bar{r}+H(0)] + \alpha_2 A_2 \ell n\varepsilon + O(\varepsilon) \qquad \text{A.12.1}$$

$$\phi^{r} \simeq ie^{-kh} + \frac{ie^{-kh}}{\ell n\varepsilon}[\ell n\bar{r}+H(0)] - \alpha_2 A_2 \ell n\varepsilon \qquad \text{A.12.2}$$

4. 2 term inner expansion:

$$\psi \simeq C + \beta_1 \{Q_1 R_e \cosh^{-1} i\bar{z} + q_1\}$$

5. Rewrite in outer variables:

$$\psi \simeq C + \beta_1 \{Q_1 R_e \cosh^{-1}(iz/\varepsilon) + q_1\}$$

6. Expand for small ε (z fixed):

$$\psi \simeq C + \beta_1 \{\pm Q_1 \ \ln\frac{2r}{\varepsilon} + q_1\}$$

("+" for $x > 0$, "−" for $x < 0$)

7. 3 term outer expansion (of 2 term inner)

$$\psi \simeq C \mp \beta_1 Q_1 \ln\varepsilon \pm \beta_1 Q_1 \ln 2r + \beta_1 q_1$$

If we now rewrite this in inner coordinates, we get:

$$\psi \simeq C \pm \beta_1 Q_1 \ln 2\bar{r} + \beta_1 q_1 \qquad \text{A.13}$$

First, comparing the $\ln\bar{r}$ terms, which must match, we find:

$$\beta_1 Q_1 = \frac{ie^{-kh}}{\ln\varepsilon},$$

from which we deduce that $\beta_1 = 1/\ln\varepsilon$ and $Q_1 = -A_1 = ie^{-kh}$. The next terms to match are of $O(1/\ln\varepsilon)$. In order for A.12 to match with A. , we must set $\alpha_2 = (1/\ln\varepsilon)^2$ to obtain (setting $Q_1 = -A_1$):

$$-A_1\ln 2 + q_1 = -A_1 H(0) - A_2$$

$$+A_1\ln 2 + q_1 = A_1 H(0) + A_2$$

from which we deduce

$$q_1 = 0$$

$$A_2 = A_1[\ln 2 - H(0)] \qquad \text{A.14}$$

Combining the results so far with A.2 and A.6, we can write the outer expansion as

$$\phi^{\ell} \simeq 2ie^{-ky}\cos kx - ie^{-kh}[\ln r + H(\vec{r})]\left\{\frac{1}{\ln\varepsilon} + \frac{\ln 2 - H(0)}{(\ln\varepsilon)^2} + \dots\right\}$$

A.15.1

$$\phi^r \approx ie^{-kh}[\ell nr+H(\vec{r})]\left\{-\frac{1}{\ell n\varepsilon} + \frac{\ell n2-H(0)}{(\ell n\varepsilon)^2} + \ldots\right\} \quad A.15.2$$

The above process ca: of course be extended indefinitely, yielding in this case an asymptotic series in $(1/\ell n\varepsilon)^n$ carried to an infinite number of terms. Actually, at some point the series should be truncated since the accuracy gained by adding a term of $(1/\ell n\varepsilon)^N$ will, for finite values of ε, be less than that lost by ignoring $0(\varepsilon)$ terms. This happens when $N = -\ell n\varepsilon/\ell n|\ell n\varepsilon|$. Notice that N becomes infinite as $\varepsilon \to 0$.

Further terms in the above expansions may be added with increasing tedium.

Comparison with "Semi-Intuitive" Matching

It is much easier to find the solution to this problem directly by setting

$$\phi^\ell(x,y) \approx 2ie^{+ky}\cos kx + A(\varepsilon)[\ell nr+H(\vec{r})] \quad A.16.1$$

$$\phi^r(x,y) \approx -A(\varepsilon)[\ell nr+H(\vec{r})] \quad A.16.2$$

for the outer solution, and

$$\psi(x,y,\varepsilon) = P + Q(\varepsilon)\mathrm{Re}\cosh^{-1}(iz/\varepsilon) \quad A.17$$

for the inner solution. These representations are of course valid to whatever order the particular form of the solutions is valid, since the same expressions could be derived by factoring the $[\ell nr+H(\vec{r})]$ and the $[\mathrm{Re}\cosh^{-1}(i\bar{z})]$ expressions from A.2 and A.9 respectively. In particular, we see immediately that

$$A(\varepsilon) = \sum_{n=1}^{N} \alpha_n A_n \qquad \text{A.18}$$

$$Q(\varepsilon) = \sum_{n=1}^{N} \beta_n Q_n \qquad \text{A.19}$$

and

$$P = C + \sum_{n=1}^{N} \beta_n q_n \qquad \text{A.20}$$

To show the equivalence of the two forms of matching, we need only set the outer limit of the inner solution (A.17) equal to the inner limit of the outer solution (A.16) to obtain (setting A = -Q for continuity)

$$2ie^{-kh} + A[\ell nr + H(0)] = P + A\ell n(2r/\varepsilon) \qquad \text{A.21.1}$$

$$-A[\ell nr + H(0)] = P - A\ell n(2r/\varepsilon) \qquad \text{A.21.2}$$

which yields

$$P = ie^{-kh} \qquad \text{A.22}$$

$$A = \frac{ie^{-kh}}{\ell n2 - H(0) - \ell n\varepsilon} \qquad \text{A.23}$$

Expanding $A(\varepsilon)$ in powers of $(1/\ell n\varepsilon)$ yields

$$A(\varepsilon) = \frac{1}{\ell n\varepsilon}\left[\frac{-ie^{-kh}}{1 - \frac{\ell n2-H(0)}{\ell n\varepsilon}}\right] \simeq -\frac{ie^{-kh}}{\ell n\varepsilon}\left[1 + \frac{\ell n2-H(0)}{\ell n\varepsilon} + \ldots\right] \qquad \text{A.24}$$

Comparing A.15 and A.16 using A.24 shows that both matching procedures do indeed yield the same result.

APPENDIX B

GREEN'S FUNCTION

The Green's function is the potential of a source at (ξ,η) which satisfies the free surface condition, the bottom boundary condition, and the radiation conditions at $x = \pm\infty$. If this function is $G(x,y|\xi,\eta)$, when the time dependence has been superseded as in Chapter II, then

$$\nabla^2 G(x,y|\xi,\eta) = - 2\pi\ \delta(x-\xi)\delta(y-\eta) \qquad \text{B.1}$$

$$(\nu - \partial/\partial y)\ G(x,D|\xi,\eta) = 0 \qquad \text{B.2}$$

$$\frac{G(x,0|\xi,\eta)}{\partial y} = 0 \qquad \text{B.3}$$

$$G \simeq e^{\pm iKx} \qquad x \to \pm\infty \qquad \text{B.4}$$

where $\nu = \omega^2/g$

The equations have been written in dimensional form. These equations have been solved by numerous authors. Thorne (1953) writes $G(x,y|\xi,\eta)$ in the form

$$G(x,y|\xi,\eta) = \ell n(r/r') + \phi_1(x,y|\xi,\eta) + i\phi_c(x,y|\xi,\eta),$$

$$\text{where} \quad r^2 = (x-\xi)^2 + (y-\eta)^2$$

$$r'^2 = (x-\xi)^2 + (y+\eta-2D)^2$$

He then solves for ϕ_1 by writing

$$\phi_1(x,y|\xi,\eta) = \int_0^\infty [f_1(\xi,\eta,k)\ \sinh ky$$

$$+ f_2(\xi,\eta,k)\ \cosh k(D-y)]\ \cos kx\ dk$$

and selecting f_1 and f_2 so that the boundary conditions B.2 and B.3 are satisfied. ϕ_2 is selected so the radiation conditions are satisfied.

Wehausen and Laitone solve the same problem using the complex potential function, and Mei (1969) finds the Green's function by Fourier transform techniques. Only the results will be presented here.

As given by Thorne, and with a substitution indicated by Wehausen*, the functions ϕ_1 and ϕ_2 may be written

$$\phi_1(x,y|\xi,\eta) = -\,2\ell nD$$
$$-\,2\oint_0^\infty \left\{\frac{K+}{k}\;\frac{e^{-kD}\cosh k(D+\eta)\cosh k(D+y)\cos k(x-\xi)}{k\sinh kD - \nu\cosh kD} + \frac{e^{-kD}}{k}\right\} dk$$

$$\phi_2(x,y|\xi,\eta) = \frac{K^2-\nu^2}{K(K^2D-\nu^2D+\nu)}\cosh K(D+\eta)\cosh K(D+y)\cos K(x-\xi)$$

The asymptotic form may be written

$$\lim_{x\to\pm\infty} G(x,y|\xi,\eta) = \frac{2\pi(K^2-\nu^2)}{K(K^2D-\nu^2D+\nu)}\cosh K(D+y)\cosh K(D+\xi)\,e^{iK|x-\xi|-i\pi/2}$$

The value of the integral for $_1$ is computed by taking (numerically) the limit

---

*Wehausen introduces the identity

$$\frac{e^{-KD}\sinh KD}{\nu D + \sinh^2 KD} = \frac{K-\nu}{K^2D - \nu^2D +}$$

$$\oint_0^{\infty} \frac{f(k)\ dk}{k \sinh kD - \nu \cosh kD} \approx \lim_{\Delta \to 0} \left\{ \int_0^{K-\Delta} (\ )dk + \int_{K-\Delta}^{\infty} (\ )dk \right\}$$

for each set of values $(x,y|\xi,\eta)$ on the cylinder.

APPENDIX C

ASYMPTOTIC LIMITS OF $\cosh^{-1} iZ$

The solution to the inner problem was obtained in Chapter III by performing a conformal mapping:

$$Z = -i \cosh \zeta \qquad \text{III.21}$$

$$\text{where } Z = (x \pm 1)/\varepsilon + iy/\varepsilon$$

This mapping is illustrated in Figures III.3,4. The asymptotic limits may be taken, for the left side of the gap,

$$\lim_{\substack{\xi \to -\infty \\ 0<\eta<\pi}} Z = \frac{-ie^{-(\xi+i\eta)}}{2} \qquad \text{C.1}$$

and, for the right side of the gap,

$$\lim_{\substack{\xi \to +\infty \\ 0<\eta<\pi}} Z = \frac{-ie^{(\xi+i\eta)}}{2} \qquad \text{C.2}$$

Thus, we may take the mapping in the two limits to be:

$$\zeta = -\ \ln 2iZ \quad \text{(left side)}$$

$$\zeta = \ln 2iZ \quad \text{(right side)}$$

which yields the complex velocity potential from equation III.22,

$$W(Z) \to \pm\, U \ln 2iZ + C,$$

which yields the asymptotic form of the velocity potential when only the real part is taken, i.e.,

$$\phi(X,Y) = \pm U\ln 2|Z| + C.$$

This "outer limit" has been utilized in Chapter IV for the matching.

APPENDIX D

NUMERICAL FILTERING OF DATA

If we desire to low pass filter a time function, $x(t)$, we must pass it through a linear system with the following transfer function

$$H(\omega) = 1.0 \qquad -\omega_c < \omega < \omega_c$$

$$H(\omega) = 0.0 \qquad |\omega| > \omega_c$$

In this manner, if $X(\omega)$ is the Fourier transform of $x(t)$ (cf. Davenport and Root)

$$X(\omega) = \frac{1}{\sqrt{2\pi}} \int_{-\infty}^{+\infty} x(t) e^{-i\omega t} dt \qquad \text{D.1}$$

The Fourier transform of the output, $y(t)$, will be

$$Y(\omega) = H(\omega)\ X(\omega), \qquad \text{D.2}$$

so that $y(t)$ will be $x(t)$ with frequencies of $|\omega| > \omega_c$ removed.

$y(t)$ may be found by taking the inverse Fourier transform of D.2

$$y(t) = \frac{1}{\sqrt{2\pi}} \int_{-\infty}^{+\infty} H(\omega)\ X(\omega)\ e^{i\omega t}\ d\omega \qquad \text{D.3}$$

Noting that

$$H(\omega) = \frac{1}{\sqrt{2\pi}} \int_{-\infty}^{+\infty} h(t)\ e^{-i\omega t}\ dt,$$

write

$$y(t) = \frac{1}{2\pi} \int_{-\infty}^{\infty} dZ'h(t') \int_{-\infty}^{\infty} d\omega X(\omega) e^{i\omega(t-t')}$$

$$= \frac{1}{\sqrt{2\pi}} \int_{-\infty}^{\infty} h(t')\ x(t-t')\ dt' \qquad \text{D.4}$$

Equation D.1 is the familiar convolution integral (cf. Blackman and Tuckey, p. 72). Equation D.4 is helpful in our case since we may find the filtered function, y(t), approximately by performing the integration numerically. To do this, we must determine h(t):

$$h(t) = \frac{1}{\sqrt{2\pi}} \int_{-\infty}^{+\infty} H(\omega) e^{i\omega t} d\omega$$

$$= \frac{1}{\sqrt{2\pi}} \int_{-\omega_c}^{\omega} e^{i\omega t} d\omega$$

$$= \sqrt{\frac{2}{\pi}} \frac{\sin \omega_c t}{t} \qquad \text{D.5}$$

Equation D.4 may now be written

$$y(t) = \frac{1}{\pi} \int_{-\infty}^{+\infty} x(t-t') \frac{\sin \omega_c t'}{t'} dt' \qquad \text{D.6}$$

Since we cannot obtain a wave record of infinite length, the above integral must be approximated by one over a finite time period. The actual records were taken over several (at least 5) wave cycles. Since we are only interested in the filtered values over one period, we will calculate y(t) for t's lying within a length of the record representing no more than 1/5 of the total record. If the total sample time is T_s (sec.), the punched data will consist of 250 T_s points for each of seven channels of information (for a sample rate of 250 Hz.). The point t - T/2 may arbitrarily be selected to correspond to the ℓth point of the data, ℓ = 125 T_s, so that t = T/2 lies in the middle of the recorded data. The points t=0 and t=T will thus lie an equal number of points to each side of the midpoint. The situation is shown graphically in Figure D.1.

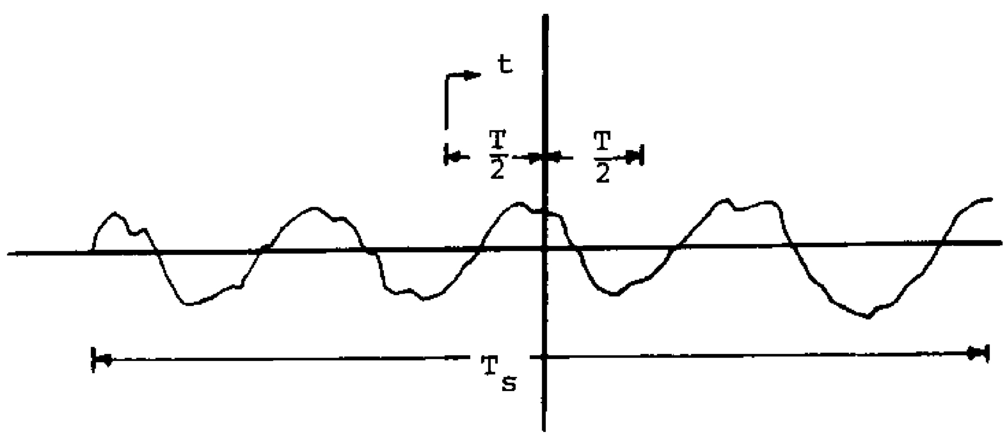

Figure D.1

ILLUSTRATION OF RECORDED SIGNAL

gration over a finite time,

In order that the i

$$\text{:-t')}\ \frac{\sin \omega_o t'\, dt'}{t'}, \qquad \text{D.7}$$

$$y(t) \simeq \frac{1}{\pi} \int_{-T_o}^{T_o}$$

he limits of the

would not require values of x(t) beyo

/2 - M, where M is a

record length, we must select T_o = T_s

hash that might

buffer to protect us from picking up a

exist at the ends of the record. M is typically selected to equal 50.

Now, selecting the data points so that

$$y_i(t_j) = Y_{ij} = Y_{\ell+j}$$

where $y_i(t_j)$ is the signal for channel i at time $t = t_j$

$$t_j = (j-1)\Delta\tau$$

$$\Delta\tau = T/N$$

N = number of points to be calculated for one cycle

and letting $t_j = t - t'$ in we may write

$$y(t_i) = \frac{1}{\pi} \int_{t_i-T_o}^{t_i+T_o} x(t_j) \frac{\sin \omega_c(t_j-t_i)}{t_j - t_i} dt_j$$

This may be written in numerical form

$$Y_i = \Delta\tau \sum_{j=i-N_o}^{i+N_o} x_j A_k \qquad \text{D.8}$$

$$\text{where } A_k = \frac{1}{\pi} \frac{\sin \omega_c(t_j-t_i)}{t_j - t_i}$$

$$= \frac{1}{\pi} \frac{\sin k\omega_c\Delta\tau}{k\Delta\tau}$$

$$N_o = 125\ T_o$$

Program DATA reads the cards punched on the IBM 1130 and applies the filter D.8 to all channels prior to Fourier analysis.

APPENDIX E

RADIATION FROM AN OSCILLATING CYLINDER

The solution for an oscillating cylinder in calm water is of interest because the damping coefficient may be directly related to the magnitude (but not the phase) of the force coefficient by means of the Haskind relations (see Newman, 1962). The velocity potentials, the added mass and [illegible] damping coefficients, are readily computed by the same pro gram used to compute the wave forces with minor alterat[illegible] These computations serve two purposes. First, a compariso of the computed added mass coefficients with those measure in the cylinder vibration studies (Table provides ar alternate means of comparing the linear theory with experi ment. Secondly, by computing the wave force coefficint or via direct computation, and once via the Haskind relations using computed damping coefficients, the reliability of th computer program may be checked since the Haskind relatior holds only between the exact linear damping coefficient ar the exact wave force coefficient.

The formulation of this problem follows closely that the wave force problem. We will again denote the potentia outside the cylinder by $\overline{\phi}(\vec{r})$, that inside by $\tilde{\phi}(\vec{r})$, and the "inner" gap potential by $\hat{\phi}(\vec{r})$.

The cylinder will be assumed oscillating in the hori- zontal plane with a velocity

$$U(t) = U_o \cos \omega t. \qquad \text{E.1}$$

The fluid is assumed incompressible and the motion irrotational.

E.1 The Outside Region

$\overline{\phi}(\vec{r})$ then satisfies the following conditions:

$$\nabla^2\overline{\phi}(\vec{r}) = 0 \qquad \text{E.2.1}$$

$$\overline{\phi}_y(x,D) - \frac{\omega^2 R}{g}\,\overline{\phi}(x,D) = 0 \qquad \text{E.2.2}$$

$$\overline{\phi}_y(x,0) = 0 \qquad |x| > 1 \qquad \text{E.2.3}$$

$$\overline{\phi}_n(x_s,y_s) = U \cos\theta \qquad \text{E.2.4}$$

$$\text{where } x_s^2 + y_s^2 = 1$$

$$\theta = \tan^{-1}(x_s/y_s)$$

In addition, $\overline{\phi}(x,y)$ satisfies the radiation condition at $|x| \to \infty$.

We will again write $\overline{\phi}(\vec{r})$ as a first order term plus a source and a sink perturbation term to account for the gap. We will introduce the same non-uniformities as before and will solve by matching the solutions near each gap.

Let

$$\overline{\phi}(\vec{r}) = \overline{\phi}_o(\vec{r}) + Q(\varepsilon)\overline{\phi}_1(\vec{r}) \qquad \text{E.3.1}$$

$$\overline{\phi}_1(r) = \ell n(r_L/r_R) + H(\vec{r}) \qquad \text{E.3.2}$$

The conditions on $\overline{\phi}_1$ and $\overline{\phi}_2$ are the same with the exception of the boundary condition on the cylinder.

$$\overline{\Phi}_{1n}(x_s\ \ _s) = U\cos\theta \qquad \text{E.4.1}$$

$$\overline{\Phi}_{2n}(x_s, y_s) = 0 \qquad \text{E.4.2}$$

We can see immediately that $H(\vec{r})$ is identical to $H(\vec{r})$ in eqn. for the wave force calculation.

The first order outside potential, $\overline{\Phi}_1$, may be found numerically by the same integral equation as was $\phi_{so}(\vec{r})$ for the wave force, namely

$$\overline{\Phi}_1(x_s, y_s) = -\frac{1}{\pi}\int \overline{\Phi}_1(\xi,\eta)\,\frac{\partial G}{\partial n}\,(x_s y_s|\xi,\eta)\,d\ell$$

$$+\frac{1}{\pi}\int G(x_s, y_s|\xi,\eta)\,\frac{\partial\overline{\Phi}_1}{\partial n}\,(x_s y_s)\,d\ell$$

$$= -\frac{1}{\pi}\int \phi_1\,\frac{\partial G}{\partial n}\,d\ell + \frac{U}{\pi}\int G\cos\theta\,d\ell \qquad \text{E.5}$$

where the integrations are taken over the cylinder's surface as before. E.5 may be solved numerically by the same program used to compute $\phi_{so}(\vec{r})$ by simply making the substitution

$$\frac{\partial\phi_i}{\partial n} = U\cos\theta \qquad \text{E.6}$$

in the program, i.e., by using the oscillating velocities rather than the incident wave velocities.

Assuming this computation has been carried out, we may ... write as before:

$$\overline{\Phi}_o(1,0) = \overline{\Phi}_{OR} \qquad \text{E.7.1}$$

$$\overline{\Phi}_o(-1,0) = \overline{\Phi}_{OL} \qquad \text{E.7.2}$$

$$H(1,0) = H_R \tag{E.7.3}$$

$$H(-1,0) = H_L \tag{E.7.4}$$

E.2 The Inside Region

The conditions to be satisfied by $\phi(r)$ are simplified by the absence of a free surface.

$$\nabla^2\tilde{\phi}(\vec{r}) = 0 \tag{E.8.1}$$

$$\tilde{\phi}_y(x,0) = 0 \tag{E.8.2}$$

$$\tilde{\phi}_n(x_s,y_s) = U\cos\theta \tag{E.8.3}$$

The potential which satisfies these conditions is the same as that for a fixed cylinder with an added term to satisfy E.8.2:

$$\tilde{\phi}(\vec{r}) = B(\varepsilon) + Ux + Q(\varepsilon)\ell n(r_R/r_L) \tag{E.9}$$

E.3 The Inner Solution

The inner solution, like the inside solution, remains the same as before with the addition of a term to account for the motion of the cylinder wall. Thus we may write

$$\hat{\phi}_L(X_L,Y_L) = C_L + Q(\varepsilon)\ \text{Re}\ \{\cosh^{-1}(iZ_L)\} + Ux \qquad \text{E.10.1}$$

$$\hat{\phi}_R(X_R,Y_R) = C_R + Q(\varepsilon)\ \text{Re}\ \{\cosh^{-1}(iZ_R)\} + Ux \qquad \text{E.10.2}$$

where the inner variables are again defined as

$$X_L = (x+1)/\varepsilon$$
$$Y_L = y/\varepsilon$$
$$X_R = (x-1)/\varepsilon$$
$$Y_R = y/\varepsilon$$

The term Ux is written in outer coordinates since matching will be carried out in that system.

E.4

The outer limits of the inner solutions may be written as follows:

$$\lim_{\substack{\varepsilon\to 0 \\ X_L, Y_L \text{ fixed} \\ x \lessgtr 0}} \hat{\phi}_L(X_L,Y_L) = C_L \pm Q(\varepsilon)\ln(2r_L/\varepsilon) \qquad \text{E.11.1}$$

$$\lim_{\substack{\varepsilon\to 0 \\ X_R, Y_R \text{ fixed} \\ x \lessgtr 0}} \hat{\phi}_R(X_R.Y_R) = C_R \pm Q(\varepsilon)\ln(2r_R/\varepsilon) \qquad \text{E.11.2}$$

where $r_L = \sqrt{(x+1)^2 + y^2}$

$$r_R = \sqrt{(x-1)^2 + y^2}$$

The inner limits of the outer solutions may be taken as

$$\lim_{\vec{r}\to(-1,0)} \overline{\phi}(\vec{r}) = \overline{\phi}_{oL} + Q[\ell n r_L - \ell n_2 + H_L] \qquad \text{E.12.1}$$

$$\lim_{\vec{r}\to(1,0)} \overline{\phi}(\vec{r}) = \overline{\phi}_{oR} + Q[\ell n 2 - \ell n r_R + H_R] \qquad \text{E.12.2}$$

$$\lim_{\vec{r}\to(-1,0)} \tilde{\phi}(\vec{r}) = B - U + Q(\ell n 2 - \ell n r_L) \qquad \text{E.13.1}$$

$$\lim_{\vec{r}\to(1,0)} \tilde{\phi}(\vec{r}) = B + U + Q(\ell n r_R - \ell n 2) \qquad \text{E.13.2}$$

We may now find the source strength by writing the total circulation in terms of the potential differences across each region (i.e., the method presented in Section   The equation for the circulation becomes

$$\begin{aligned}
&\overline{\phi}_{oL} + Q[\ell n r_L - \ell n 2 + H_L] - \phi_{oR} - Q[\ell n 2 - \ell n r_R + H_R] \\
&+ C_L - Q[\ell n 2 + \ell n r_L - \ell n \varepsilon] - C_L - Q[\ell n 2 + \ell n r_L - \ell n \varepsilon] \\
&+ B + U + Q[\ell n r_R - \ell n 2] - B + U - Q[\ell n 2 - \ell n r_L] \\
&+ C_R - Q[\ell n 2 + \ell n r_R - \ell n \varepsilon] - C_R - Q[\ell n 2 + \ell n r_R - \ell n \varepsilon] \\
&= 0 \qquad \text{E.14}
\end{aligned}$$

Cancelling terms in E.14 and solving for Q yields

$$Q = \frac{\overline{\phi}_{oR} - \overline{\phi}_{oL} - 2U}{H_L - H_R - 8\ell n 2 + 4\ell n \varepsilon} \qquad \text{E.15}$$

E.5 Matching

Using E.15 instead of

in program MAIN yields the forces per unit velocity (setting $U = 1.0$) on a cylinder oscillating in the horizontal plane. If we write these forces as

$$F = f_1 + if_2,$$

we can identify f_1 with the damping coefficient of the cylinder and f_2 with its added mass. In particular, if f_1 and f_2 are in units of lbs. force per foot per second velocity, we may write the damping coefficient and the added mass respectively

$$B_{11} = f_1 \qquad \text{E.16.1}$$

$$A_{11} = f_2/\omega \qquad \text{E.16.2}$$

Haskind's relation for horizontal wave force may be written (Newman, 1962)

$$|F_H| = a\sqrt{\rho g^2/\omega \; B_{11}} \; . \qquad \text{E.17}$$

This may be written in terms of the Morison mass coefficient C_M as

$$|C_M| = \frac{2 \; F_H \cosh KD}{\rho g \pi R^2 Ka} = \frac{2 \cosh KD}{\rho g \pi K R^2} \sqrt{\frac{\rho g^2}{\omega} B_{11}} \qquad \text{E.18}$$

Table E.1 shows values of C_M computed by the two methods. The column marked C_M presents values computed via the wave scattering program; the column marked C_M' shows values computed via the radiation solution and Haskind's relations.

KD	R/D	ε	C_M	C_M'
.873	.50	0.0	2.013	1.935
.873	.50	.01	1.393	1.351
6.817	.50	0.0	1.582	1.532
6.817	.50	.01	1.740	1.712

TABLE E.1

The difference between C_M and C_M' is due entirely to numerical errors. These results indicate, therefore, the relative accuracy of the computer program used for calculating wave forces.

Appendices F, G and H have been omitted from this report. They may be found in the original Thesis or obtained from the author. Contact the Department of Ocean Engineering, M.I.T., Cambridge, Massachusetts 02139